Elsevier Editorial System(tm) for Science of the Total Environment
Manuscript Draft

Manuscript Number: STOTEN-D-19-14613R2

Title: Gravimetry-based water storage shifting over the China-India border area controlled by regional climate variability

Article Type: Research Paper

Keywords: Water storage shifting; Gravity Recovery and Climate Experiment; climate variability; China-India border area

Corresponding Author: Dr. Kwok Pan Chun,

Corresponding Author's Institution: Hong Kong Baptist University

First Author: Kwok Pan Chun

Order of Authors: Kwok Pan Chun; Qing He; Hok Sum Fok; Subimal Ghosh; Omer Yetemen; Qiang Chen; Ana Mijic

Abstract: The regional water storage shifting causes nonstationary spatial distribution of droughts and flooding, leading to water management challenges, environmental degradation and economic losses. The regional water storage shifting is becoming evident due to the increasing climate variability. However, the previous studies for climate drivers behind the water storage shifting are not rigorously quantified. In this study, the terrestrial water storage (TWS) spatial shifting pattern during 2002-2017 over the China-India border area (CIBA) is developed using the Gravity Recovery and Climate Experiment (GRACE), suggesting that the northwestern India were wetting while western China was drying. Similar drying and wetting patterns were also found in the precipitation, snow depth, Palmer Drought Severity Index (PDSI) and potential evaporation data. Based on our newly proposed Indian monsoon (IM) and western North Pacific monsoon (WNPM) variation indices, the water shifting pattern over the CIBA was found to be affected by the weakening of the variation of IM and WNPM through modulating the regional atmospheric circulation. The weakening of IM and WNPM variations has shown to be attributed to the decreasing temperature gradient between the CIBA and the Indian Ocean, and possibly related to increasing regional temperatures associated with the increasing global temperature. As the global warming intensifies, it is expected that the regional TWS shifting pattern over the CIBA will be further exaggerated, stressing the need of advancing water resources management for local communities in the region.

Response to Reviewers: Dear Dr Ouyang,
Thank you for being the editor of this manuscript. We also would like to thank the reviewers' comments and suggestions.
Please find the revised version of "Gravimetry-based water storage shifting over the China-India border area controlled by regional climate variability" with one author's new affiliation. We also provide new supporting materials for this manuscript.
Below are our responses to the reviewers' comments.
Reviewer #2: Authors have addressed the review comments satisfactorily, and improved the presentation in the manuscript.

For the benefit of readers, Authors should include the supporting codes used in the study as supporting material (or provide it in links/open source platform)

Response to Reviewer 2 comment: Thank you for the comments. Following the suggestion, we have provided new supporting documents including a data resource list, codes and a data file of the new indices mentioned in the manuscript. The details are described in the Readme file.

Gravimetry-based water storage shifting over the China-India border area controlled by regional climate variability

Kwok Pan Chun[1], Qing He[1], Hok Sum Fok[2], Subimal Ghosh[3], Omer Yetemen[4], Qiang Chen[5], Ana Mijic[6]

[1] Department of Geography, Hong Kong Baptist University, Hong Kong, China.

[2] School of Geodesy and Geomatics, Wuhan University, Wuhan 430079, China.

[3] Department of Civil Engineering, Indian Institute of Technology Bombay, Mumbai, India.

[4] Civil, Surveying, and Environmental Engineering, The University of Newcastle, Australia.

[5] Geophysics Laboratory, Faculty of Science, Technology and Communication, University of Luxembourg, 2, avenue de l'Université, L-4365 Esch-sur-Alzette, Luxembourg.

[6] Imperial College London, Department of Civil and Environmental Engineering, London SW7 2AZ, UK.

Corresponding author: Kwok Pan Chun (kpchun@hkbu.edu.hk)

Dear Dr Ouyang,

Thank you for being the editor of this manuscript. We also would like to thank the reviewers' comments and suggestions.

Please find the revised version of "Gravimetry-based water storage shifting over the China-India border area controlled by regional climate variability" with one author's new affiliation. We also provide new supporting materials for this manuscript.

Below are our responses to the reviewers' comments.

Reviewer #2: Authors have addressed the review comments satisfactorily, and improved the presentation in the manuscript.
For the benefit of readers, Authors should include the supporting codes used in the study as supporting material (or provide it in links/open source platform)

Response to Reviewer 2 comment: Thank you for the comments. Following the suggestion, we have provided new supporting documents including a data resource list, codes and a data file of the new indices mentioned in the manuscript. The details are described in the Readme file.

Gravimetry-based water storage shifting over the China-India border area controlled by regional climate variability

Kwok Pan Chun[1], Qing He[1], Hok Sum Fok[2], Subimal Ghosh[3], Omer Yetemen[4,7], Qiang Chen[5], Ana Mijic[6]

[1] Department of Geography, Hong Kong Baptist University, Hong Kong, China.

[2] School of Geodesy and Geomatics, Wuhan University, Wuhan 430079, China.

[3] Department of Civil Engineering, Indian Institute of Technology Bombay, Mumbai, India.

[4] Civil, Surveying, and Environmental Engineering, The University of Newcastle, Australia.

[5] Geophysics Laboratory, Faculty of Science, Technology and Communication, University of Luxembourg, 2, avenue de l'Université, L-4365 Esch-sur-Alzette, Luxembourg.

[6] Imperial College London, Department of Civil and Environmental Engineering, London SW7 2AZ, UK.

[7] Eurasia Institute of Earth Sciences, Istanbul Technical University, Maslak 34469, Istanbul, Turkey.

Corresponding author: Kwok Pan Chun (kpchun@hkbu.edu.hk)

Formatted: Superscript

Highlights:

- Terrestrial water storage showed a clear shifting pattern
- Pattern showed wetting in western China and drying in northwestern India.
- The shifting patterns were mainly due to the weakening of the monsoon variations.
- Weakening monsoon were related to decreasing regional temperature gradients.

Abstract

The regional water storage shifting causes nonstationary spatial distribution of droughts and flooding, leading to water management challenges, environmental degradation and economic losses. The regional water storage shifting is becoming evident due to the increasing climate variability. However, the previous studies for climate drivers behind the water storage shifting are not rigorously quantified. In this study, the terrestrial water storage (TWS) spatial shifting pattern during 2002-2017 over the China-India border area (CIBA) is developed using the Gravity Recovery and Climate Experiment (GRACE), suggesting that the northwestern India were wetting while western China was drying. Similar drying and wetting patterns were also found in the precipitation, snow depth, Palmer Drought Severity Index (PDSI) and potential evaporation data. Based on our newly proposed Indian monsoon (IM) and western North Pacific monsoon (WNPM) variation indices, the water shifting pattern over the CIBA was found to be affected by the weakening of the variation of IM and WNPM through modulating the regional atmospheric circulation. The weakening of IM and WNPM

variations has shown to be attributed to the decreasing temperature gradient between the CIBA and the Indian Ocean, and possibly related to increasing regional temperatures associated with the increasing global temperature. As the global warming intensifies, it is expected that the regional TWS shifting pattern over the CIBA will be further exaggerated, stressing the need of advancing water resources management for local communities in the region.

Keywords

Water storage shifting; Gravity Recovery and Climate Experiment; climate variability; China-India border area

1 Introduction

Terrestrial water storage (TWS), including canopy water, glaciers, snow, surface water in rivers, lakes, wetlands and reservoirs, and underground water, determines global and regional hydrological resilience (Alsdorf et al., 2007). It plays a major role in the exchange of water with the atmosphere and oceans, and affects climate variability (Kim et al., 2009). Therefore, the TWS monitoring as well as the underlying drivers for its spatiotemporal dynamics are crucial for understanding the climatic-hydrological system (Humphrey et al., 2016). With the launch of the Gravity Recovery and Climate Experiment (GRACE) in March 2002, it provides a novel and reliable tool for TWS monitoring (e.g., Long et al., 2015; Long et al., 2017; Reager and Famiglietti, 2009b; Scanlon et al., 2019; Schmidt et al., 2006b; Sinha et al., 2016; Syed et al., 2008; Tapley et al., 2004).

In recent years, the GRACE data has been widely used to assess the TWS variability (e.g., Güntner et al., 2007; Long et al., 2015; Schmidt et al., 2006a), to monitor droughts (e.g., Houborg et al., 2012; Thomas et al., 2014; Yi and Wen, 2016; Zhao et al., 2017) and flooding (e.g., Chen et al., 2010; Reager and Famiglietti, 2009a; Reager et al., 2014); it is also used to evaluate groundwater depletion (e.g., Long et al., 2016; Rodell et al., 2009; Thomas and Famiglietti, 2019), and to estimate ice sheet or glacier loss (e.g., Chen et al., 2009; Farinotti et al., 2015; Shepherd et al., 2018). These studies have demonstrated the capability of GRACE to observe regional hydrological variability and global climate abnormalities, which are used for investigated water cycles linked with global and regional climates. For investigating the GRACE long-term trend variability, Rodell et al. (2018) quantified the global TWS trends during 2002-2016 and provided their corresponding causes. They found a general wetting pattern at high- and low-latitudes and a drying pattern at mid-latitudes, and these patterns are mainly due to the regular natural variability, groundwater depletion, and climate change. Meanwhile, Scanlon et al. (2018) found the TWS in some mid-latitude basins were decreasing, including Arkansas, Indus, Ganges, Brahmaputra, Hai River, Euphrates. On the other hand, high- and low-latitude regions showed an increasing TWS trend including Missouri, Amazon, Okavango, and Murray basin.

The increasing water loss at mid-latitudes exerts great pressure on the water supply in mid-latitude countries, in particular populous China and India. The China-India border area (CIBA, Figure 1), covering the Qinghai-Tibet Plateau (QTP), and Indus-Ganges-Brahmaputra basin (IGBB), is shared by multiple nations, including China, India, Nepal, Bhutan, Bangladesh, and Pakistan. The Tibetan Plateau, known as the ‘third pole’ of the Earth (Yao et al., 2012), affects regional thermal gradients which modulate local circulations (Duan et al., 2018; Wu et al., 2014; Zhao and Chen, 2001). Therefore, exploring how local climate mechanisms affect the TWS variability over the CIBA can provide information to decision makers for managing water resources shared among multiple populous nations. Over the IGBB, there have been several studies focusing on the water storage variations over the IGBB (e.g., Khandu et al., 2016; Scanlon et al., 2018) and QTP regions (e.g., Song et al., 2015; Xiang et al., 2016; Zhang et al., 2017). Related to the glacial processes, sharp water mass losses were observed in the southeast QTP between 2003 and 2011 (Song et al., 2015). Moreover, the lake volume in QTP region increased from 1970s to 2015 (Zhang et al., 2017). Over the IGBB, the TWS declined rapidly due to decreasing precipitation during 2002-2014 (Khandu et al., 2016) and increasing irrigation (Scanlon et al., 2018). Overall, previous studies clearly showed the separate trend variations of TWS in QTP and IGBB. Although they attempted to explain the TWS variations using meteorological forcing (e.g. precipitation and temperature) and human influences (e.g. irrigation), the TWS variations over the IGBB can be associated with the water conditions over the QTP, since the headwaters of the Indus, Ganges and Brahmaputra rivers originate in the QTP region (Kuehl et al., 2011). Therefore, there is a need to investigate the TWS dynamic in the QTP and the IGBB as an integral system rather than individual separate components. Furthermore, the

TWS variations are not only directly controlled by the local precipitation and temperature, but also indirectly affected by regional atmospheric circulations and temperature gradients between land and ocean.

Over the IGBB, the spatiotemporal dynamic of the hydrological regime is mainly under the control of the Indian monsoon (IM) (Khandu et al., 2017). Over the IGBB from July to September, the IM contributes to around 60-90% of the annual precipitation (Khandu et al., 2016). Due to the complex climate types, (Figure 1b), the IGBB has unevenly distributed precipitation over the sub-basins. In the Ganges basin, the northwest region is dryer than the coast area; in the Brahmaputra basin, there is heavy precipitation because of the rain shadow effect (Mirza et al., 1998). The upper Indus basin receives more precipitation than the lower basin, especially in the mountain region (Archer et al., 2010). Furthermore, the formation and variation of the IM are closely related to the QTP heating (Feng and Hu, 2005; Molnar et al., 1993; Sato and Kimura, 2007), and the IM affects precipitation patterns and river distributions over the QTP (Yao et al., 2009). Therefore, the IM plays an crucial role in the water dynamics over the whole CIBA.

Apart from the influence of IM, the regional temperature gradient could be an indirect contributor to the hydrological variability over the IGBB region. For instance, Roxy et al. (2015) found that the decreasing land-sea thermal gradient weakens the summer monsoon circulation and leads to the rainfall variations in India, due to rapid Indian Ocean warming. Over the past decades, the regional temperature increase caused wetter conditions in central and northern QTP (Yang et al., 2014). Moreover, changing hydroclimatic extreme events over the QTP and IGBB region are suggested to be related to shifting atmospheric and hydrological patterns due to increasing global average temperatures (Wijngaard et al., 2017). In recent years, more frequent droughts occurred in central India (Mallya et al., 2016; Rajeevan and Bhate, 2009), Nepal (Baidya et al., 2008), and Bangladesh (Shahid, 2011), while the extreme precipitation events were increased over the most parts of the India (Roxy et al., 2017; Sen Roy and Balling, 2004). In the central QTP, grasslands were affected by flooding due to the expansion of the surrounding lakes since the early 2000s (Zhu et al., 2010).

Over the CIBA, the changes of precipitation driven by IM variability affect the TWS dynamic (e.g., Khandu et al., 2016; Papa et al., 2010; 2015). The relationships between the IM and the TWS over the CIBA were only discussed qualitatively in almost all previous studies, but few studies have quantified these relationships and analyzed their mechanisms associated with regional temperature gradients at a seasonal scale. In this study, a new IM variation index was proposed to explore how the TWS is related to atmospheric circulations and regional temperature gradients. Given the close interaction between the IM and the western North Pacific monsoon (WNPM) (e.g., Gu et al., 2010; Li and Hsu, 2018; Wang et al., 2001), the WNPM was also considered to be a possible contributor to the TWS shifting. Furthermore, the spatiotemporal variability of precipitation and the Palmer Drought Severity Index were also explored because the PDSI represents the soil moisture state which is a difference between precipitation and potential evapotranspiration.

Overall, the main objectives of this study are: (1) to evaluate spatio-temporal characteristics of TWS associated with the other meteorological patterns in CIBA (2) to quantify the relationships between the TWS variations and monsoons (i.e. the IM and the WNPM); (3) to identify the temperature drivers related to monsoons and TWS variations; and (4) to develop a framework for explaining the relationships of temperature, monsoons and the TWS.

This study was organized as follows. A summary of various data sets and data analysis approaches employed in this study were given in Section 2. The results were given in Section 3, and they are followed by the corresponding discussion in Section 4. In Section 5, the major findings and implications of shifting TWS over the CIBA were summarized.

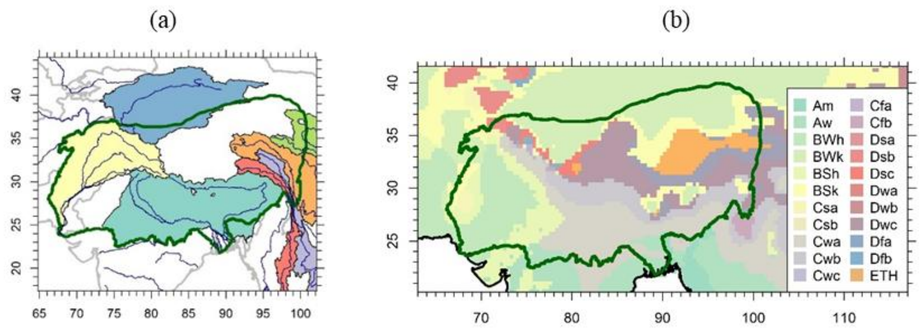

Figure 1. The general features (a) and Koppen climate types (b) of the CIBA. The yellow and cyan shaded areas are Indus Basin and Ganges-Brahmaputra Basin respectively in Figure 1a.

2 Materials and methods

2.1 Gravity Recovery and Climate Experiment (GRACE) data

The GRACE was designed to monitor the temporal and spatial variability of the Earth's gravity field. Using the algorithm of Wahr et al. (1998), the gravity field can be converted to the equivalent water height (EWH) for monitoring the TWS. In this study, we used GRACE Level-2 Release 06 (RL06) from the Center for Space Research (CSR; derived from ftp://isdcftp.gfz-potsdam.de/grace/Level-2/CSR/RL06/) at University of Texas to explore the spatiotemporal dynamics of TWS over the CIBA, in the form of Stokes spherical harmonic coefficients (SHCs) up to a degree and order of 60. The TWS grid data derived from GRACE spans from April 2002 to March 2017 (total 15 years), with a spatial resolution of 1 degree and a global coverage. For reducing the estimation errors of gravity anomalies, the pre-processing and post-processing procedures for GRACE data were applied, and these procedures include adding the degree-1 SHCs representing the geocenter motion (Swenson et al., 2008), replacing of the C_{20} term with the results from Satellite Laser Ranging (SLR) (Cheng and Ries, 2017), destripping, and applying the Gaussian filter with a radius of 350 km (Swenson and Wahr, 2006).

2.2 Meteorological data

For linking the TWS variation to precipitation pattern, the Tropical Rainfall Measuring Mission (TRMM) 3B43 version 7 was used in this study. This TRMM Multi-satellite Precipitation Analysis (TMPA) product were produced from assimilating data from multiple precipitation satellites, radiometers, and rain gauges by Huffman et al. (2007). The product was obtained from the NASA Goddard Space Flight Center (https://pmm.nasa.gov/data-access/downloads/trmm), with a time span ranging from 1998 to present, and a spatial coverage of 50°S-50°N with a resolution of 0.25 degree.

Apart from the TWS and precipitation data, drought indices are used for investigating the shift of hydrological conditions. In this study, the self-calibrating Palmer drought severity index (PDSI) (Wells et al., 2004) was used due to its better spatial comparability than traditional PDSI (Palmer, 1965), derived from the Research Data Archive at National Center for Atmospheric Research (NCAR) (https://rda.ucar.edu/datasets/ds299.0/) (Dai, 2017). The self-calibrating PDSI (hereafter just called PDSI for simplicity) data ranges from 1850 to 2014 with a monthly scale, covering the global land areas with a spatial resolution of 2.5 degree.

Other meteorological variables like the potential evaporation, snow melting and temperature also play important roles in the hydrological dynamics. These meteorological variables were derived from the ERA5-Land monthly averaged datasets (https://cds.climate.copernicus.eu/cdsapp#!/dataset/reanalysis-era5-land-monthly-means?tab=form), produced by the European Centre for Medium-Range Weather Forecasts (ECMWF). The ERA5 datasets covers the period from 2001 to present, with a high spatial resolution of 0.1×0.1°. In addition, the sea surface temperature (SST) data are derived form the extended reconstructed SST version 5 (ERSST.v5; https://www.esrl.noaa.gov/psd/data/gridded/data.noaa.ersst.v5.html) of the National Climate Data Centre (Huang et al., 2017).

2.3 Monsoon indices

The monsoon interaction zone of the IM and the WNPM is close to the edge of our study area (i.e., the CIBA) over the Indochina Peninsula (Wang and LinHo, 2002). In order to quantify the effect of IM on the TWS variability over the CIBA, the IM index was calculated, using the difference of zonal winds at 850-hPa between a southern region (5°-15°N, 40°-80°E) and a northern region (20°-30°N, 70°-90°E) (Wang et al., 2001). Based on the definition of Wang et al. (2001), the WNPM index was also calculated, using the difference of zonal winds at 850-hPa a southern region (5°-15°N, 100°-130°E) and a northern region (20°-30°N, 110°-140°E). The wind data for the calculation of IM and WNPM indices were extracted from the National Centers Environmental Prediction (NCEP) data (https://www.ncep.noaa.gov/).

2.4 Methodology

2.4.1 Moving standard deviation

Instead of using the conventional monsoon indices, we proposed to use the moving standard deviation of monsoon indices, to examine how the monsoon weakening affects the hydrological regimes over the CIBA. The moving standard deviation of a given monsoon time series can be calculated as:

$$S(t)=\sqrt{\frac{\sum_{i=t}^{t+M}\left(x(i)-\mu(t)\right)^2}{M-1}} \quad (1)$$

where $S(t)$ and $\mu(t)$ represent the standard deviation and average value of monsoon index *x* for the period from *t* to $t+M$ at time *t*, respectively. *M* is the size of moving window, which is chosen as 12 months in this study. The time series formed by these standard deviations is hereafter called the monsoon variation index in this study.

2.4.2 Local Indicators of Spatial Association (LISA)

The LISA was proposed to measure the local association between one observations and its neighboring observations (Anselin, 1995). The general LISA for an observation Z_i at location i can be expressed as

$$L_i = f\left(Z_i, Z_{J_i}\right) \quad (2)$$

where f is a function for association calculation, and the Z_{J_i} are the observations at the neighboring locations J_i of i. In this study, we used Moran's I (Moran, 1950) to be the calculation function. The LISA based on Moran's I for location i can be written as

$$I_i = \frac{(Z_i-\bar{Z})}{S_i^2}\sum_{j=1,j\neq i}^{n} w_{ij}\left(Z_j-\bar{Z}\right) \quad (3)$$

where

$$S_i^2 = \frac{\sum_{j=1,j\neq i}^{n} w_{ij}}{n-1} - \bar{Z}^2$$

where n is the total number of observations, Z_i and Z_j are the observations at location i and j; w_{ij} is the spatial weight between location i and j.

2.4.3 Singular spectral analysis

To capture the spatiotemporal characteristics of the precipitation, the singular spectral analysis (SSA) method was applied in this study. The SSA was introduced by Broomhead and King (1986), aiming at decomposing a time series into a sum of independent series identified as trend, periodic component, and noise (Hassani, 2007). The decomposition process of the SSA can be divided into two steps: embedding and singular value decomposition (SVD). Given a univariate time series $Y = (y_1, \ldots, y_N)$, the embedding procedure means transferring one dimensional Y into H-dimensional vectors $\boldsymbol{X} = (X_1, \ldots, X_H)$, where $X_i = (y_i, \ldots, y_K)^T, i = 1, \ldots, K = N - L + 1$. The parameter $2 \leq L \leq N$ is the window length, and its selection is very important for the SSA.

The covariance matrix $\boldsymbol{C}$ should be firstly derived from the trajectory matrix $\boldsymbol{X}$:

$$\boldsymbol{C} = \frac{\mathbf{1}}{K}\boldsymbol{X}^{\boldsymbol{T}}\boldsymbol{X} = \boldsymbol{E}\boldsymbol{\Lambda}\boldsymbol{E}^{\boldsymbol{T}} \quad (4)$$

where $\boldsymbol{\Lambda} = \mathrm{diag}(\lambda_1, \ldots, \lambda_d)$, a diagonal matrix, consists of the eigenvalues of the covariance matrix, and *d* is the rank of the $\boldsymbol{X}$. The matrix $\boldsymbol{E} = (\boldsymbol{e}_{\boldsymbol{1}}, \ldots, \boldsymbol{e}_{\boldsymbol{d}})$ includes corresponding eigenvectors.

Based on the SVD, the trajectory matrix X can be written as follows

$$\boldsymbol{X} = \boldsymbol{U}\sum\boldsymbol{V}^{\boldsymbol{T}} \quad (5)$$

where the columns of U and V are orthogonal, containing the left and right eigenvectors of X,$\sum$ is a diagonal matrix. Combined equation (1) and (2), the covariance matrix can be also denoted as

$$\boldsymbol{C} = \boldsymbol{U}(\sum^2/K)\boldsymbol{U}^{\boldsymbol{T}} \quad (6)$$

Thus $\boldsymbol{U} = (\boldsymbol{u_1}, \ldots, \boldsymbol{u_d}) = \boldsymbol{E} = (\boldsymbol{e_1}, \ldots, \boldsymbol{e_d})$, $\sum = \sqrt{K}\boldsymbol{\Lambda}^{1/2} = diag\left(\sqrt{K\lambda_1}, \ldots, \sqrt{K\lambda_d}\right)$, and $\boldsymbol{V} = (\boldsymbol{v_1}, \ldots, \boldsymbol{v_d})$ can also be easily obtained based on the equation (2). The $\boldsymbol{u}_i$ and $\boldsymbol{v}_i$ are called temporal empirical orthogonal functions (EOFs) and principal components (PCs), respectively.

In addition, the SVD of the trajectory matrix can be also written as

$$\boldsymbol{X} = \boldsymbol{X}_1 + \cdots + \boldsymbol{X}_d \quad (7)$$

where $\boldsymbol{X}_i = \sqrt{K\lambda_i}\boldsymbol{u}_i\boldsymbol{v}_i^T (i = 1, \ldots, d)$, are elementary matrices.

3 Results

3.1 The water shifting characteristics

Hovmöller diagrams (Hovmöller, 1949) were plotted to investigate the TWS spatiotemporal dynamic over the CIBA (66°E-101°E, 21°N-40°N) between 2002 and 2017. According to the temporal variances of TWS along longitude and latitude, seasonal clusters were found along both longitude and latitude. Moreover, TWS showed an increasing trend over 80°E-90°E (the Chinese side) but a decreasing trend between 75°E and 80°E (the Indian side) (Figure 2a). In terms of latitude, the shift of TWS was even clearer. Figure 2b shows a decreasing trend between 28°N and 32°N and an increasing trend over 32°N-38°N. In order to get more apparent trend pattern, the Hovmöller diagram of seasonal TWS anomalies was shown in Figure 2c. It displays a distinctive increasing trend between 32°N and 38°N and a decreasing trend between 28°N and 32°N. The dividing line between increasing and decreasing trends was around the 32°N latitude.

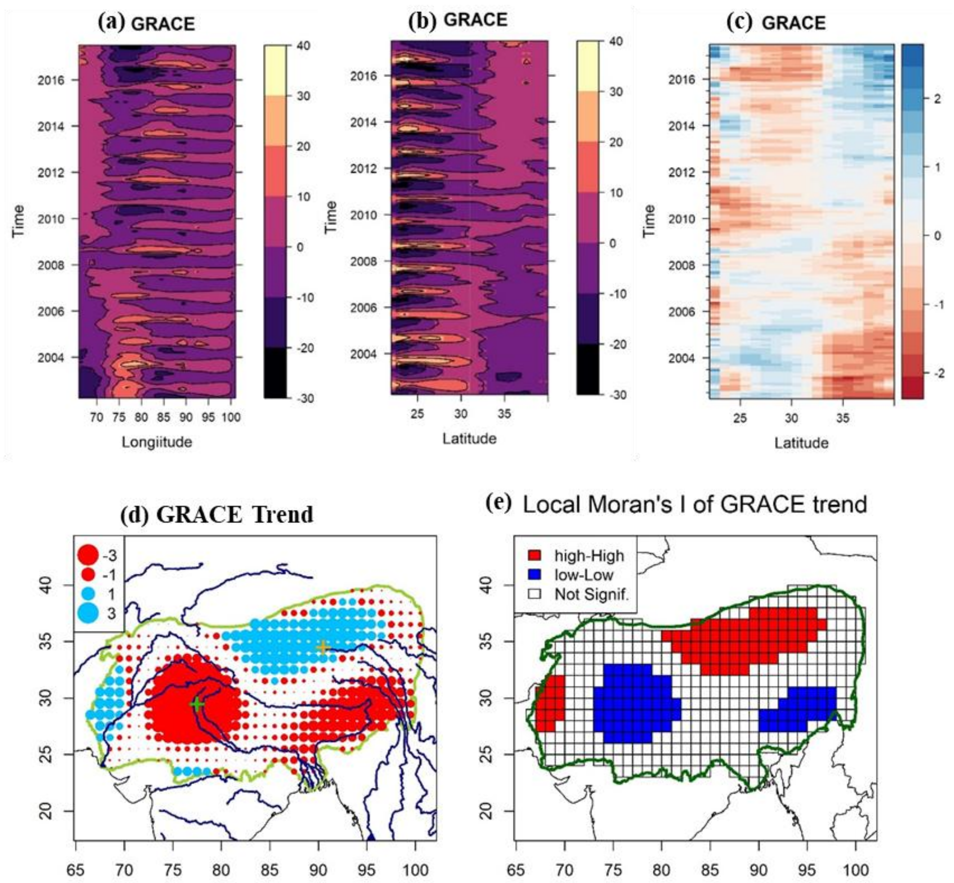

Figure 2. Hovmöller diagrams of TWS (mm) along longitude (a) and latitude (b), and the seasonal anomalies along latitude (c) over the CIBA region. Spatial trend distribution of the TWS (d) and corresponding local Moran's I distribution (e) over the CIBA. The blue and red circles represent the increasing and decreasing trend, respectively. The orange and green crosses are the locations in western China and northwestern India, respectively. The red and blue in (e) represent the high-high hotspots and low-low hotspots respectively.

According to Figure 2a-c, the temporal TWS variances had clear spatial shifts over the CIBA. Moreover, the spatial trend distribution of TWS and its LISA map displayed three clusters (also called hot spots); two of them represented decreasing trend, and one was increasing trend (Figure 2d-e). The increasing hot spot was located at the region of 80°E-95°E, 32°N-37°N (i.e., western China), while decreasing hot spots covered the regions of 72°E-82°E, 26°N-32°N (northwestern India) and 85°E-100°E, 25°N-31°N (Bangladesh, Figure 2d-e). The spatial trend pattern of TWS was consistent with the Hovmöller diagrams of TWS (Figure 2a-c), indicating there was a TWS shifting over the CIBA during 2002-2017.

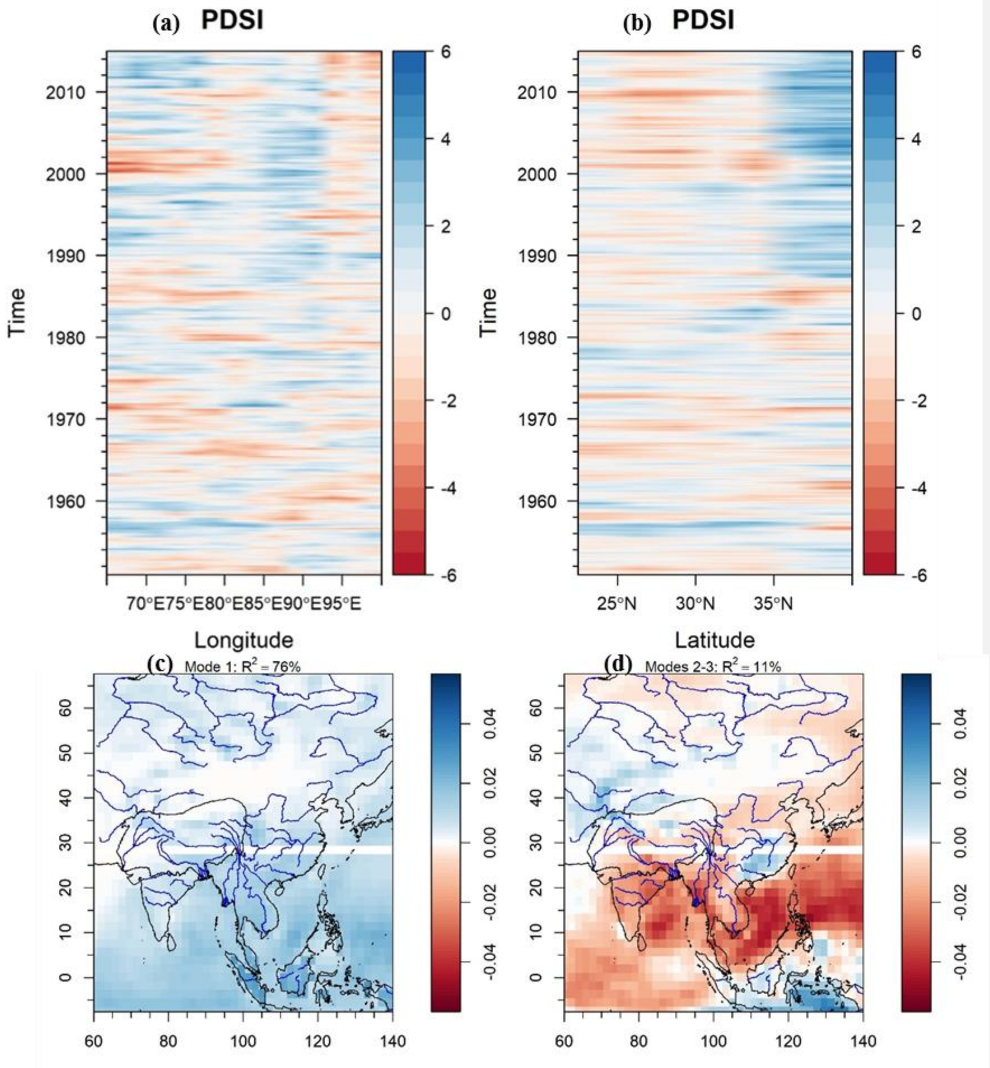

Figure 3. Hovmöller diagrams of PDSI along longitude (a) and latitude (b) over the GBB. The mode 1 (c) and combination of mode 2 and mode 3 (d) of TRMM precipitation based on the SSA.

Apart from the TWS, the Hovmöller diagrams of TRMM derived-precipitation and PDSI were shown in Figure 3. The Hovmöller diagrams of PDSI showed that central QTP (87°E-92°E, 35°N-40°N) has been wetting (blue regions in the diagrams) since the late 1980s (Figures 3a-b). After 2000, the northwestern India (26°N-32°N) has been drying (red regions in the diagram; Figure 3b). For precipitation, its seasonal signals are very strong, which can mask the trend signals, leading to unclear precipitation shifting pattern in the precipitation Hovmöller diagrams (not shown in this paper). Therefore, we used SSA method to separate the seasonal and trend signals (Figure 3c-d). The precipitation mode 1 represented the seasonal signal, which accounts for 76% of the total variances. It explains 7 times of the variance explained by the combination of mode 2 and mode 3 (hereafter called mode 2-3). The mode 2-3 accounts for 11% of the total precipitation variances, representing the secular trend variances. It showed similar pattern with the spatial TWS trend distribution, suggesting an increasing trend in western China and decreasing trend in other regions of the GBB (Figure 3d).

In addition, the potential evaporation distribution in Figure S1a showed a drying-wetting trend pattern which is similar with that of the TWS. Changing TWS over the IGBB during 2002-2017 can be directly caused by a more precipitation (and less evaporation) trend over the central QTP and a precipitation decline (and strengthened evaporation) over the IGBB (Figure 3d and Figure S1a). Similarly, Figure S1b showed sharp declines of snow depths during 2002-2017 over the northwest and the southeast corners of the QTP. These downward trends corresponded well with the rising temperatures (Figure S1c). With the rising of the local temperatures, a reducing snow depth trend (i.e., more snow melting) during 2002-2017 can be linked to increasing downstream surface waters such as the expansion of lakes in the central QTP (Zhang et al., 2017). Therefore, for the QTP region, the snow melting could be another important contributor to the TWS variations.

In summary, the TWS water shifting pattern over the CIBA is wetting for the western China and drying for the northwestern India. This shifting pattern could be directly affected by precipitation, potential evaporation and snow melting, which are mainly driven by the Asian monsoons modulated by regional temperature gradients. Therefore, the impacts of Asian monsoons, including IM and WNPM, on the water shifting since 2002 were investigated in next section.

3.2 Monsoon as a driving mechanism behind the TWS shifting

The summer IM index (for the months of JJA) had a decreasing trend, whereas the winter IM index (for the months of DJF) had an increasing trend (Figure 4a). However, for the monsoon intensity, the IM was weakening in both summer and winter. Although it is less clear, the WNPM index showed similar weakening trend. The weakening of the IM and WNPM could be the underlying drivers of water shifting over the CIBA. To quantify this weakening effect, IM and WNPM variation (hereafter called IMV and WNPMV) index were proposed based on the moving standard deviation of the IM and WNPM index, showing the both IM and WNPM strength were decreasing during 2002 and 2017 (Figure 4c-d). Particularly, the IMV index fell abruptly since 2010.

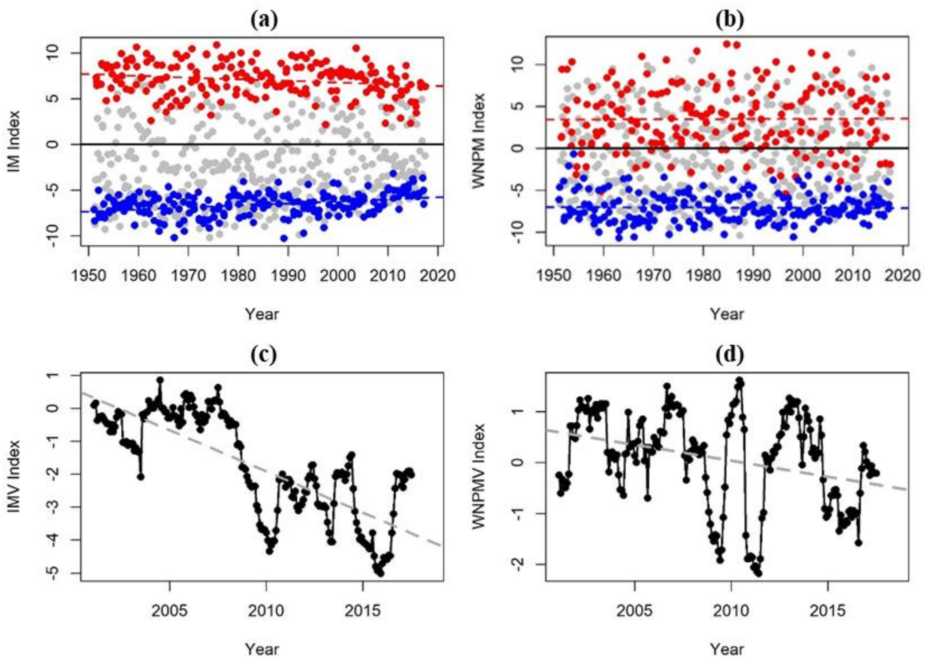

Figure 4. The monthly values of IM and WNPM indices during 1950-2017 (a-b) and the corresponding IMV and WNPMV indices during 2002-2017 (c-d). The red dots are the boreal summer (JJA) data and the blue dots are the winter (DJF) data in Figure 4a and 4b.

For investigating the relationships between IM (and WNPM) and TWS over the CIBA, two TWS time series located in western China and northwestern India (orange and green cross respectively in Figure 2d) were extracted. There were no significant relationships between IM (and WNPM) and TWS in both the western China and northwestern India (Figure S2). However, a significant negative trend for the western China and a significant positive trend for the northwestern India between the IMV (and WNPMV) index and TWS were shown in Figure 5a-d. The results revealed that the weakening IM and WNPM could lead to an increasing TWS trend in western China and a decreasing trend in northwestern India. Moreover, the LISA map of the partial correlation of the IMV and TWS shared the similar pattern with that of the WNPMV, showing significant negative and positive spatial clusters in western China and northwestern India, respectively (Figure 5e-f), which was consistent with the TWS trend patterns. Therefore, Figure 5a-f demonstrated that the TWS shifting over the whole CIBA results from the weakening of the Asian monsoons. Additionally, for the above-mentioned precipitation mode 2-3, representing the spatial precipitation trend pattern, its temporal variation (hereafter called mode strength) was consistent with the IMV and WNPMV step change (Figures S3), indicating that the precipitation redistribution over the GBB was attributed to the IMV and WNPMV.

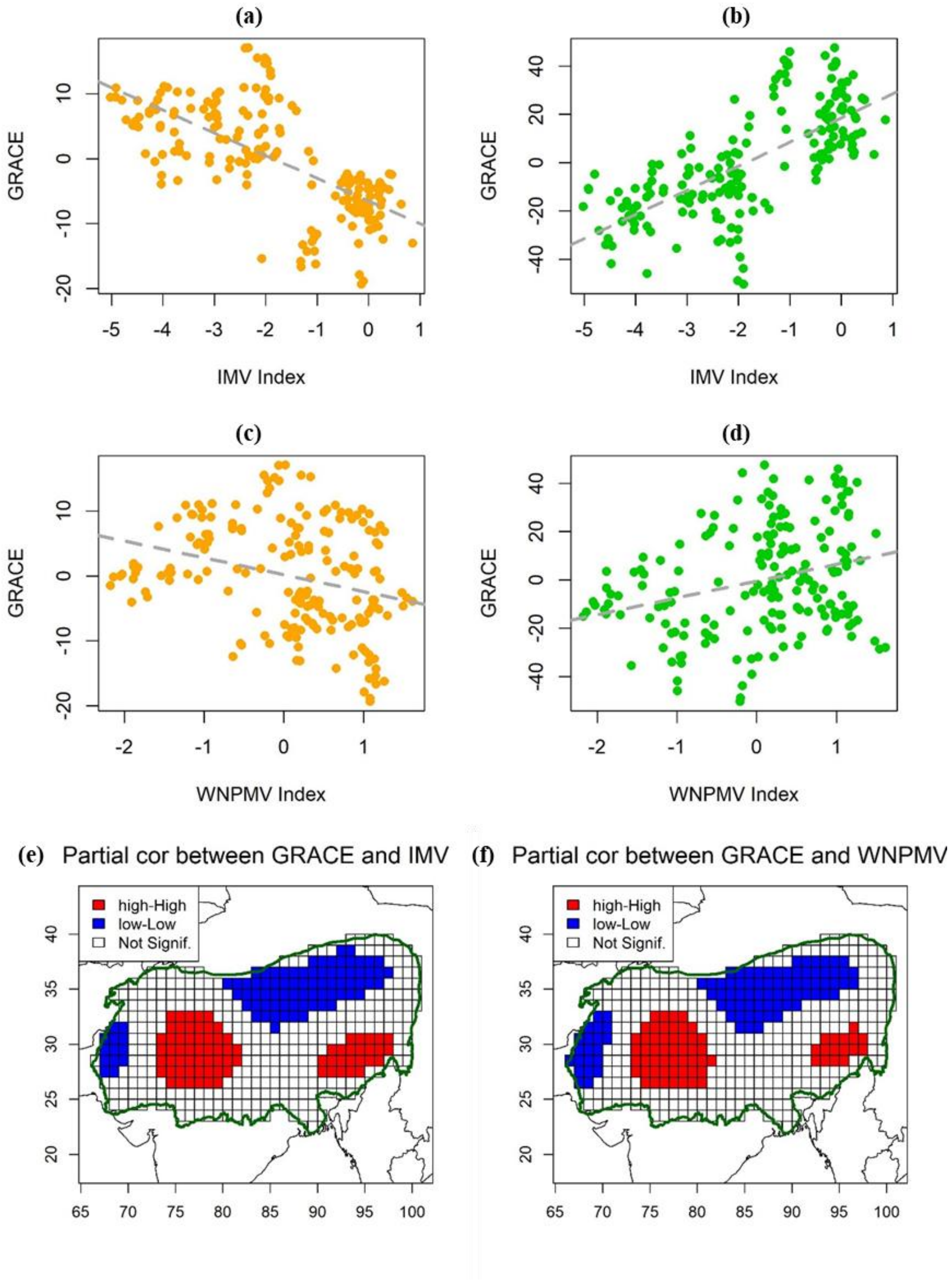
(a)
(b)
GRACE
IMV Index
(c)
(d)
WNPMV Index
(e) Partial cor between GRACE and IMV
(f) Partial cor between GRACE and WNPMV
high-High
low-Low
Not Signif.

377

Figure 5. IMV and WNPMV against the TWS over the China (a, c) and India region (b, d). The LISA map of partial correlation between TWS and IMV (e), and WNPMV (f) over the CIBA.

3.3 Temperature drivers behind monsoons and TWS

The above results showed that the TWS shifting over the CIBA was caused by the weakening of the IMV and WNPMV through modulating the precipitation distribution. The IM and WNPM variability have been showed to be related to the sea surface temperature (SST) (e.g., Annamalai et al., 2005; Weare, 1979; Xu et al., 2019), the temperature of the QTP (e.g., Boos and Kuang, 2010; Zhao and Chen, 2001; Zhisheng et al., 2015), and the land-ocean thermal difference (e.g., Roxy et al., 2015; Tao et al., 2016; Yang et al., 2007). Therefore, to explore the relationship between monsoons and surface temperatures, the average temperature over three regions located in the Indian Ocean (hereafter called Region A), the Ganges (hereafter called Region B) and the Brahmaputra (hereafter called Region C) were extracted (Figure S4).

The Figure 6 showed the relationships between mean annual temperature in different regions and monsoon indices for 70 years. Both the IM and WNPM indices were not related to the mean SST of Region A (Figure 6a and 6c), while the IMV and WNPMV fitted well with negative and positive relationship for the SST, respectively (Figure 6b and 6d). Moreover, negative relationships between the IMV and the near surface air temperature (NSAT) were found in all regions (Figure 6e-g). For the

WNPMV, it showed a positive relation with the NSAT at Region A, but negatively correlated with the NASTs at Region B and Region C (Figure 6h-j). These outcomes showed that the local and ocean temperature can modulate the monsoon variations. The negative relationships between temperatures and the IMV at three regions revealed that rising regional air temperatures and SST caused by increasing global temperatures may be the driver of the IM weakening. In addition, the IMV had a positively weak but statistically significant relationship with the thermal difference between Region A and Region C, while the WNPMV showed no significant relationship with the land-ocean thermal difference (Figures 6k-l), because it was more likely related to the thermal difference between the Asian land surface and the tropical Pacific Ocean based on its definition (Li and Hsu, 2018). Therefore, the land-Indian Ocean thermal difference may play a weak role for changing monsoons and thus the TWS spatial patterns.

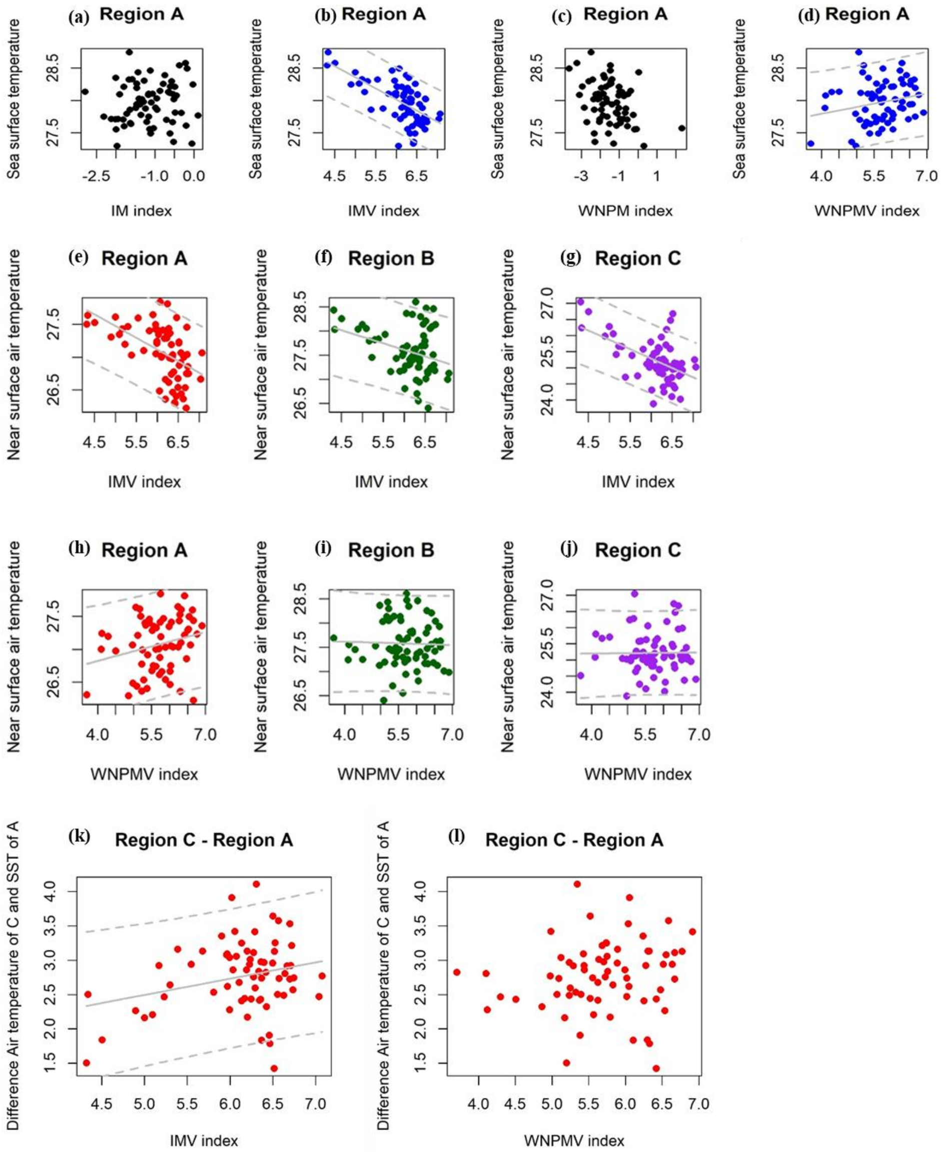

Figure 6. IM, IMV, WNPM and WNPMV index against the SST in Region A (a-d); IMV and WNPMV index against the NSAT in Region A, Region B and Region C (e-j); IMV and WNPMV index against the air temperature difference between Region A and Region C (k-l).

4 Discussion

The TWS trend pattern and the Hovmöller diagrams clearly showed the spatial clusters over the CIBA. There were (1) a significant decreasing cluster over the upper Indus and Ganges (i.e., northwestern India), (2) an increasing cluster over the central QTP (i.e., western China) and (3) a decreasing cluster over the southeastern Brahmaputra basin (i.e., Bangladesh). In addition to decreasing precipitation and increasing potential evaporation, the TWS decline in the IGBB was also probably attributed to the over-exploitation of underground water for water supply in agriculture and industrial sectors in northern India and Bangladesh (Rodell et al., 2009; Shamsudduha et al., 2012). Given the TWS decline and population increase, the IGBB region has now been facing severe water scarcity (Babel and Wahid, 2009), and the situation will become more serious if no measure is taken.

Apart from the anthropogenic effect, the monsoon variability is a main natural driver to the TWS shifting over the CIBA. Based on the monsoon variation analysis, the weakening of the IMV and WNPMV were significant contributors to the increasing TWS over the western China and the decreasing TWS over the northwestern India. During winter (Figures 7a and 7c), less strong dry monsoon winds come from the Himalaya over the Qinghai-Tibet Plateau; during summer (Figures 7b and 7d), weak monsoons would bring less moist winds from the Arabian Sea to India. Weaker and less moist winds would lead to drying windward side and wetting leeward side of the Himalaya, and thus an increasing TWS over the western China and a decreasing TWS over the northwestern India.

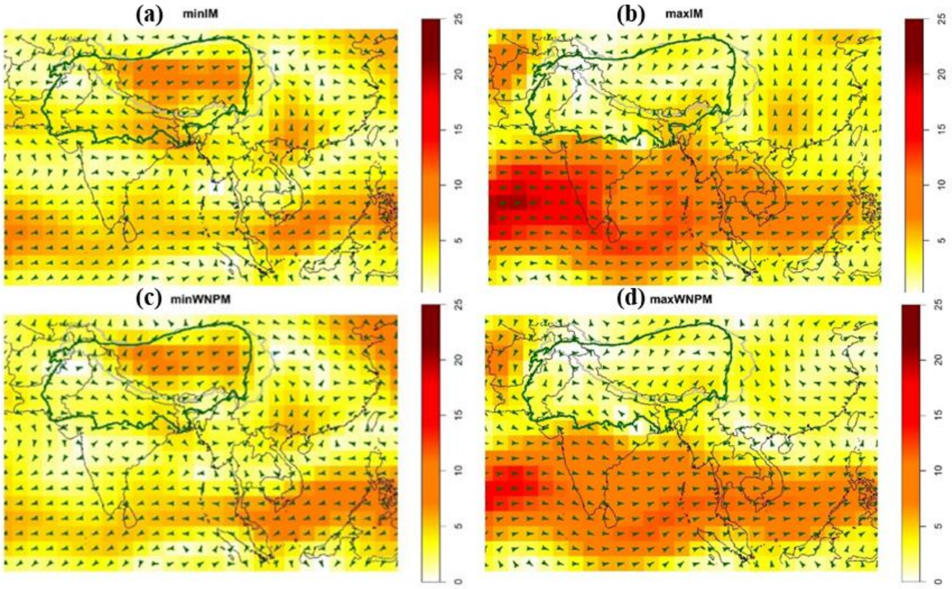

Figure 7. The average wind field of the lowest and highest 10% IM index (a-b), representing the winter monsoons and summer monsoons, respectively. (c-d) are same as (a-b) but for the WNPM.

According to the Figures 8a-b, the Indian Ocean (Region A) had a clear temperature increasing in both summer and winter. This temperature change led to the weakening of the IM, based on the negative relationship between IMV and SST in Region A (Figure 6b). The temperature over the Region B showed no obvious trend in both summer and winter (Figures 8c-d). The QTP (Region C) showed an increasing temperature trend in winter (Figure 8e), but no obvious trend in summer (Figure 8f). The increasing trends of temperature over the Indian Ocean were larger than that over the QTP in both winter and summer, indicating that the thermal difference between the Indian Ocean and QTP was decreasing, leading to the decrease in the IM intensity based on the positive relationship between IMV and temperature difference shown in the Figure 6k. For the WNPMV, the increasing temperature over the Region A indicated the strengthening of the WNPMV based on the positive relationship between WNPMV and SST over Region A (Figure 6d). However, this result is not consistent with the WNPMV weakening. This inconsistency can be explained by the complex interactions between the Indian Ocean and the Pacific Ocean, and the WNPM is less important for the CIBA, compared to the IM (Luo et al., 2010; 2012).

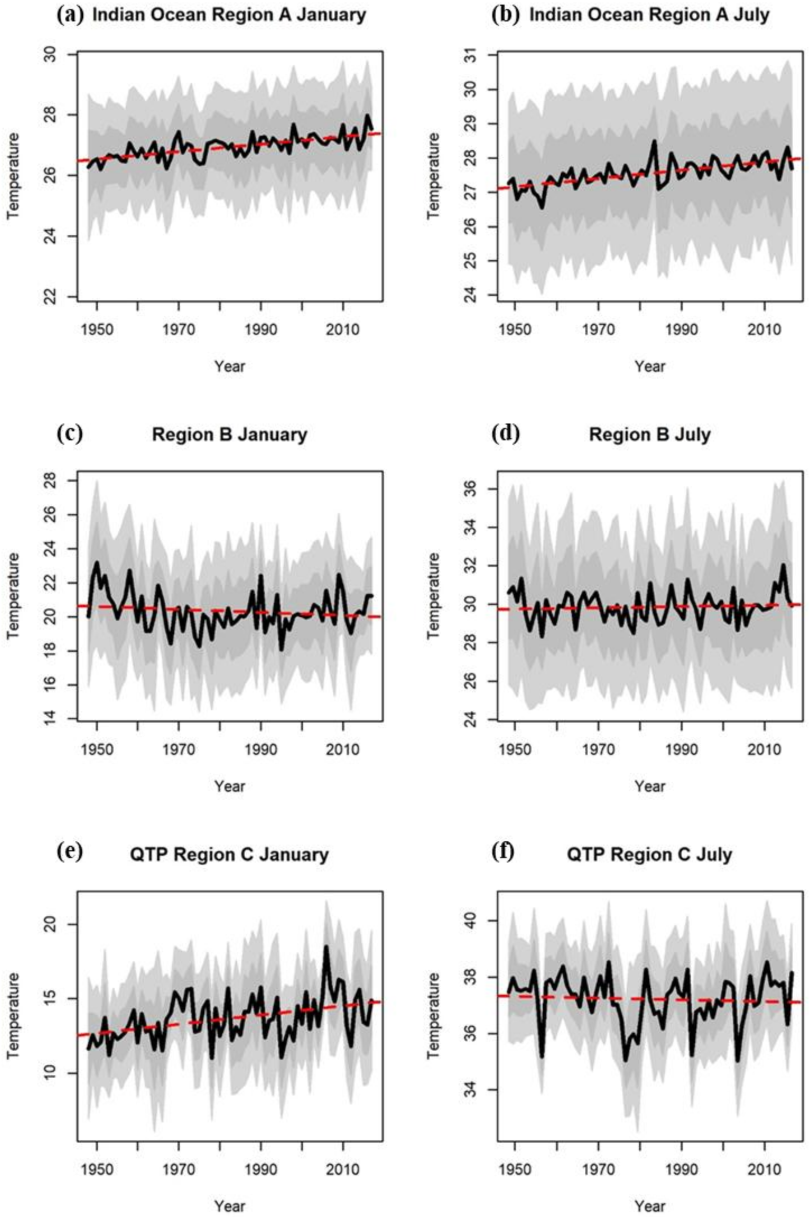

Figure 8. The average temperature variation over time in winter (January) and summer (July) over the Region A (a-b), Region B (c-d) and Region C (e-f).

5 Conclusion

In this study, we use the Hovmöller diagrams, the spatial TWS trend patterns and their LISA maps to show that the TWS over the western China part was increasing and the TWS over the northwestern India part was decreasing. The precipitation and potential evaporation showed similar drying and wetting patterns with the TWS, and snow melting due to the rising temperature can be an important contributor to the TWS increase over western China (i.e., central QTP). The water shifting pattern between 2002 and 2017 over the CIBA were controlled by the changing Asian monsoon (i.e., IM and WNPM) and local temperature through the modulation of precipitation, evaporation and snow melting.

The intensity of both IM and WNPM showed a gentle decreasing trend during 1950-2017. Furthermore, in order to emphasize the monsoon variation, IMV and WNPMV were calculated based on the traditional monsoon indices, revealing that the monsoon decreased dramatically during 2002-2017. In addition, the TWS over the drying region (i.e., northwestern India) was positively correlated with IMV (and WNPM), whereas the relationship between the TWS over the wetting zone (i.e., western China) and IMV (and WNPMV) was negative. This result suggested that the weakening of the IM led to the decreasing and increasing trends of TWS over two different regions of the CIBA. Moreover, similar clusters on the LISA maps further show that the weakening monsoons caused the TWS redistribution over the CIBA.

Finally, the ocean and continental temperature difference changes modulated the IM and WNPM variability, and they led to the TWS shifting over the CIBA. The temperatures over the QTP, the Ganges, and the Indian Ocean were negatively correlated with the IMV, indicating that increasing local temperatures weakened the IM, and thus affecting the TWS shifting. Meanwhile, the decrease in the thermal difference between the QTP and the Indian Ocean can also explain the weakening of the IM because of their positive relationship.

In this study, we looked at monsoon roles for changing TWS. Although the Glacial Isostatic Adjustment (GIA) were applied to the TWS data, the glacier effect can be important for explaining the observed TWS shifts. The observed drying center at the headwater of the Ganges can be related to the Gangotri glacier which is one of the largest glaciers in the Himalayas. The Gangotri glacier has been retreating at a significant rate between 22 and 27 m/year (Bhambri et al., 2011; Jain, 2008). The glacier retreat could be another explanation of decreasing TWS over the Ganges due to the temperature changes.

In summary, our findings have linked spatial water shifting over the CIBA to monsoon variations and changing local or even global temperature gradients. The main limitation of the study is whether the detected TWS shifting will last after 2017. For future studies, it will be worthwhile to project future TWS distributions using the temperature gradients derived from climate model outputs based on different Representative Concentration Pathways (RCPs). Then, these projected water conditions can help decision-makers to propose water management designs, including (1) establishing water consumption quotas for regions having declining TWS and (2) setting up flood control measures for places having increasing TWS. Therefore, the dynamic relationships between temperature gradient, TWS and monsoons in this study is not only building blocks for exploring the mechanisms of shifting hydroclimatic systems, but also providing new insights for future water management designs to the region.

Acknowledgments

This research was funded by the Hong Kong Baptist University Faculty research Fund (FRG1/1617/005, FRG2/1617/082, FRG2/1516/085), ~~and~~ the National Natural Science Foundation of China (NSFC) (Grant No. 41974003, 41674007), and The Scientific and Technological Research Council of Turkey (TUBITAK) 2232 grant (118C329). This research was conducted using the resources of the High Performance Cluster Computing Centre, Hong Kong Baptist University, which receives funding from Research Grant Council, University Grant Committee of the HKSAR and Hong Kong Baptist University. The datasets used in this study are publicly available, and the corresponding URLs are provided in the section 2.

References:

Alsdorf DE, Rodriguez E, Lettenmaier DP. Measuring surface water from space. Reviews of Geophysics 2007; 45.

Annamalai H, Liu P, Xie S-P. Southwest Indian Ocean SST Variability: Its Local Effect and Remote Influence on Asian Monsoons. Journal of Climate 2005; 18: 4150-4167.

Anselin L. Local Indicators of Spatial Association—LISA. Geographical Analysis 1995; 27: 93-115.

Archer DR, Forsythe N, Fowler HJ, Shah SM. Sustainability of water resources management in the Indus Basin under changing climatic and socio economic conditions. Hydrol. Earth Syst. Sci. 2010; 14: 1669-1680.

Babel MS, Wahid SM. Freshwater Under Threat South Asia: Vulnerability Assessment of Freshwater Resources to Environmental Change: Ganges-Brahmaputra-Meghna River Basin, Helmand River Basin, Indus River Basin: UNEP, 2009.

Baidya SK, Shrestha ML, Sheikh MM. Trends in daily climatic extremes of temperature and precipitation in Nepal. Journal of Hydrology and Meteorology 2008; 5: 38-51.

Bhambri R, Bolch T, Chaujar RK, Kulshreshtha SC. Glacier changes in the Garhwal Himalaya, India, from 1968 to 2006 based on remote sensing. Journal of Glaciology 2011; 57: 543-556.

Boos WR, Kuang Z. Dominant control of the South Asian monsoon by orographic insulation versus plateau heating. Nature 2010; 463: 218-22.

Broomhead DS, King GP. Extracting qualitative dynamics from experimental data. Physica D: Nonlinear Phenomena 1986; 20: 217-236.

Chen JL, Wilson CR, Blankenship D, Tapley BD. Accelerated Antarctic ice loss from satellite gravity measurements. Nature Geoscience 2009; 2: 859.

Chen JL, Wilson CR, Tapley BD. The 2009 exceptional Amazon flood and interannual terrestrial water storage change observed by GRACE. Water Resources Research 2010; 46.

Cheng M, Ries J. The unexpected signal in GRACE estimates of $$C_{20}$$C20. Journal of Geodesy 2017; 91: 897-914.

Dai A. Dai Global Palmer Drought Severity Index (PDSI). Research Data Archive at the National Center for Atmospheric Research, Computational and Information Systems Laboratory, Boulder, CO, 2017.

Duan A, Liu S, Zhao Y, Gao K, Hu W. Atmospheric heat source/sink dataset over the Tibetan Plateau based on satellite and routine meteorological observations. Big Earth Data 2018; 2: 179-189.

Farinotti D, Longuevergne L, Moholdt G, Duethmann D, Mölg T, Bolch T, et al. Substantial glacier mass loss in the Tien Shan over the past 50 years. Nature Geoscience 2015; 8: 716.

Feng S, Hu Q. Regulation of Tibetan Plateau heating on variation of Indian summer monsoon in the last two millennia. Geophysical Research Letters 2005; 32.

Gu D, Li T, Ji Z, Zheng B. On the Phase Relations between the Western North Pacific, Indian, and Australian Monsoons. Journal of Climate 2010; 23: 5572-5589.

Güntner A, Stuck J, Werth S, Döll P, Verzano K, Merz B. A global analysis of temporal and spatial variations in continental water storage. Water Resources Research 2007; 43.

Hassani H. Singular Spectrum Analysis: Methodology and Comparison. University Library of Munich, Germany, 2007.

Houborg R, Rodell M, Li B, Reichle R, Zaitchik BF. Drought indicators based on model- assimilated Gravity Recovery and Climate Experiment (GRACE) terrestrial water storage observations. Water Resources Research 2012; 48.

Hovmöller E. The Trough-and-Ridge diagram. Tellus 1949; 1: 62-66.

Huang B, Thorne PW, Banzon VF, Boyer T, Chepurin G, Lawrimore JH, et al. Extended Reconstructed Sea Surface Temperature, Version 5 (ERSSTv5): Upgrades, Validations, and Intercomparisons. Journal of Climate 2017; 30: 8179-8205.

Huffman GJ, Bolvin DT, Nelkin EJ, Wolff DB, Adler RF, Gu G, et al. The TRMM Multisatellite Precipitation Analysis (TMPA): Quasi-Global, Multiyear, Combined-Sensor Precipitation Estimates at Fine Scales. Journal of Hydrometeorology 2007; 8: 38-55.

Humphrey V, Gudmundsson L, Seneviratne SI. Assessing Global Water Storage Variability from GRACE: Trends, Seasonal Cycle, Subseasonal Anomalies and Extremes. Surveys in Geophysics 2016; 37: 357-395.

Jain SK. Impact of retreat of Gangotri glacier on the flow of Ganga River. Current Science 2008; 95: 1012-1014.

Khandu, Awange JL, Anyah R, Kuhn M, Fukuda Y. Assessing regional climate simulations of the last 30 years (1982–2012) over Ganges–Brahmaputra–Meghna River Basin. Climate Dynamics 2017; 49: 2329-2350.

Khandu, Forootan E, Schumacher M, Awange JL, Müller Schmied H. Exploring the influence of precipitation extremes and human water use on total water storage (TWS) changes in the Ganges-Brahmaputra-Meghna River Basin. Water Resources Research 2016; 52: 2240-2258.

Kim H, Yeh PJ-F, Oki T, Kanae S. Role of rivers in the seasonal variations of terrestrial water storage over global basins. Geophysical Research Letters 2009; 36.

Kuehl SA, Allison MA, Goodbred SL, Kudrass H. The Ganges–Brahmaputra Delta. 2011: 413-434.

Li T, Hsu P-c. Monsoon Dynamics and Its Interactions with Ocean. Fundamentals of Tropical Climate Dynamics. Springer International Publishing, Cham, 2018, pp. 185-229.

Long D, Chen X, Scanlon BR, Wada Y, Hong Y, Singh VP, et al. Have GRACE satellites overestimated groundwater depletion in the Northwest India Aquifer? Scientific Reports 2016; 6: 24398.

Long D, Longuevergne L, Scanlon BR. Global analysis of approaches for deriving total water storage changes from GRACE satellites. Water Resources Research 2015; 51: 2574-2594.

Long D, Pan Y, Zhou J, Chen Y, Hou X, Hong Y, et al. Global analysis of spatiotemporal variability in merged total water storage changes using multiple GRACE products and global hydrological models. Remote Sensing of Environment 2017; 192: 198-216.

Luo J-J, Zhang R, Behera SK, Masumoto Y, Jin F-F, Lukas R, et al. Interaction between El Niño and Extreme Indian Ocean Dipole. Journal of Climate 2010; 23: 726-742.

Luo JJ, Sasaki W, Masumoto Y. Indian Ocean warming modulates Pacific climate change. Proc Natl Acad Sci U S A 2012; 109: 18701-6.

Mallya G, Mishra V, Niyogi D, Tripathi S, Govindaraju RS. Trends and variability of droughts over the Indian monsoon region. Weather and Climate Extremes 2016; 12: 43-68.

Mirza MQ, Warrick RA, Ericksen NJ, Kenny GJ. Trends and persistence in precipitation in the Ganges, Brahmaputra and Meghna river basins. Hydrological Sciences Journal 1998; 43: 845-858.

Molnar P, England P, Martinod J. Mantle dynamics, uplift of the Tibetan Plateau, and the Indian Monsoon. Reviews of Geophysics 1993; 31: 357-396.

Moran PAP. Notes on Continuous Stochastic Phenomena. Biometrika 1950; 37: 17-23.

Palmer WC. Meteorological drought (Vol. 30). Washington, DC, USA: US Department of Commerce. Weather Bureau 1965.

Papa F, Durand F, Rossow WB, Rahman A, Bala SK. Satellite altimeter-derived monthly discharge of the Ganga-Brahmaputra River and its seasonal to interannual variations from 1993 to 2008. Journal of Geophysical Research: Oceans 2010; 115.

Papa F, Frappart F, Malbeteau Y, Shamsudduha M, Vuruputur V, Sekhar M, et al. Satellite-derived surface and sub-surface water storage in the Ganges–Brahmaputra River Basin. Journal of Hydrology: Regional Studies 2015; 4: 15-35.

Rajeevan M, Bhate J. A high resolution daily gridded rainfall dataset (1971–2005) for mesoscale meteorological studies. Current Science 2009; 96: 558-562.

Reager JT, Famiglietti JS. Global terrestrial water storage capacity and flood potential using GRACE. Geophysical Research Letters 2009a; 36.

Reager JT, Famiglietti JS. Global terrestrial water storage capacity and flood potential using GRACE. Geophysical Research Letters 2009b; 36: L23402.

Reager JT, Thomas BF, Famiglietti JS. River basin flood potential inferred using GRACE gravity observations at several months lead time. Nature Geoscience 2014; 7: 588.

Rodell M, Famiglietti J, Wiese D, Reager J, Beaudoing H, Landerer FW, et al. Emerging trends in global freshwater availability. Nature 2018; 557: 651.

Rodell M, Velicogna I, Famiglietti JS. Satellite-based estimates of groundwater depletion in India. Nature 2009; 460: 999.

Roxy MK, Ghosh S, Pathak A, Athulya R, Mujumdar M, Murtugudde R, et al. A threefold rise in widespread extreme rain events over central India. Nature Communications 2017; 8: 708.

Roxy MK, Ritika K, Terray P, Murtugudde R, Ashok K, Goswami BN. Drying of Indian subcontinent by rapid Indian Ocean warming and a weakening land-sea thermal gradient. Nat Commun 2015; 6: 7423.

Sato T, Kimura F. How Does the Tibetan Plateau Affect the Transition of Indian Monsoon Rainfall? Monthly Weather Review 2007; 135: 2006-2015.

Scanlon BR, Zhang Z, Rateb A, Sun A, Wiese D, Save H, et al. Tracking Seasonal Fluctuations in Land Water Storage Using Global Models and GRACE Satellites. Geophysical Research Letters 2019; 46: 5254-5264.

Scanlon BR, Zhang Z, Save H, Sun AY, Schmied HM, van Beek LP, et al. Global models underestimate large decadal declining and rising water storage trends relative to GRACE satellite data. Proceedings of the National Academy of Sciences 2018; 115: E1080-E1089.

Schmidt R, Schwintzer P, Flechtner F, Reigber C, Güntner A, Döll P, et al. GRACE observations of changes in continental water storage. Global and Planetary Change 2006a; 50: 112-126.

Schmidt R, Schwintzer P, Flechtner F, Reigber C, Güntner A, Döll P, et al. GRACE observations of changes in continental water storage. Global and Planetary Change 2006b; 50: 112-126.

Sen Roy S, Balling RC. Trends in extreme daily precipitation indices in India. International Journal of Climatology 2004; 24: 457-466.

Shahid S. Trends in extreme rainfall events of Bangladesh. Theoretical and Applied Climatology 2011; 104: 489-499.

Shamsudduha M, Taylor RG, Longuevergne L. Monitoring groundwater storage changes in the highly seasonal humid tropics: Validation of GRACE measurements in the Bengal Basin. Water Resources Research 2012; 48.

Shepherd A, Ivins E, Rignot E, Smith B, van den Broeke M, Velicogna I, et al. Mass balance of the Antarctic Ice Sheet from 1992 to 2017. Nature 2018; 558: 219-222.

Sinha D, Syed TH, Famiglietti JS, Reager JT, Thomas RC. Characterizing Drought in India Using GRACE Observations of Terrestrial Water Storage Deficit. Journal of Hydrometeorology 2016; 18: 381-396.

Song C, Ke L, Huang B, Richards KS. Can mountain glacier melting explains the GRACE-observed mass loss in the southeast Tibetan Plateau: From a climate perspective? Global and Planetary Change 2015; 124: 1-9.

Swenson S, Chambers D, Wahr J. Estimating geocenter variations from a combination of GRACE and ocean model output. Journal of Geophysical Research: Solid Earth 2008; 113.

Swenson S, Wahr J. Post-processing removal of correlated errors in GRACE data. Geophysical Research Letters 2006; 33: L08402.

Syed TH, Famiglietti JS, Rodell M, Chen J, Wilson CR. Analysis of terrestrial water storage changes from GRACE and GLDAS. Water Resources Research 2008; 44.

Tao Y, Cao J, Lan G, Su Q. The zonal movement of the Indian–East Asian summer monsoon interface in relation to the land–sea thermal contrast anomaly over East Asia. Climate Dynamics 2016; 46: 2759-2771.

Tapley BD, Bettadpur S, Watkins M, Reigber C. The gravity recovery and climate experiment: Mission overview and early results. Geophysical Research Letters 2004; 31.

Thomas AC, Reager JT, Famiglietti JS, Rodell M. A GRACE-based water storage deficit approach for hydrological drought characterization. Geophysical Research Letters 2014; 41: 1537-1545.

Thomas BF, Famiglietti JS. Identifying Climate-Induced Groundwater Depletion in GRACE Observations. Scientific Reports 2019; 9: 4124.

Wahr J, Molenaar M, Bryan F. Time variability of the Earth's gravity field: Hydrological and oceanic effects and their possible detection using GRACE. Journal of Geophysical Research: Solid Earth 1998; 103: 30205-30229.

Wang B, LinHo. Rainy Season of the Asian–Pacific Summer Monsoon. Journal of Climate 2002; 15: 386-398.

Wang B, Wu R, Lau K-M. Interannual Variability of the Asian Summer Monsoon: Contrasts between the Indian and the Western North Pacific–East Asian Monsoons. Journal of Climate 2001; 14: 4073-4090.

Weare BC. A Statistical Study of the Relationships between Ocean Surface Temperatures and the Indian Monsoon. Journal of the Atmospheric Sciences 1979; 36: 2279-2291.

Wells N, Goddard S, Hayes MJ. A Self-Calibrating Palmer Drought Severity Index. Journal of Climate 2004; 17: 2335-2351.

Wijngaard RR, Lutz AF, Nepal S, Khanal S, Pradhananga S, Shrestha AB, et al. Future changes in hydro-climatic extremes in the Upper Indus, Ganges, and Brahmaputra River basins. PLOS ONE 2017; 12: e0190224.

Wu G, Duan A, Liu Y, Mao J, Ren R, Bao Q, et al. Tibetan Plateau climate dynamics: recent research progress and outlook. National Science Review 2014; 2: 100-116.

Xiang L, Wang H, Steffen H, Wu P, Jia L, Jiang L, et al. Groundwater storage changes in the Tibetan Plateau and adjacent areas revealed from GRACE satellite gravity data. Earth and Planetary Science Letters 2016; 449: 228-239.

Xu K, Lu R, Kim B-J, Mao J, Park J-K. Influence of Tropical SSTs on the Interannual Variation of the Summer Monsoon Break over the Western North Pacific. Journal of Climate 2019; 32: 2807-2821.

Yang J, Liu Q, Xie S-P, Liu Z, Wu L. Impact of the Indian Ocean SST basin mode on the Asian summer monsoon. Geophysical Research Letters 2007; 34.

Yang K, Wu H, Qin J, Lin C, Tang W, Chen Y. Recent climate changes over the Tibetan Plateau and their impacts on energy and water cycle: A review. Global and Planetary Change 2014; 112: 79-91.

Yao T, Thompson L, Yang W, Yu W, Gao Y, Guo X, et al. Different glacier status with atmospheric circulations in Tibetan Plateau and surroundings. Nature Climate Change 2012; 2: 663-667.

Yao T, Zhou H, Yang X. Indian monsoon influences altitude effect of δ18O in precipitation/river water on the Tibetan Plateau. Chinese Science Bulletin 2009; 54: 2724-2731.

Yi H, Wen L. Satellite gravity measurement monitoring terrestrial water storage change and drought in the continental United States. Scientific Reports 2016; 6: 19909.

Zhang G, Yao T, Shum CK, Yi S, Yang K, Xie H, et al. Lake volume and groundwater storage variations in Tibetan Plateau's endorheic basin. Geophysical Research Letters 2017; 44: 5550-5560.

Zhao M, Velicogna I, Kimball JS. Satellite observations of regional drought severity in the continental United States using GRACE-based terrestrial water storage changes. Journal of Climate 2017; 30: 6297-6308.

Zhao P, Chen L. Climatic features of atmospheric heat source/sink over the Qinghai-Xizang Plateau in 35 years and its relation to rainfall in China. Science in China Series D: Earth Sciences 2001; 44: 858-864.

Zhisheng A, Guoxiong W, Jianping L, Youbin S, Yimin L, Weijian Z, et al. Global Monsoon Dynamics and Climate Change. Annual Review of Earth and Planetary Sciences 2015; 43: 29-77.

Zhu L, Xie M, Wu Y. Quantitative analysis of lake area variations and the influence factors from 1971 to 2004 in the Nam Co basin of the Tibetan Plateau. Chinese Science Bulletin 2010; 55: 1294-1303.

Appendix

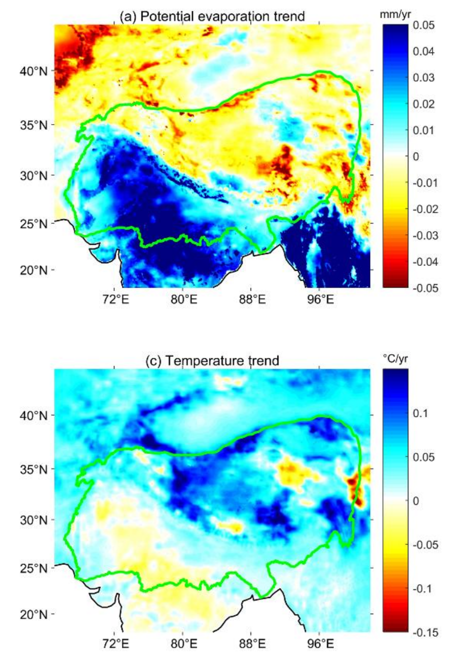

Figure S1. The potential evaporation (a), snow depth (b) and temperature trend (c) pattern over the CIBA.

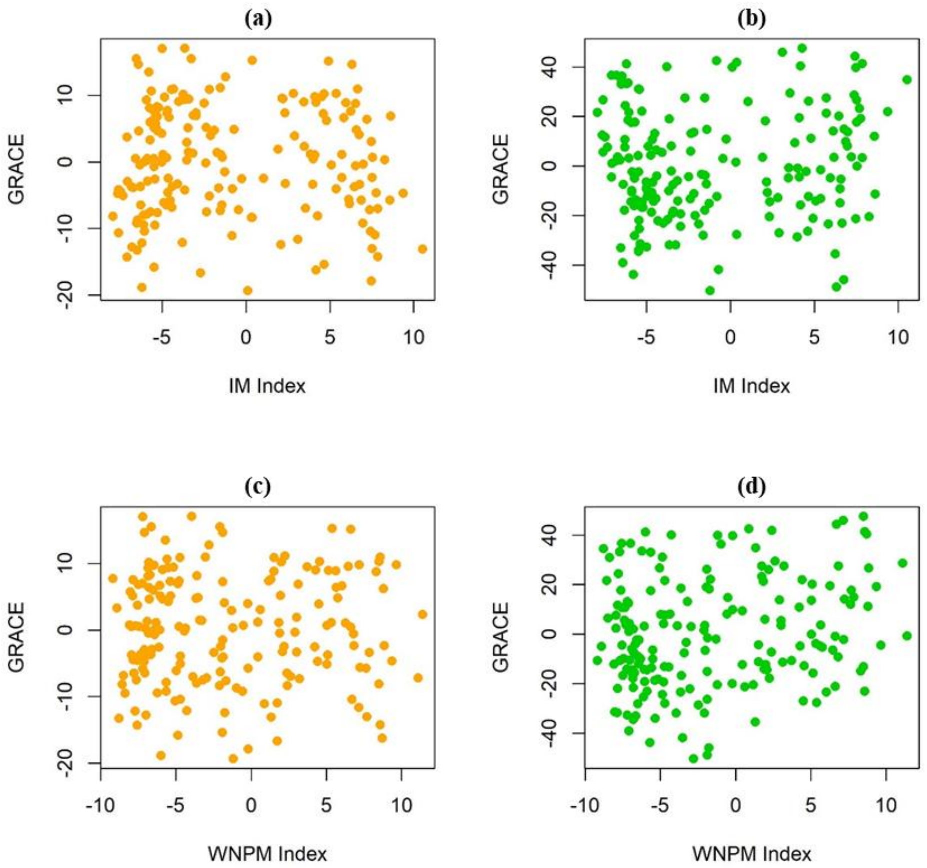

Figure S2. The IM and WNPM index against the TWS over the China (a, c) and India region (b, d) of CIBA.

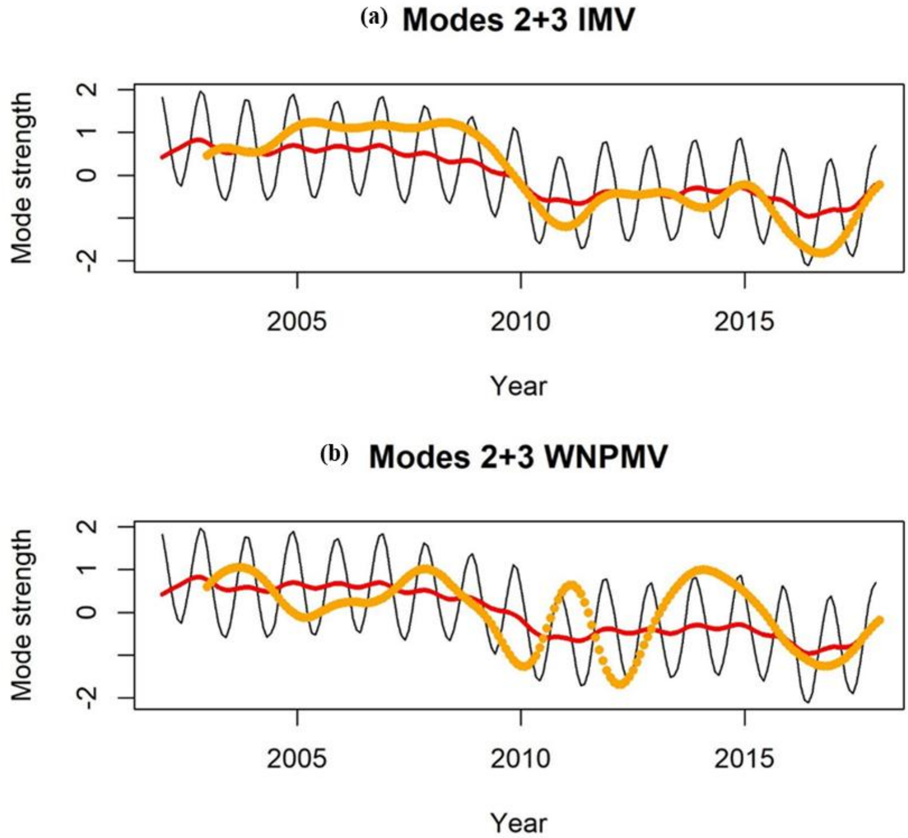

Figure S3. The mode strength of precipitation mode 2-3 (red) against the IMV (a) and WNPM step change (orange) (b).

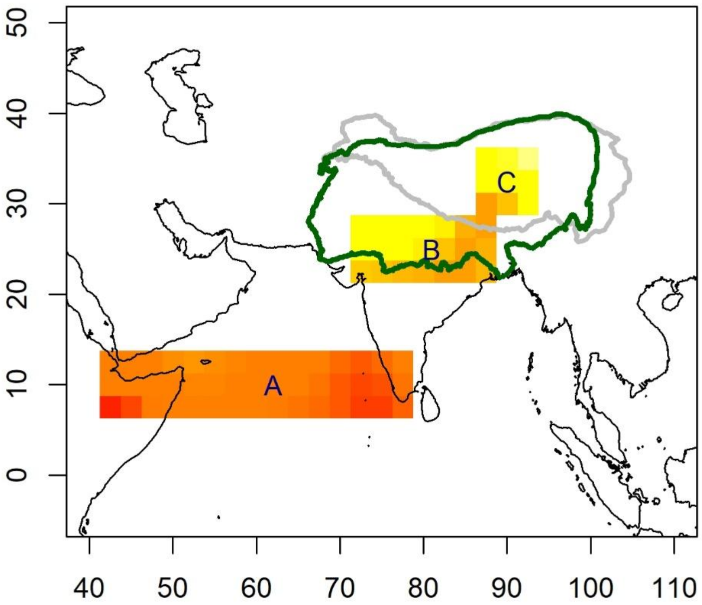

Figure S4. The selected temperature locations.

Graphical Abstract

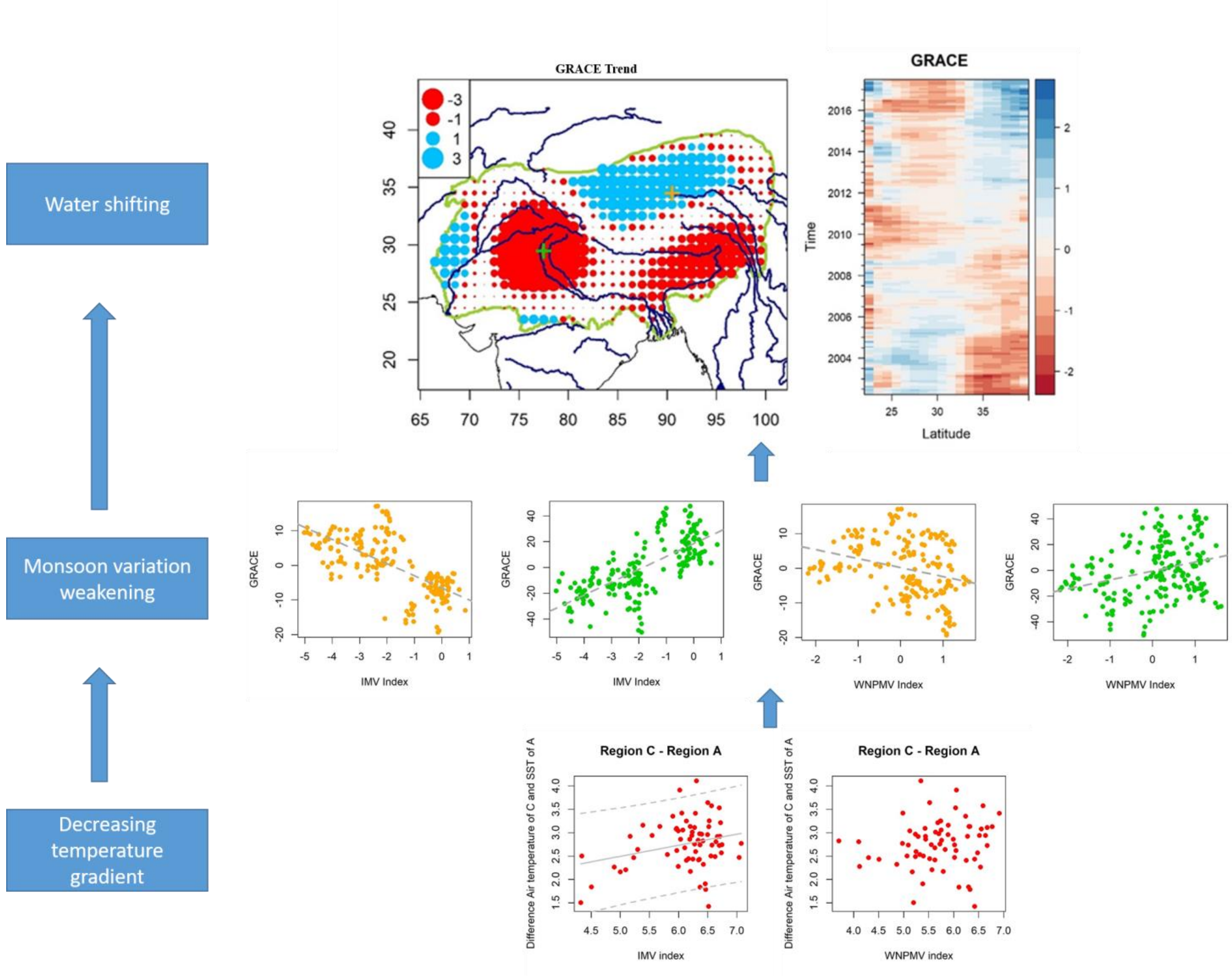

***Highlights (for review : 3 to 5 bullet points (maximum 85 characters including spaces per bullet point)**

Highlights:

- Terrestrial water storage showed a clear shifting pattern
- Pattern showed wetting in western China and drying in northwestern India.
- The shifting patterns were mainly due to the weakening of the monsoon variations.
- Weakening monsoon were related to decreasing regional temperature gradients.

Gravimetry-based water storage shifting over the China-India border area controlled by regional climate variability

Kwok Pan Chun[1], Qing He[1], Hok Sum Fok[2], Subimal Ghosh[3], Omer Yetemen[4,7], Qiang Chen[5], Ana Mijic[6]

[1] Department of Geography, Hong Kong Baptist University, Hong Kong, China.

[2] School of Geodesy and Geomatics, Wuhan University, Wuhan 430079, China.

[3] Department of Civil Engineering, Indian Institute of Technology Bombay, Mumbai, India.

[4] Civil, Surveying, and Environmental Engineering, The University of Newcastle, Australia.

[5] Geophysics Laboratory, Faculty of Science, Technology and Communication, University of Luxembourg, 2, avenue de l'Université, L-4365 Esch-sur-Alzette, Luxembourg.

[6] Imperial College London, Department of Civil and Environmental Engineering, London SW7 2AZ, UK.

[7] Eurasia Institute of Earth Sciences, Istanbul Technical University, Maslak 34469, Istanbul, Turkey.

Corresponding author: Kwok Pan Chun (kpchun@hkbu.edu.hk)

Highlights:

- Terrestrial water storage showed a clear shifting pattern
- Pattern showed wetting in western China and drying in northwestern India.
- The shifting patterns were mainly due to the weakening of the monsoon variations.
- Weakening monsoon were related to decreasing regional temperature gradients.

Abstract

The regional water storage shifting causes nonstationary spatial distribution of droughts and flooding, leading to water management challenges, environmental degradation and economic losses. The regional water storage shifting is becoming evident due to the increasing climate variability. However, the previous studies for climate drivers behind the water storage shifting are not rigorously quantified. In this study, the terrestrial water storage (TWS) spatial shifting pattern during 2002-2017 over the China-India border area (CIBA) is developed using the Gravity Recovery and Climate Experiment (GRACE), suggesting that the northwestern India were wetting while western China was drying. Similar drying and wetting patterns were also found in the precipitation, snow depth, Palmer Drought Severity Index (PDSI) and potential evaporation data. Based on our newly proposed Indian monsoon (IM) and western North Pacific monsoon (WNPM) variation indices, the water shifting pattern over the CIBA was found to be affected by the weakening of the variation of IM and WNPM through modulating the regional atmospheric circulation. The weakening of IM and WNPM

variations has shown to be attributed to the decreasing temperature gradient between the CIBA and the Indian Ocean, and possibly related to increasing regional temperatures associated with the increasing global temperature. As the global warming intensifies, it is expected that the regional TWS shifting pattern over the CIBA will be further exaggerated, stressing the need of advancing water resources management for local communities in the region.

Keywords

Water storage shifting; Gravity Recovery and Climate Experiment; climate variability; China-India border area

1 Introduction

Terrestrial water storage (TWS), including canopy water, glaciers, snow, surface water in rivers, lakes, wetlands and reservoirs, and underground water, determines global and regional hydrological resilience (Alsdorf et al., 2007). It plays a major role in the exchange of water with the atmosphere and oceans, and affects climate variability (Kim et al., 2009). Therefore, the TWS monitoring as well as the underlying drivers for its spatiotemporal dynamics are crucial for understanding the climatic-hydrological system (Humphrey et al., 2016). With the launch of the Gravity Recovery and Climate Experiment (GRACE) in March 2002, it provides a novel and reliable tool for TWS monitoring (e.g., Long et al., 2015; Long et al., 2017; Reager and Famiglietti, 2009b; Scanlon et al., 2019; Schmidt et al., 2006b; Sinha et al., 2016; Syed et al., 2008; Tapley et al., 2004).

In recent years, the GRACE data has been widely used to assess the TWS variability (e.g., Güntner et al., 2007; Long et al., 2015; Schmidt et al., 2006a), to monitor droughts (e.g., Houborg et al., 2012; Thomas et al., 2014; Yi and Wen, 2016; Zhao et al., 2017) and flooding (e.g., Chen et al., 2010; Reager and Famiglietti, 2009a; Reager et al., 2014); it is also used to evaluate groundwater depletion (e.g., Long et al., 2016; Rodell et al., 2009; Thomas and Famiglietti, 2019), and to estimate ice sheet or glacier loss (e.g., Chen et al., 2009; Farinotti et al., 2015; Shepherd et al., 2018). These studies have demonstrated the capability of GRACE to observe regional hydrological variability and global climate abnormalities, which are used for investigated water cycles linked with global and regional climates. For investigating the GRACE long-term trend variability, Rodell et al. (2018) quantified the global TWS trends during 2002-2016 and provided their corresponding causes. They found a general wetting pattern at high- and low-latitudes and a drying pattern at mid-latitudes, and these patterns are mainly due to the regular natural variability, groundwater depletion, and climate change. Meanwhile, Scanlon et al. (2018) found the TWS in some mid-latitude basins were decreasing, including Arkansas, Indus, Ganges, Brahmaputra, Hai River, Euphrates. On the other hand, high- and low-latitude regions showed an increasing TWS trend including Missouri, Amazon, Okavango, and Murray basin.

The increasing water loss at mid-latitudes exerts great pressure on the water supply in mid-latitude countries, in particular populous China and India. The China-India border area (CIBA, Figure 1), covering the Qinghai-Tibet Plateau (QTP), and Indus-Ganges-Brahmaputra basin (IGBB), is shared by multiple nations, including China, India, Nepal, Bhutan, Bangladesh, and Pakistan. The Tibetan Plateau, known as the ‘third pole’ of the Earth (Yao et al., 2012), affects regional thermal gradients which modulate local circulations (Duan et al., 2018; Wu et al., 2014; Zhao and Chen, 2001). Therefore, exploring how local climate mechanisms affect the TWS variability over the CIBA can provide information to decision makers for managing water resources shared among multiple populous nations. Over the IGBB, there have been several studies focusing on the water storage variations over the IGBB (e.g., Khandu et al., 2016; Scanlon et al., 2018) and QTP regions (e.g., Song et al., 2015; Xiang et al., 2016; Zhang et al., 2017). Related to the glacial processes, sharp water mass losses were observed in the southeast QTP between 2003 and 2011 (Song et al., 2015). Moreover, the lake volume in QTP region increased from 1970s to 2015 (Zhang et al., 2017). Over the IGBB, the TWS declined rapidly due to decreasing precipitation during 2002-2014 (Khandu et al., 2016) and increasing irrigation (Scanlon et al., 2018). Overall, previous studies clearly showed the separate trend variations of TWS in QTP and IGBB. Although they attempted to explain the TWS variations using meteorological forcing (e.g. precipitation and temperature) and human influences (e.g. irrigation), the TWS variations over the IGBB can be associated with the water conditions over the QTP, since the headwaters of the Indus, Ganges and Brahmaputra rivers originate in the QTP region (Kuehl et al., 2011). Therefore, there is a need to investigate the TWS dynamic in the QTP and the IGBB as an integral system rather than individual separate components. Furthermore, the

TWS variations are not only directly controlled by the local precipitation and temperature, but also indirectly affected by regional atmospheric circulations and temperature gradients between land and ocean.

Over the IGBB, the spatiotemporal dynamic of the hydrological regime is mainly under the control of the Indian monsoon (IM) (Khandu et al., 2017). Over the IGBB from July to September, the IM contributes to around 60-90% of the annual precipitation (Khandu et al., 2016). Due to the complex climate types, (Figure 1b), the IGBB has unevenly distributed precipitation over the sub-basins. In the Ganges basin, the northwest region is dryer than the coast area; in the Brahmaputra basin, there is heavy precipitation because of the rain shadow effect (Mirza et al., 1998). The upper Indus basin receives more precipitation than the lower basin, especially in the mountain region (Archer et al., 2010). Furthermore, the formation and variation of the IM are closely related to the QTP heating (Feng and Hu, 2005; Molnar et al., 1993; Sato and Kimura, 2007), and the IM affects precipitation patterns and river distributions over the QTP (Yao et al., 2009). Therefore, the IM plays an crucial role in the water dynamics over the whole CIBA.

Apart from the influence of IM, the regional temperature gradient could be an indirect contributor to the hydrological variability over the IGBB region. For instance, Roxy et al. (2015) found that the decreasing land-sea thermal gradient weakens the summer monsoon circulation and leads to the rainfall variations in India, due to rapid Indian Ocean warming. Over the past decades, the regional temperature increase caused wetter conditions in central and northern QTP (Yang et al., 2014). Moreover, changing hydroclimatic extreme events over the QTP and IGBB region are suggested to be related to shifting atmospheric and hydrological patterns due to increasing global average temperatures (Wijngaard et al., 2017). In recent years, more frequent droughts occurred in central India (Mallya et al., 2016; Rajeevan and Bhate, 2009), Nepal (Baidya et al., 2008), and Bangladesh (Shahid, 2011), while the extreme precipitation events were increased over the most parts of the India (Roxy et al., 2017; Sen Roy and Balling, 2004). In the central QTP, grasslands were affected by flooding due to the expansion of the surrounding lakes since the early 2000s (Zhu et al., 2010).

Over the CIBA, the changes of precipitation driven by IM variability affect the TWS dynamic (e.g., Khandu et al., 2016; Papa et al., 2010; 2015). The relationships between the IM and the TWS over the CIBA were only discussed qualitatively in almost all previous studies, but few studies have quantified these relationships and analyzed their mechanisms associated with regional temperature gradients at a seasonal scale. In this study, a new IM variation index was proposed to explore how the TWS is related to atmospheric circulations and regional temperature gradients. Given the close interaction between the IM and the western North Pacific monsoon (WNPM) (e.g., Gu et al., 2010; Li and Hsu, 2018; Wang et al., 2001), the WNPM was also considered to be a possible contributor to the TWS shifting. Furthermore, the spatiotemporal variability of precipitation and the Palmer Drought Severity Index were also explored because the PDSI represents the soil moisture state which is a difference between precipitation and potential evapotranspiration.

Overall, the main objectives of this study are: (1) to evaluate spatio-temporal characteristics of TWS associated with the other meteorological patterns in CIBA (2) to quantify the relationships between the TWS variations and monsoons (i.e. the IM and the WNPM); (3) to identify the temperature drivers related to monsoons and TWS variations; and (4) to develop a framework for explaining the relationships of temperature, monsoons and the TWS.

This study was organized as follows. A summary of various data sets and data analysis approaches employed in this study were given in Section 2. The results were given in Section 3, and they are followed by the corresponding discussion in Section 4. In Section 5, the major findings and implications of shifting TWS over the CIBA were summarized.

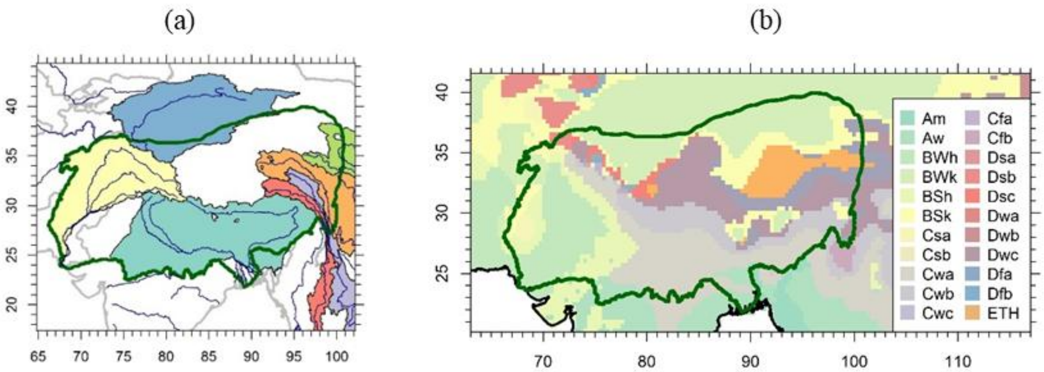

Figure 1. The general features (a) and Koppen climate types (b) of the CIBA. The yellow and cyan shaded areas are Indus Basin and Ganges-Brahmaputra Basin respectively in Figure 1a.

2 Materials and methods

2.1 Gravity Recovery and Climate Experiment (GRACE) data

The GRACE was designed to monitor the temporal and spatial variability of the Earth's gravity field. Using the algorithm of Wahr et al. (1998), the gravity field can be converted to the equivalent water height (EWH) for monitoring the TWS. In this study, we used GRACE Level-2 Release 06 (RL06) from the Center for Space Research (CSR; derived from ftp://isdcftp.gfz-potsdam.de/grace/Level-2/CSR/RL06/) at University of Texas to explore the spatiotemporal dynamics of TWS over the CIBA, in the form of Stokes spherical harmonic coefficients (SHCs) up to a degree and order of 60. The TWS grid data derived from GRACE spans from April 2002 to March 2017 (total 15 years), with a spatial resolution of 1 degree and a global coverage. For reducing the estimation errors of gravity anomalies, the pre-processing and post-processing procedures for GRACE data were applied, and these procedures include adding the degree-1 SHCs representing the geocenter motion (Swenson et al., 2008), replacing of the C_{20} term with the results from Satellite Laser Ranging (SLR) (Cheng and Ries, 2017), destripping, and applying the Gaussian filter with a radius of 350 km (Swenson and Wahr, 2006).

2.2 Meteorological data

For linking the TWS variation to precipitation pattern, the Tropical Rainfall Measuring Mission (TRMM) 3B43 version 7 was used in this study. This TRMM Multi-satellite Precipitation Analysis (TMPA) product were produced from assimilating data from multiple precipitation satellites, radiometers, and rain gauges by Huffman et al. (2007). The product was obtained from the NASA Goddard Space Flight Center (https://pmm.nasa.gov/data-access/downloads/trmm), with a time span ranging from 1998 to present, and a spatial coverage of 50°S-50°N with a resolution of 0.25 degree.

Apart from the TWS and precipitation data, drought indices are used for investigating the shift of hydrological conditions. In this study, the self-calibrating Palmer drought severity index (PDSI) (Wells et al., 2004) was used due to its better spatial comparability than traditional PDSI (Palmer, 1965), derived from the Research Data Archive at National Center for Atmospheric Research (NCAR) (https://rda.ucar.edu/datasets/ds299.0/) (Dai, 2017). The self-calibrating PDSI (hereafter just called PDSI for simplicity) data ranges from 1850 to 2014 with a monthly scale, covering the global land areas with a spatial resolution of 2.5 degree.

Other meteorological variables like the potential evaporation, snow melting and temperature also play important roles in the hydrological dynamics. These meteorological variables were derived from the ERA5-Land monthly averaged datasets (https://cds.climate.copernicus.eu/cdsapp#!/dataset/reanalysis-era5-land-monthly-means?tab=form), produced by the European Centre for Medium-Range Weather Forecasts (ECMWF). The ERA5 datasets covers the period from 2001 to present, with a high spatial resolution of 0.1×0.1°. In addition, the sea surface temperature (SST) data are derived form the extended reconstructed SST version 5 (ERSST.v5; https://www.esrl.noaa.gov/psd/data/gridded/data.noaa.ersst.v5.html) of the National Climate Data Centre (Huang et al., 2017).

2.3 Monsoon indices

The monsoon interaction zone of the IM and the WNPM is close to the edge of our study area (i.e., the CIBA) over the Indochina Peninsula (Wang and LinHo, 2002). In order to quantify the effect of IM on the TWS variability over the CIBA, the IM index was calculated, using the difference of zonal winds at 850-hPa between a southern region (5°-15°N, 40°-80°E) and a northern region (20°-30°N, 70°-90°E) (Wang et al., 2001). Based on the definition of Wang et al. (2001), the WNPM index was also calculated, using the difference of zonal winds at 850-hPa a southern region (5°-15°N, 100°-130°E) and a northern region (20°-30°N, 110°-140°E). The wind data for the calculation of IM and WNPM indices were extracted from the National Centers Environmental Prediction (NCEP) data (https://www.ncep.noaa.gov/).

2.4 Methodology

2.4.1 Moving standard deviation

Instead of using the conventional monsoon indices, we proposed to use the moving standard deviation of monsoon indices, to examine how the monsoon weakening affects the hydrological regimes over the CIBA. The moving standard deviation of a given monsoon time series can be calculated as:

$$S(t)=\sqrt{\frac{\sum_{i=t}^{t+M}\left(x(i)-\mu(t)\right)^{2}}{M-1}} \tag{1}$$

where $S(t)$ and $\mu(t)$ represent the standard deviation and average value of monsoon index x for the period from t to $t+M$ at time t, respectively. M is the size of moving window, which is chosen as 12 months in this study. The time series formed by these standard deviations is hereafter called the monsoon variation index in this study.

2.4.2 Local Indicators of Spatial Association (LISA)

The LISA was proposed to measure the local association between one observations and its neighboring observations (Anselin, 1995). The general LISA for an observation Z_i at location i can be expressed as

$$L_i = f\left(Z_i, Z_{J_i}\right) \tag{2}$$

where f is a function for association calculation, and the Z_{J_i} are the observations at the neighboring locations J_i of i. In this study, we used Moran's I (Moran, 1950) to be the calculation function. The LISA based on Moran's I for location i can be written as

$$I_i = \frac{(Z_i - \bar{Z})}{S_i^2}\sum_{j=1, j\neq i}^{n} w_{ij}\left(Z_j - \bar{Z}\right) \tag{3}$$

where

$$S_i^2 = \frac{\sum_{j=1, j\neq i}^{n} w_{ij}}{n-1} - \bar{Z}^2$$

where n is the total number of observations, Z_i and Z_j are the observations at location i and j; w_{ij} is the spatial weight between location i and j.

2.4.3 Singular spectral analysis

To capture the spatiotemporal characteristics of the precipitation, the singular spectral analysis (SSA) method was applied in this study. The SSA was introduced by Broomhead and King (1986), aiming at decomposing a time series into a sum of independent series identified as trend, periodic component, and noise (Hassani, 2007). The decomposition process of the SSA can be divided into two steps: embedding and singular value decomposition (SVD). Given a univariate time series $Y = (y_1, \dots, y_N)$, the embedding procedure means transferring one dimensional Y into H-dimensional vectors $\boldsymbol{X} = (X_1, \dots, X_H)$, where $X_i = (y_i, \dots, y_K)^T, i = 1, \dots, K = N - L + 1$. The parameter $2 \leq L \leq N$ is the window length, and its selection is very important for the SSA.

The covariance matrix $\boldsymbol{C}$ should be firstly derived from the trajectory matrix $\boldsymbol{X}$:

$$\boldsymbol{C} = \frac{\boldsymbol{1}}{K}\boldsymbol{X}^{\boldsymbol{T}}\boldsymbol{X} = \boldsymbol{E\Lambda E}^{\boldsymbol{T}} \tag{4}$$

where $\boldsymbol{\Lambda} = \mathrm{diag}(\lambda_1, \dots, \lambda_d)$, a diagonal matrix, consists of the eigenvalues of the covariance matrix, and d is the rank of the $\boldsymbol{X}$. The matrix $\boldsymbol{E} = (\boldsymbol{e_1}, \dots, \boldsymbol{e_d})$ includes corresponding eigenvectors.

Based on the SVD, the trajectory matrix X can be written as follows

$$\boldsymbol{X} = \boldsymbol{U}\sum\boldsymbol{V}^{\boldsymbol{T}} \tag{5}$$

where the columns of U and V are orthogonal, containing the left and right eigenvectors of X,$\sum$ is a diagonal matrix. Combined equation (1) and (2), the covariance matrix can be also denoted as

$$\boldsymbol{C} = \boldsymbol{U}(\sum^2/K)\boldsymbol{U}^{\boldsymbol{T}} \tag{6}$$

Thus $\boldsymbol{U} = (\boldsymbol{u_1}, \ldots, \boldsymbol{u_d}) = \boldsymbol{E} = (\boldsymbol{e_1}, \ldots, \boldsymbol{e_d})$, $\sum = \sqrt{K}\boldsymbol{\Lambda}^{1/2} = diag\left(\sqrt{K\lambda_1}, \ldots, \sqrt{K\lambda_d}\right)$, and $\boldsymbol{V} = (\boldsymbol{v_1}, \ldots, \boldsymbol{v_d})$ can also be easily obtained based on the equation (2). The $\boldsymbol{u}_i$ and $\boldsymbol{v}_i$ are called temporal empirical orthogonal functions (EOFs) and principal components (PCs), respectively.

In addition, the SVD of the trajectory matrix can be also written as

$$\boldsymbol{X} = \boldsymbol{X}_1 + \cdots + \boldsymbol{X}_d \tag{7}$$

where $\boldsymbol{X}_i = \sqrt{K\lambda_i}\boldsymbol{u}_i\boldsymbol{v}_i^T (i = 1, \ldots, d)$, are elementary matrices.

3 Results

3.1 The water shifting characteristics

Hovmöller diagrams (Hovmöller, 1949) were plotted to investigate the TWS spatiotemporal dynamic over the CIBA (66°E-101°E, 21°N-40°N) between 2002 and 2017. According to the temporal variances of TWS along longitude and latitude, seasonal clusters were found along both longitude and latitude. Moreover, TWS showed an increasing trend over 80°E-90°E (the Chinese side) but a decreasing trend between 75°E and 80°E (the Indian side) (Figure 2a). In terms of latitude, the shift of TWS was even clearer. Figure 2b shows a decreasing trend between 28°N and 32°N and an increasing trend over 32°N-38°N. In order to get more apparent trend pattern, the Hovmöller diagram of seasonal TWS anomalies was shown in Figure 2c. It displays a distinctive increasing trend between 32°N and 38°N and a decreasing trend between 28°N and 32°N. The dividing line between increasing and decreasing trends was around the 32°N latitude.

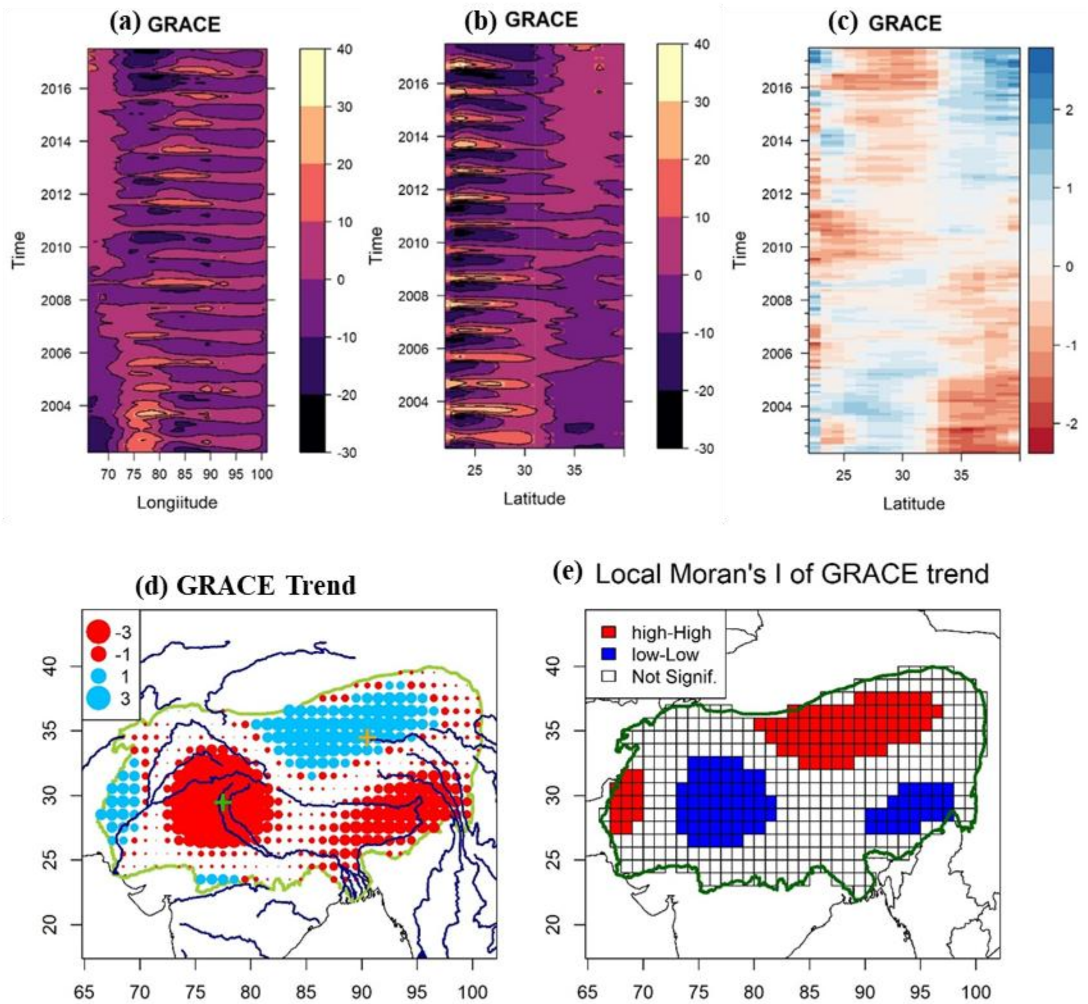

Figure 2. Hovmöller diagrams of TWS (mm) along longitude (a) and latitude (b), and the seasonal anomalies along latitude (c) over the CIBA region. Spatial trend distribution of the TWS (d) and corresponding local Moran's I distribution (e) over the CIBA. The blue and red circles represent the increasing and decreasing trend, respectively. The orange and green crosses are the locations in western China and northwestern India, respectively. The red and blue in (e) represent the high-high hotspots and low-low hotspots respectively.

According to Figure 2a-c, the temporal TWS variances had clear spatial shifts over the CIBA. Moreover, the spatial trend distribution of TWS and its LISA map displayed three clusters (also called hot spots); two of them represented decreasing trend, and one was increasing trend (Figure 2d-e). The increasing hot spot was located at the region of 80°E-95°E, 32°N-37°N (i.e., western China), while decreasing hot spots covered the regions of 72°E-82°E, 26°N-32°N (northwestern India) and 85°E-100°E, 25°N-31°N (Bangladesh, Figure 2d-e). The spatial trend pattern of TWS was consistent with the Hovmöller diagrams of TWS (Figure 2a-c), indicating there was a TWS shifting over the CIBA during 2002-2017.

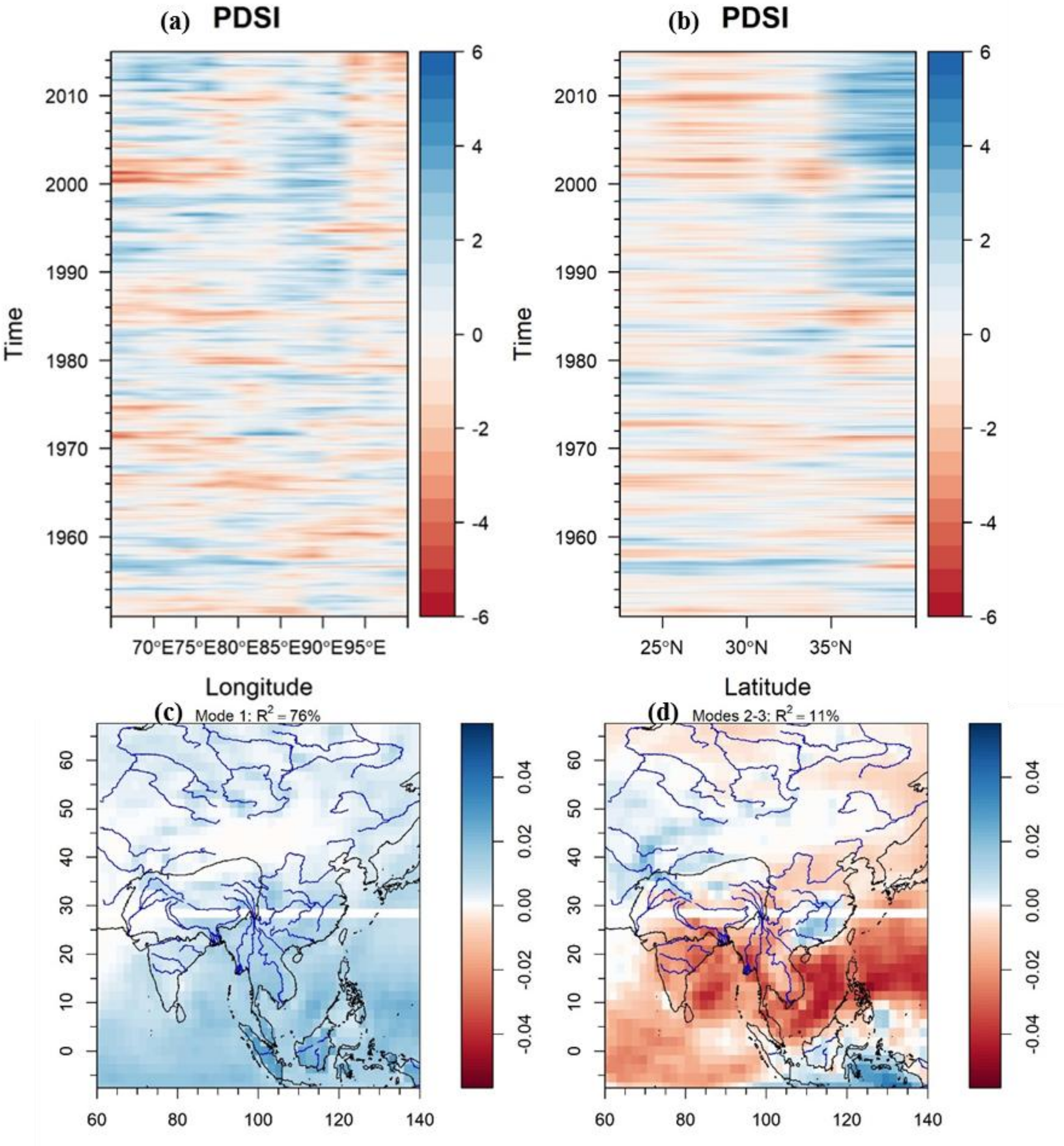

Figure 3. Hovmöller diagrams of PDSI along longitude (a) and latitude (b) over the GBB. The mode 1 (c) and combination of mode 2 and mode 3 (d) of TRMM precipitation based on the SSA.

Apart from the TWS, the Hovmöller diagrams of TRMM derived-precipitation and PDSI were shown in Figure 3. The Hovmöller diagrams of PDSI showed that central QTP (87°E-92°E, 35°N-40°N) has been wetting (blue regions in the diagrams) since the late 1980s (Figures 3a-b). After 2000, the northwestern India (26°N-32°N) has been drying (red regions in the diagram; Figure 3b). For precipitation, its seasonal signals are very strong, which can mask the trend signals, leading to unclear precipitation shifting pattern in the precipitation Hovmöller diagrams (not shown in this paper). Therefore, we used SSA method to separate the seasonal and trend signals (Figure 3c-d). The precipitation mode 1 represented the seasonal signal, which accounts for 76% of the total variances. It explains 7 times of the variance explained by the combination of mode 2 and mode 3 (hereafter called mode 2-3). The mode 2-3 accounts for 11% of the total precipitation variances, representing the secular trend variances. It showed similar pattern with the spatial TWS trend distribution, suggesting an increasing trend in western China and decreasing trend in other regions of the GBB (Figure 3d).

In addition, the potential evaporation distribution in Figure S1a showed a drying-wetting trend pattern which is similar with that of the TWS. Changing TWS over the IGBB during 2002-2017 can be directly caused by a more precipitation (and less evaporation) trend over the central QTP and a precipitation decline (and strengthened evaporation) over the IGBB (Figure 3d and Figure S1a). Similarly, Figure S1b showed sharp declines of snow depths during 2002-2017 over the northwest and the southeast corners of the QTP. These downward trends corresponded well with the rising temperatures (Figure S1c). With the rising of the local temperatures, a reducing snow depth trend (i.e., more snow melting) during 2002-2017 can be linked to increasing downstream surface waters such as the expansion of lakes in the central QTP (Zhang et al., 2017). Therefore, for the QTP region, the snow melting could be another important contributor to the TWS variations.

In summary, the TWS water shifting pattern over the CIBA is wetting for the western China and drying for the northwestern India. This shifting pattern could be directly affected by precipitation, potential evaporation and snow melting, which are mainly driven by the Asian monsoons modulated by regional temperature gradients. Therefore, the impacts of Asian monsoons, including IM and WNPM, on the water shifting since 2002 were investigated in next section.

3.2 Monsoon as a driving mechanism behind the TWS shifting

The summer IM index (for the months of JJA) had a decreasing trend, whereas the winter IM index (for the months of DJF) had an increasing trend (Figure 4a). However, for the monsoon intensity, the IM was weakening in both summer and winter. Although it is less clear, the WNPM index showed similar weakening trend. The weakening of the IM and WNPM could be the underlying drivers of water shifting over the CIBA. To quantify this weakening effect, IM and WNPM variation (hereafter called IMV and WNPMV) index were proposed based on the moving standard deviation of the IM and WNPM index, showing the both IM and WNPM strength were decreasing during 2002 and 2017 (Figure 4c-d). Particularly, the IMV index fell abruptly since 2010.

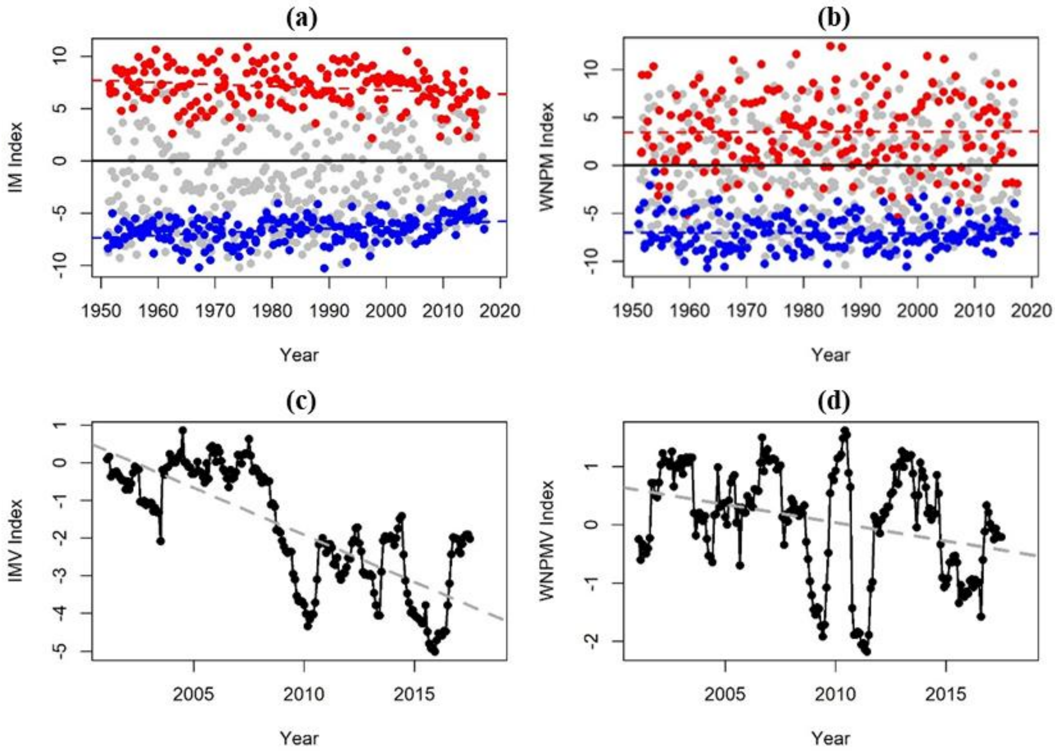

Figure 4. The monthly values of IM and WNPM indices during 1950-2017 (a-b) and the corresponding IMV and WNPMV indices during 2002-2017 (c-d). The red dots are the boreal summer (JJA) data and the blue dots are the winter (DJF) data in Figure 4a and 4b.

For investigating the relationships between IM (and WNPM) and TWS over the CIBA, two TWS time series located in western China and northwestern India (orange and green cross respectively in Figure 2d) were extracted. There were no significant relationships between IM (and WNPM) and TWS in both the western China and northwestern India (Figure S2). However, a significant negative trend for the western China and a significant positive trend for the northwestern India between the IMV (and WNPMV) index and TWS were shown in Figure 5a-d. The results revealed that the weakening IM and WNPM could lead to an increasing TWS trend in western China and a decreasing trend in northwestern India. Moreover, the LISA map of the partial correlation of the IMV and TWS shared the similar pattern with that of the WNPMV, showing significant negative and positive spatial clusters in western China and northwestern India, respectively (Figure 5e-f), which was consistent with the TWS trend patterns. Therefore, Figure 5a-f demonstrated that the TWS shifting over the whole CIBA results from the weakening of the Asian monsoons. Additionally, for the above-mentioned precipitation mode 2-3, representing the spatial precipitation trend pattern, its temporal variation (hereafter called mode strength) was consistent with the IMV and WNPMV step change (Figures S3), indicating that the precipitation redistribution over the GBB was attributed to the IMV and WNPMV.

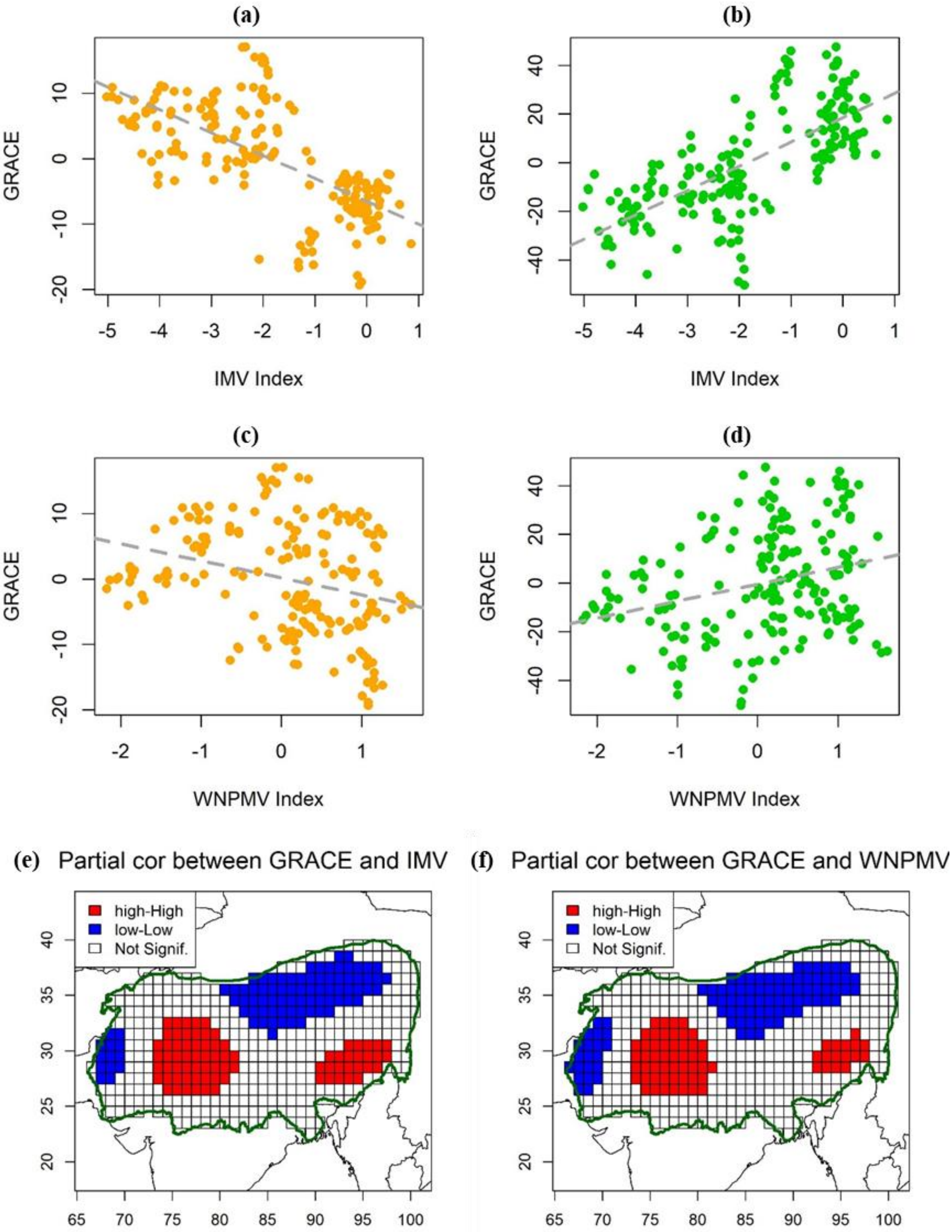
(a)
(b)
GRACE
IMV Index
(c)
(d)
WNPMV Index
(e) Partial cor between GRACE and IMV
(f) Partial cor between GRACE and WNPMV
high-High
low-Low
Not Signif.

Figure 5. IMV and WNPMV against the TWS over the China (a, c) and India region (b, d). The LISA map of partial correlation between TWS and IMV (e), and WNPMV (f) over the CIBA.

3.3 Temperature drivers behind monsoons and TWS

The above results showed that the TWS shifting over the CIBA was caused by the weakening of the IMV and WNPMV through modulating the precipitation distribution. The IM and WNPM variability have been showed to be related to the sea surface temperature (SST) (e.g., Annamalai et al., 2005; Weare, 1979; Xu et al., 2019), the temperature of the QTP (e.g., Boos and Kuang, 2010; Zhao and Chen, 2001; Zhisheng et al., 2015), and the land-ocean thermal difference (e.g., Roxy et al., 2015; Tao et al., 2016; Yang et al., 2007). Therefore, to explore the relationship between monsoons and surface temperatures, the average temperature over three regions located in the Indian Ocean (hereafter called Region A), the Ganges (hereafter called Region B) and the Brahmaputra (hereafter called Region C) were extracted (Figure S4).

The Figure 6 showed the relationships between mean annual temperature in different regions and monsoon indices for 70 years. Both the IM and WNPM indices were not related to the mean SST of Region A (Figure 6a and 6c), while the IMV and WNPMV fitted well with negative and positive relationship for the SST, respectively (Figure 6b and 6d). Moreover, negative relationships between the IMV and the near surface air temperature (NSAT) were found in all regions (Figure 6e-g). For the

WNPMV, it showed a positive relation with the NSAT at Region A, but negatively correlated with the NASTs at Region B and Region C (Figure 6h-j). These outcomes showed that the local and ocean temperature can modulate the monsoon variations. The negative relationships between temperatures and the IMV at three regions revealed that rising regional air temperatures and SST caused by increasing global temperatures may be the driver of the IM weakening. In addition, the IMV had a positively weak but statistically significant relationship with the thermal difference between Region A and Region C, while the WNPMV showed no significant relationship with the land-ocean thermal difference (Figures 6k-l), because it was more likely related to the thermal difference between the Asian land surface and the tropical Pacific Ocean based on its definition (Li and Hsu, 2018). Therefore, the land-Indian Ocean thermal difference may play a weak role for changing monsoons and thus the TWS spatial patterns.

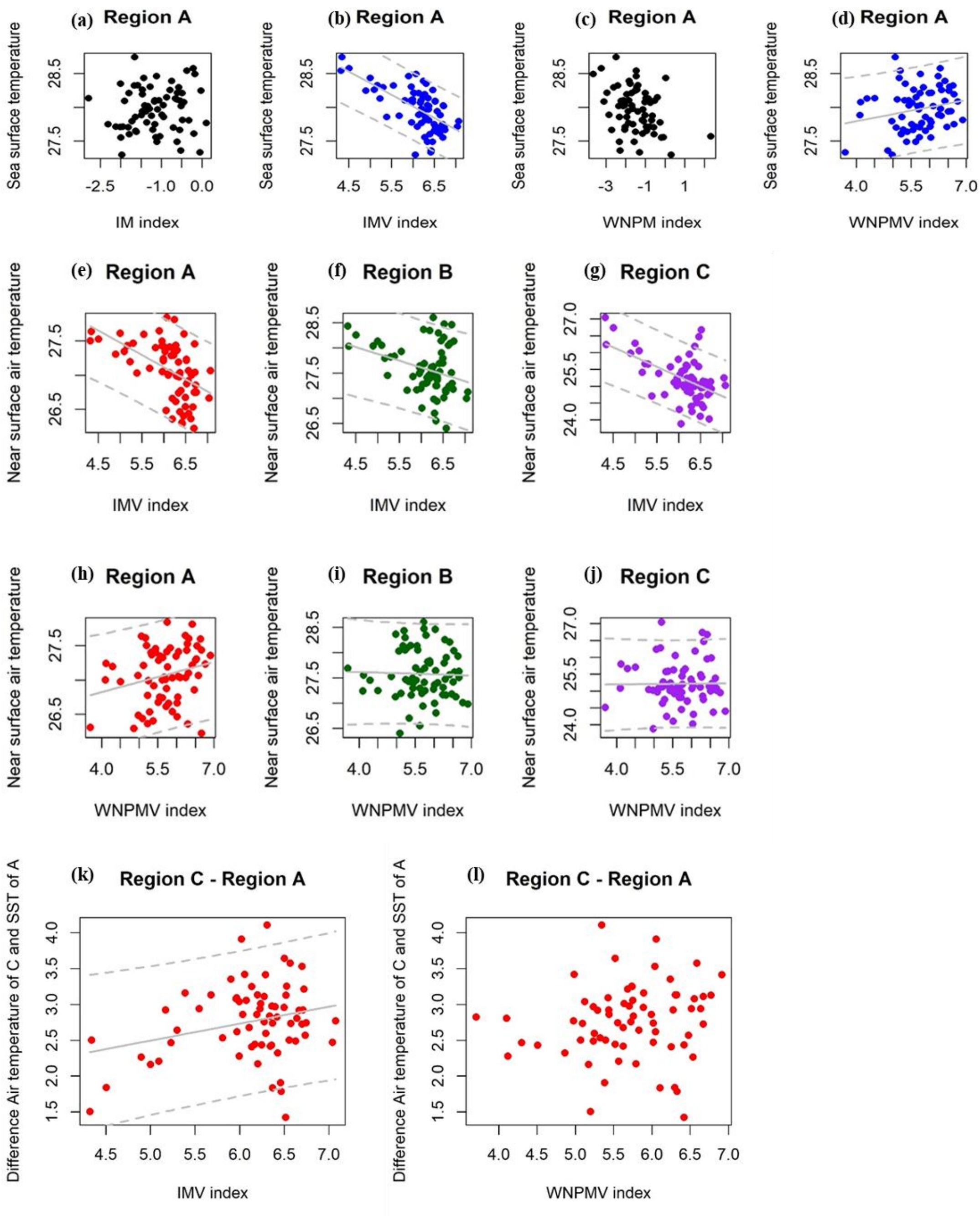

Figure 6. IM, IMV, WNPM and WNPMV index against the SST in Region A (a-d); IMV and WNPMV index against the NSAT in Region A, Region B and Region C (e-j); IMV and WNPMV index against the air temperature difference between Region A and Region C (k-l).

4 Discussion

The TWS trend pattern and the Hovmöller diagrams clearly showed the spatial clusters over the CIBA. There were (1) a significant decreasing cluster over the upper Indus and Ganges (i.e., northwestern India), (2) an increasing cluster over the central QTP (i.e., western China) and (3) a decreasing cluster over the southeastern Brahmaputra basin (i.e., Bangladesh). In addition to decreasing precipitation and increasing potential evaporation, the TWS decline in the IGBB was also probably attributed to the over-exploitation of underground water for water supply in agriculture and industrial sectors in northern India and Bangladesh (Rodell et al., 2009; Shamsudduha et al., 2012). Given the TWS decline and population increase, the IGBB region has now been facing severe water scarcity (Babel and Wahid, 2009), and the situation will become more serious if no measure is taken.

Apart from the anthropogenic effect, the monsoon variability is a main natural driver to the TWS shifting over the CIBA. Based on the monsoon variation analysis, the weakening of the IMV and WNPMV were significant contributors to the increasing TWS over the western China and the decreasing TWS over the northwestern India. During winter (Figures 7a and 7c), less strong dry monsoon winds come from the Himalaya over the Qinghai-Tibet Plateau; during summer (Figures 7b and 7d), weak monsoons would bring less moist winds from the Arabian Sea to India. Weaker and less moist winds would lead to drying windward side and wetting leeward side of the Himalaya, and thus an increasing TWS over the western China and a decreasing TWS over the northwestern India.

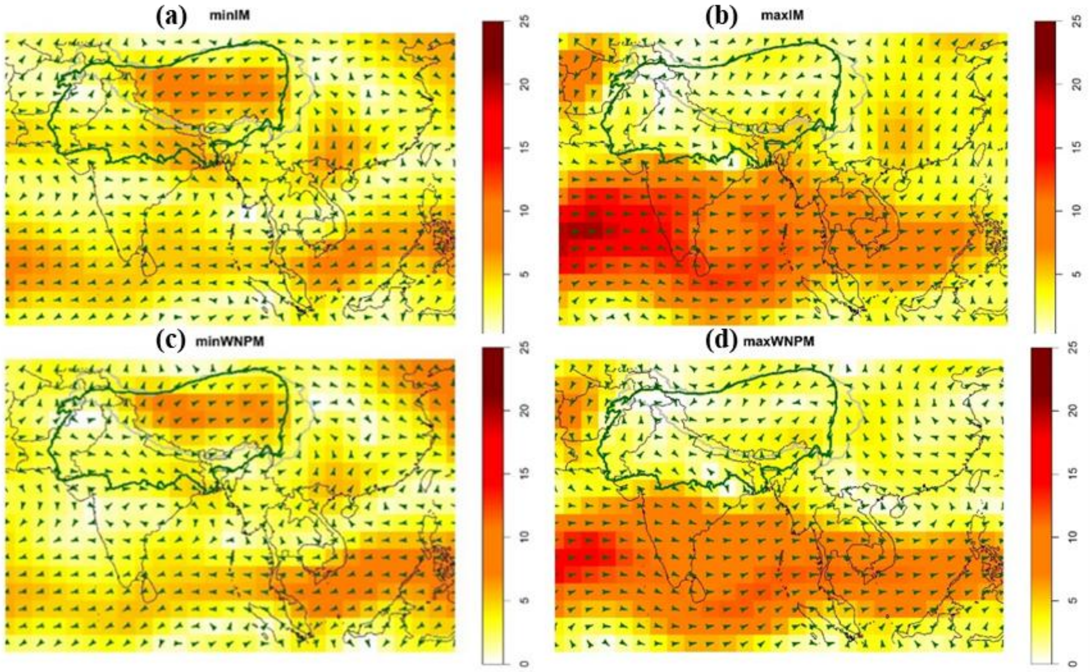

Figure 7. The average wind field of the lowest and highest 10% IM index (a-b), representing the winter monsoons and summer monsoons, respectively. (c-d) are same as (a-b) but for the WNPM.

According to the Figures 8a-b, the Indian Ocean (Region A) had a clear temperature increasing in both summer and winter. This temperature change led to the weakening of the IM, based on the negative relationship between IMV and SST in Region A (Figure 6b). The temperature over the Region B showed no obvious trend in both summer and winter (Figures 8c-d). The QTP (Region C) showed an increasing temperature trend in winter (Figure 8e), but no obvious trend in summer (Figure 8f). The increasing trends of temperature over the Indian Ocean were larger than that over the QTP in both winter and summer, indicating that the thermal difference between the Indian Ocean and QTP was decreasing, leading to the decrease in the IM intensity based on the positive relationship between IMV and temperature difference shown in the Figure 6k. For the WNPMV, the increasing temperature over the Region A indicated the strengthening of the WNPMV based on the positive relationship between WNPMV and SST over Region A (Figure 6d). However, this result is not consistent with the WNPMV weakening. This inconsistency can be explained by the complex interactions between the Indian Ocean and the Pacific Ocean, and the WNPM is less important for the CIBA, compared to the IM (Luo et al., 2010; 2012).

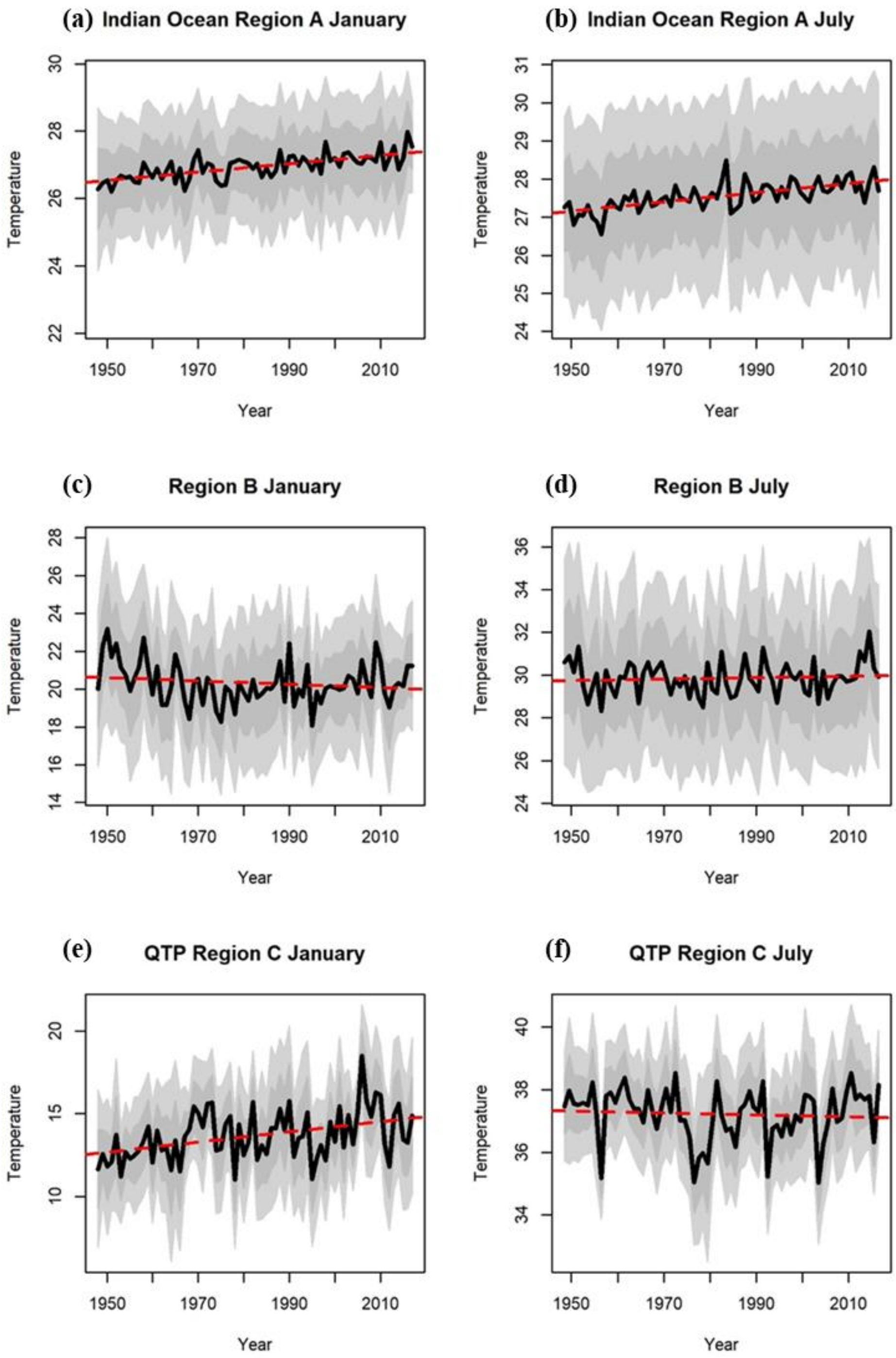

Figure 8. The average temperature variation over time in winter (January) and summer (July) over the Region A (a-b), Region B (c-d) and Region C (e-f).

5 Conclusion

In this study, we use the Hovmöller diagrams, the spatial TWS trend patterns and their LISA maps to show that the TWS over the western China part was increasing and the TWS over the northwestern India part was decreasing. The precipitation and potential evaporation showed similar drying and wetting patterns with the TWS, and snow melting due to the rising temperature can be an important contributor to the TWS increase over western China (i.e., central QTP). The water shifting pattern between 2002 and 2017 over the CIBA were controlled by the changing Asian monsoon (i.e., IM and WNPM) and local temperature through the modulation of precipitation, evaporation and snow melting.

The intensity of both IM and WNPM showed a gentle decreasing trend during 1950-2017. Furthermore, in order to emphasize the monsoon variation, IMV and WNPMV were calculated based on the traditional monsoon indices, revealing that the monsoon decreased dramatically during 2002-2017. In addition, the TWS over the drying region (i.e., northwestern India) was positively correlated with IMV (and WNPM), whereas the relationship between the TWS over the wetting zone (i.e., western China) and IMV (and WNPMV) was negative. This result suggested that the weakening of the IM led to the decreasing and increasing trends of TWS over two different regions of the CIBA. Moreover, similar clusters on the LISA maps further show that the weakening monsoons caused the TWS redistribution over the CIBA.

Finally, the ocean and continental temperature difference changes modulated the IM and WNPM variability, and they led to the TWS shifting over the CIBA. The temperatures over the QTP, the Ganges, and the Indian Ocean were negatively correlated with the IMV, indicating that increasing local temperatures weakened the IM, and thus affecting the TWS shifting. Meanwhile, the decrease in the thermal difference between the QTP and the Indian Ocean can also explain the weakening of the IM because of their positive relationship.

In this study, we looked at monsoon roles for changing TWS. Although the Glacial Isostatic Adjustment (GIA) were applied to the TWS data, the glacier effect can be important for explaining the observed TWS shifts. The observed drying center at the headwater of the Ganges can be related to the Gangotri glacier which is one of the largest glaciers in the Himalayas. The Gangotri glacier has been retreating at a significant rate between 22 and 27 m/year (Bhambri et al., 2011; Jain, 2008). The glacier retreat could be another explanation of decreasing TWS over the Ganges due to the temperature changes.

In summary, our findings have linked spatial water shifting over the CIBA to monsoon variations and changing local or even global temperature gradients. The main limitation of the study is whether the detected TWS shifting will last after 2017. For future studies, it will be worthwhile to project future TWS distributions using the temperature gradients derived from climate model outputs based on different Representative Concentration Pathways (RCPs). Then, these projected water conditions can help decision-makers to propose water management designs, including (1) establishing water consumption quotas for regions having declining TWS and (2) setting up flood control measures for places having increasing TWS. Therefore, the dynamic relationships between temperature gradient, TWS and monsoons in this study is not only building blocks for exploring the mechanisms of shifting hydroclimatic systems, but also providing new insights for future water management designs to the region.

Acknowledgments

This research was funded by the Hong Kong Baptist University Faculty research Fund (FRG1/1617/005, FRG2/1617/082, FRG2/1516/085), the National Natural Science Foundation of China (NSFC) (Grant No. 41974003, 41674007), and The Scientific and Technological Research Council of Turkey (TUBITAK) 2232 grant (118C329). This research was conducted using the resources of the High Performance Cluster Computing Centre, Hong Kong Baptist University, which receives funding from Research Grant Council, University Grant Committee of the HKSAR and Hong Kong Baptist University. The datasets used in this study are publicly available, and the corresponding URLs are provided in the section 2.

References:

Alsdorf DE, Rodriguez E, Lettenmaier DP. Measuring surface water from space. Reviews of Geophysics 2007; 45.

Annamalai H, Liu P, Xie S-P. Southwest Indian Ocean SST Variability: Its Local Effect and Remote Influence on Asian Monsoons. Journal of Climate 2005; 18: 4150-4167.

Anselin L. Local Indicators of Spatial Association—LISA. Geographical Analysis 1995; 27: 93-115.

Archer DR, Forsythe N, Fowler HJ, Shah SM. Sustainability of water resources management in the Indus Basin under changing climatic and socio economic conditions. Hydrol. Earth Syst. Sci. 2010; 14: 1669-1680.

Babel MS, Wahid SM. Freshwater Under Threat South Asia: Vulnerability Assessment of Freshwater Resources to Environmental Change: Ganges-Brahmaputra-Meghna River Basin, Helmand River Basin, Indus River Basin: UNEP, 2009.

Baidya SK, Shrestha ML, Sheikh MM. Trends in daily climatic extremes of temperature and precipitation in Nepal. Journal of Hydrology and Meteorology 2008; 5: 38-51.

Bhambri R, Bolch T, Chaujar RK, Kulshreshtha SC. Glacier changes in the Garhwal Himalaya, India, from 1968 to 2006 based on remote sensing. Journal of Glaciology 2011; 57: 543-556.

Boos WR, Kuang Z. Dominant control of the South Asian monsoon by orographic insulation versus plateau heating. Nature 2010; 463: 218-22.

Broomhead DS, King GP. Extracting qualitative dynamics from experimental data. Physica D: Nonlinear Phenomena 1986; 20: 217-236.

Chen JL, Wilson CR, Blankenship D, Tapley BD. Accelerated Antarctic ice loss from satellite gravity measurements. Nature Geoscience 2009; 2: 859.

Chen JL, Wilson CR, Tapley BD. The 2009 exceptional Amazon flood and interannual terrestrial water storage change observed by GRACE. Water Resources Research 2010; 46.

Cheng M, Ries J. The unexpected signal in GRACE estimates of $$C_{20}$$C20. Journal of Geodesy 2017; 91: 897-914.

Dai A. Dai Global Palmer Drought Severity Index (PDSI). Research Data Archive at the National Center for Atmospheric Research, Computational and Information Systems Laboratory, Boulder, CO, 2017.

Duan A, Liu S, Zhao Y, Gao K, Hu W. Atmospheric heat source/sink dataset over the Tibetan Plateau based on satellite and routine meteorological observations. Big Earth Data 2018; 2: 179-189.

Farinotti D, Longuevergne L, Moholdt G, Duethmann D, Mölg T, Bolch T, et al. Substantial glacier mass loss in the Tien Shan over the past 50 years. Nature Geoscience 2015; 8: 716.

Feng S, Hu Q. Regulation of Tibetan Plateau heating on variation of Indian summer monsoon in the last two millennia. Geophysical Research Letters 2005; 32.

Gu D, Li T, Ji Z, Zheng B. On the Phase Relations between the Western North Pacific, Indian, and Australian Monsoons. Journal of Climate 2010; 23: 5572-5589.

Güntner A, Stuck J, Werth S, Döll P, Verzano K, Merz B. A global analysis of temporal and spatial variations in continental water storage. Water Resources Research 2007; 43.

Hassani H. Singular Spectrum Analysis: Methodology and Comparison. University Library of Munich, Germany, 2007.

Houborg R, Rodell M, Li B, Reichle R, Zaitchik BF. Drought indicators based on model- assimilated Gravity Recovery and Climate Experiment (GRACE) terrestrial water storage observations. Water Resources Research 2012; 48.

Hovmöller E. The Trough-and-Ridge diagram. Tellus 1949; 1: 62-66.

Huang B, Thorne PW, Banzon VF, Boyer T, Chepurin G, Lawrimore JH, et al. Extended Reconstructed Sea Surface Temperature, Version 5 (ERSSTv5): Upgrades, Validations, and Intercomparisons. Journal of Climate 2017; 30: 8179-8205.

Huffman GJ, Bolvin DT, Nelkin EJ, Wolff DB, Adler RF, Gu G, et al. The TRMM Multisatellite Precipitation Analysis (TMPA): Quasi-Global, Multiyear, Combined-Sensor Precipitation Estimates at Fine Scales. Journal of Hydrometeorology 2007; 8: 38-55.

Humphrey V, Gudmundsson L, Seneviratne SI. Assessing Global Water Storage Variability from GRACE: Trends, Seasonal Cycle, Subseasonal Anomalies and Extremes. Surveys in Geophysics 2016; 37: 357-395.

Jain SK. Impact of retreat of Gangotri glacier on the flow of Ganga River. Current Science 2008; 95: 1012-1014.

Khandu, Awange JL, Anyah R, Kuhn M, Fukuda Y. Assessing regional climate simulations of the last 30 years (1982–2012) over Ganges–Brahmaputra–Meghna River Basin. Climate Dynamics 2017; 49: 2329-2350.

Khandu, Forootan E, Schumacher M, Awange JL, Müller Schmied H. Exploring the influence of precipitation extremes and human water use on total water storage (TWS) changes in the Ganges-Brahmaputra-Meghna River Basin. Water Resources Research 2016; 52: 2240-2258.

Kim H, Yeh PJ-F, Oki T, Kanae S. Role of rivers in the seasonal variations of terrestrial water storage over global basins. Geophysical Research Letters 2009; 36.

Kuehl SA, Allison MA, Goodbred SL, Kudrass H. The Ganges–Brahmaputra Delta. 2011: 413-434.

Li T, Hsu P-c. Monsoon Dynamics and Its Interactions with Ocean. Fundamentals of Tropical Climate Dynamics. Springer International Publishing, Cham, 2018, pp. 185-229.

Long D, Chen X, Scanlon BR, Wada Y, Hong Y, Singh VP, et al. Have GRACE satellites overestimated groundwater depletion in the Northwest India Aquifer? Scientific Reports 2016; 6: 24398.

Long D, Longuevergne L, Scanlon BR. Global analysis of approaches for deriving total water storage changes from GRACE satellites. Water Resources Research 2015; 51: 2574-2594.

Long D, Pan Y, Zhou J, Chen Y, Hou X, Hong Y, et al. Global analysis of spatiotemporal variability in merged total water storage changes using multiple GRACE products and global hydrological models. Remote Sensing of Environment 2017; 192: 198-216.

Luo J-J, Zhang R, Behera SK, Masumoto Y, Jin F-F, Lukas R, et al. Interaction between El Niño and Extreme Indian Ocean Dipole. Journal of Climate 2010; 23: 726-742.

Luo JJ, Sasaki W, Masumoto Y. Indian Ocean warming modulates Pacific climate change. Proc Natl Acad Sci U S A 2012; 109: 18701-6.

Mallya G, Mishra V, Niyogi D, Tripathi S, Govindaraju RS. Trends and variability of droughts over the Indian monsoon region. Weather and Climate Extremes 2016; 12: 43-68.

Mirza MQ, Warrick RA, Ericksen NJ, Kenny GJ. Trends and persistence in precipitation in the Ganges, Brahmaputra and Meghna river basins. Hydrological Sciences Journal 1998; 43: 845-858.

Molnar P, England P, Martinod J. Mantle dynamics, uplift of the Tibetan Plateau, and the Indian Monsoon. Reviews of Geophysics 1993; 31: 357-396.

Moran PAP. Notes on Continuous Stochastic Phenomena. Biometrika 1950; 37: 17-23.

Palmer WC. Meteorological drought (Vol. 30). Washington, DC, USA: US Department of Commerce. Weather Bureau 1965.

Papa F, Durand F, Rossow WB, Rahman A, Bala SK. Satellite altimeter-derived monthly discharge of the Ganga-Brahmaputra River and its seasonal to interannual variations from 1993 to 2008. Journal of Geophysical Research: Oceans 2010; 115.

Papa F, Frappart F, Malbeteau Y, Shamsudduha M, Vuruputur V, Sekhar M, et al. Satellite-derived surface and sub-surface water storage in the Ganges–Brahmaputra River Basin. Journal of Hydrology: Regional Studies 2015; 4: 15-35.

Rajeevan M, Bhate J. A high resolution daily gridded rainfall dataset (1971–2005) for mesoscale meteorological studies. Current Science 2009; 96: 558-562.

Reager JT, Famiglietti JS. Global terrestrial water storage capacity and flood potential using GRACE. Geophysical Research Letters 2009a; 36.

Reager JT, Famiglietti JS. Global terrestrial water storage capacity and flood potential using GRACE. Geophysical Research Letters 2009b; 36: L23402.

Reager JT, Thomas BF, Famiglietti JS. River basin flood potential inferred using GRACE gravity observations at several months lead time. Nature Geoscience 2014; 7: 588.

Rodell M, Famiglietti J, Wiese D, Reager J, Beaudoing H, Landerer FW, et al. Emerging trends in global freshwater availability. Nature 2018; 557: 651.

Rodell M, Velicogna I, Famiglietti JS. Satellite-based estimates of groundwater depletion in India. Nature 2009; 460: 999.

Roxy MK, Ghosh S, Pathak A, Athulya R, Mujumdar M, Murtugudde R, et al. A threefold rise in widespread extreme rain events over central India. Nature Communications 2017; 8: 708.

Roxy MK, Ritika K, Terray P, Murtugudde R, Ashok K, Goswami BN. Drying of Indian subcontinent by rapid Indian Ocean warming and a weakening land-sea thermal gradient. Nat Commun 2015; 6: 7423.

Sato T, Kimura F. How Does the Tibetan Plateau Affect the Transition of Indian Monsoon Rainfall? Monthly Weather Review 2007; 135: 2006-2015.

Scanlon BR, Zhang Z, Rateb A, Sun A, Wiese D, Save H, et al. Tracking Seasonal Fluctuations in Land Water Storage Using Global Models and GRACE Satellites. Geophysical Research Letters 2019; 46: 5254-5264.

Scanlon BR, Zhang Z, Save H, Sun AY, Schmied HM, van Beek LP, et al. Global models underestimate large decadal declining and rising water storage trends relative to GRACE satellite data. Proceedings of the National Academy of Sciences 2018; 115: E1080-E1089.

Schmidt R, Schwintzer P, Flechtner F, Reigber C, Güntner A, Döll P, et al. GRACE observations of changes in continental water storage. Global and Planetary Change 2006a; 50: 112-126.

Schmidt R, Schwintzer P, Flechtner F, Reigber C, Güntner A, Döll P, et al. GRACE observations of changes in continental water storage. Global and Planetary Change 2006b; 50: 112-126.

Sen Roy S, Balling RC. Trends in extreme daily precipitation indices in India. International Journal of Climatology 2004; 24: 457-466.

Shahid S. Trends in extreme rainfall events of Bangladesh. Theoretical and Applied Climatology 2011; 104: 489-499.

Shamsudduha M, Taylor RG, Longuevergne L. Monitoring groundwater storage changes in the highly seasonal humid tropics: Validation of GRACE measurements in the Bengal Basin. Water Resources Research 2012; 48.

Shepherd A, Ivins E, Rignot E, Smith B, van den Broeke M, Velicogna I, et al. Mass balance of the Antarctic Ice Sheet from 1992 to 2017. Nature 2018; 558: 219-222.

Sinha D, Syed TH, Famiglietti JS, Reager JT, Thomas RC. Characterizing Drought in India Using GRACE Observations of Terrestrial Water Storage Deficit. Journal of Hydrometeorology 2016; 18: 381-396.

Song C, Ke L, Huang B, Richards KS. Can mountain glacier melting explains the GRACE-observed mass loss in the southeast Tibetan Plateau: From a climate perspective? Global and Planetary Change 2015; 124: 1-9.

Swenson S, Chambers D, Wahr J. Estimating geocenter variations from a combination of GRACE and ocean model output. Journal of Geophysical Research: Solid Earth 2008; 113.

Swenson S, Wahr J. Post-processing removal of correlated errors in GRACE data. Geophysical Research Letters 2006; 33: L08402.

Syed TH, Famiglietti JS, Rodell M, Chen J, Wilson CR. Analysis of terrestrial water storage changes from GRACE and GLDAS. Water Resources Research 2008; 44.

Tao Y, Cao J, Lan G, Su Q. The zonal movement of the Indian–East Asian summer monsoon interface in relation to the land–sea thermal contrast anomaly over East Asia. Climate Dynamics 2016; 46: 2759-2771.

Tapley BD, Bettadpur S, Watkins M, Reigber C. The gravity recovery and climate experiment: Mission overview and early results. Geophysical Research Letters 2004; 31.

Thomas AC, Reager JT, Famiglietti JS, Rodell M. A GRACE-based water storage deficit approach for hydrological drought characterization. Geophysical Research Letters 2014; 41: 1537-1545.

Thomas BF, Famiglietti JS. Identifying Climate-Induced Groundwater Depletion in GRACE Observations. Scientific Reports 2019; 9: 4124.

Wahr J, Molenaar M, Bryan F. Time variability of the Earth's gravity field: Hydrological and oceanic effects and their possible detection using GRACE. Journal of Geophysical Research: Solid Earth 1998; 103: 30205-30229.

Wang B, LinHo. Rainy Season of the Asian–Pacific Summer Monsoon. Journal of Climate 2002; 15: 386-398.

Wang B, Wu R, Lau K-M. Interannual Variability of the Asian Summer Monsoon: Contrasts between the Indian and the Western North Pacific–East Asian Monsoons. Journal of Climate 2001; 14: 4073-4090.

Weare BC. A Statistical Study of the Relationships between Ocean Surface Temperatures and the Indian Monsoon. Journal of the Atmospheric Sciences 1979; 36: 2279-2291.

Wells N, Goddard S, Hayes MJ. A Self-Calibrating Palmer Drought Severity Index. Journal of Climate 2004; 17: 2335-2351.

Wijngaard RR, Lutz AF, Nepal S, Khanal S, Pradhananga S, Shrestha AB, et al. Future changes in hydro-climatic extremes in the Upper Indus, Ganges, and Brahmaputra River basins. PLOS ONE 2017; 12: e0190224.

Wu G, Duan A, Liu Y, Mao J, Ren R, Bao Q, et al. Tibetan Plateau climate dynamics: recent research progress and outlook. National Science Review 2014; 2: 100-116.

Xiang L, Wang H, Steffen H, Wu P, Jia L, Jiang L, et al. Groundwater storage changes in the Tibetan Plateau and adjacent areas revealed from GRACE satellite gravity data. Earth and Planetary Science Letters 2016; 449: 228-239.

Xu K, Lu R, Kim B-J, Mao J, Park J-K. Influence of Tropical SSTs on the Interannual Variation of the Summer Monsoon Break over the Western North Pacific. Journal of Climate 2019; 32: 2807-2821.

Yang J, Liu Q, Xie S-P, Liu Z, Wu L. Impact of the Indian Ocean SST basin mode on the Asian summer monsoon. Geophysical Research Letters 2007; 34.

Yang K, Wu H, Qin J, Lin C, Tang W, Chen Y. Recent climate changes over the Tibetan Plateau and their impacts on energy and water cycle: A review. Global and Planetary Change 2014; 112: 79-91.

Yao T, Thompson L, Yang W, Yu W, Gao Y, Guo X, et al. Different glacier status with atmospheric circulations in Tibetan Plateau and surroundings. Nature Climate Change 2012; 2: 663-667.

Yao T, Zhou H, Yang X. Indian monsoon influences altitude effect of δ18O in precipitation/river water on the Tibetan Plateau. Chinese Science Bulletin 2009; 54: 2724-2731.

Yi H, Wen L. Satellite gravity measurement monitoring terrestrial water storage change and drought in the continental United States. Scientific Reports 2016; 6: 19909.

Zhang G, Yao T, Shum CK, Yi S, Yang K, Xie H, et al. Lake volume and groundwater storage variations in Tibetan Plateau's endorheic basin. Geophysical Research Letters 2017; 44: 5550-5560.

Zhao M, Velicogna I, Kimball JS. Satellite observations of regional drought severity in the continental United States using GRACE-based terrestrial water storage changes. Journal of Climate 2017; 30: 6297-6308.

Zhao P, Chen L. Climatic features of atmospheric heat source/sink over the Qinghai-Xizang Plateau in 35 years and its relation to rainfall in China. Science in China Series D: Earth Sciences 2001; 44: 858-864.

Zhisheng A, Guoxiong W, Jianping L, Youbin S, Yimin L, Weijian Z, et al. Global Monsoon Dynamics and Climate Change. Annual Review of Earth and Planetary Sciences 2015; 43: 29-77.

Zhu L, Xie M, Wu Y. Quantitative analysis of lake area variations and the influence factors from 1971 to 2004 in the Nam Co basin of the Tibetan Plateau. Chinese Science Bulletin 2010; 55: 1294-1303.

Appendix

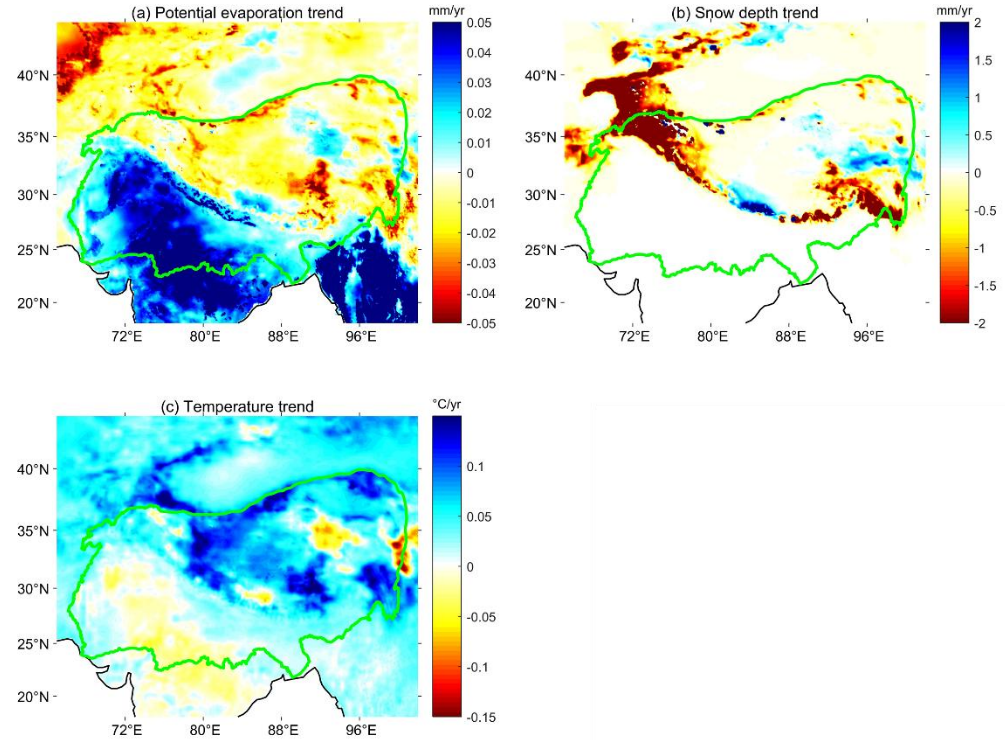

Figure S1. The potential evaporation (a), snow depth (b) and temperature trend (c) pattern over the CIBA.

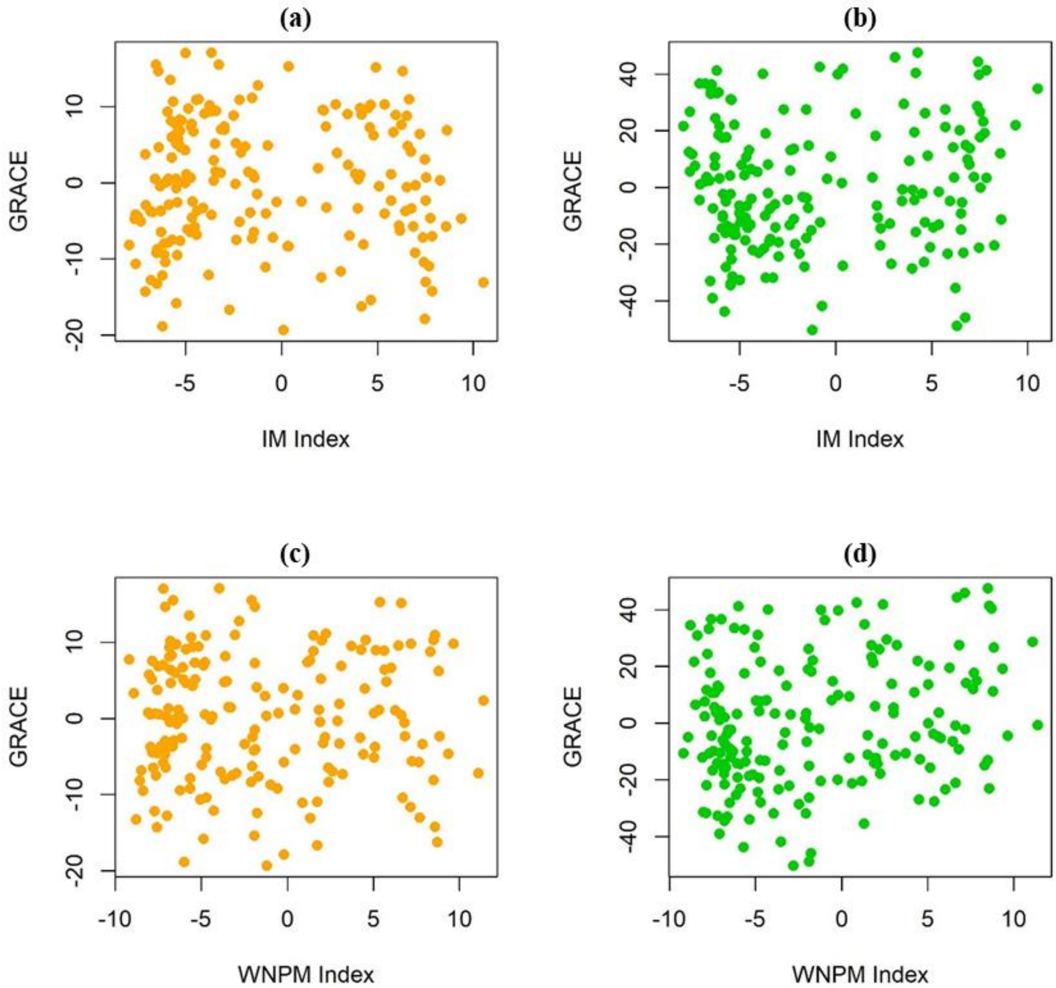

Figure S2. The IM and WNPM index against the TWS over the China (a, c) and India region (b, d) of CIBA.

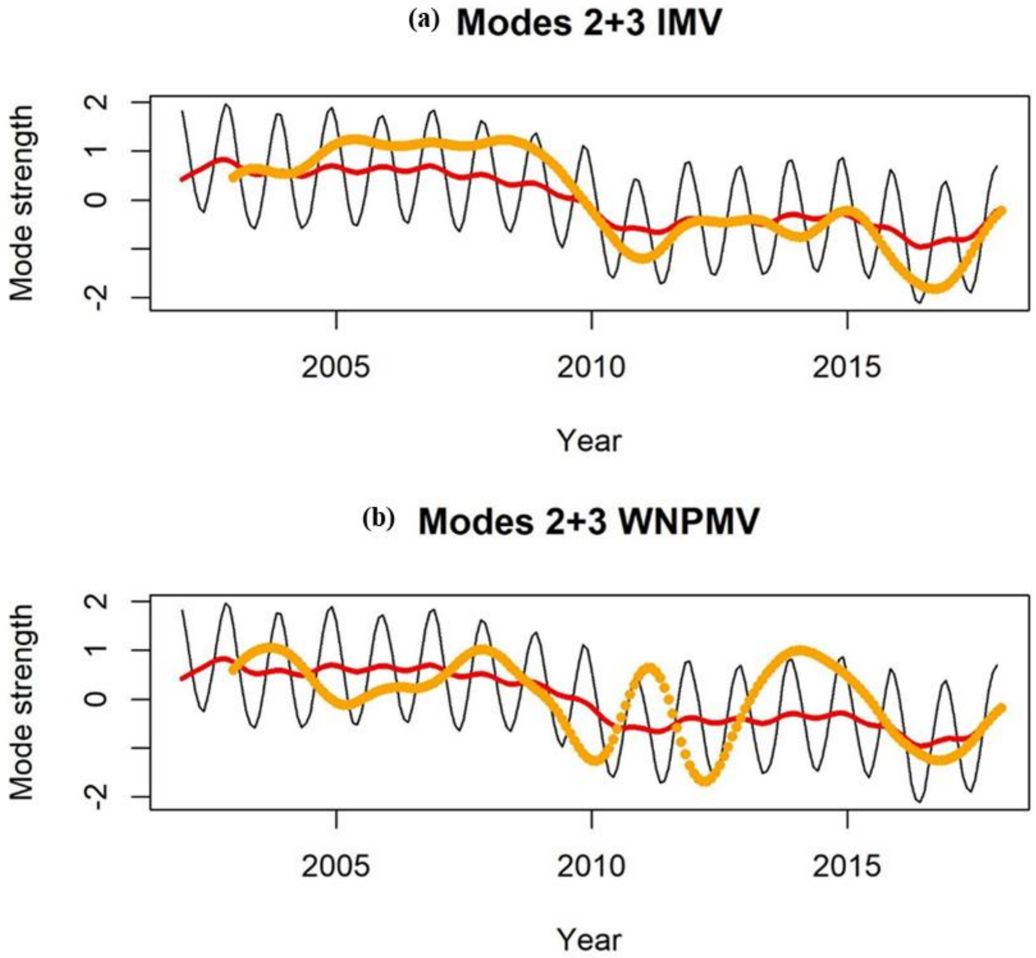

Figure S3. The mode strength of precipitation mode 2-3 (red) against the IMV (a) and WNPM step change (orange) (b).

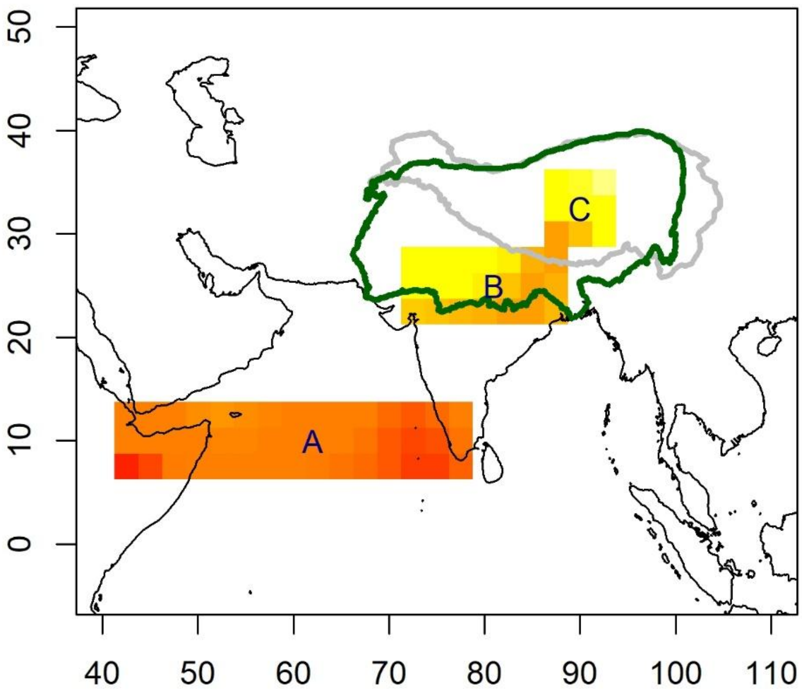

Figure S4. The selected temperature locations.

Figure

Click here to download high resolution image

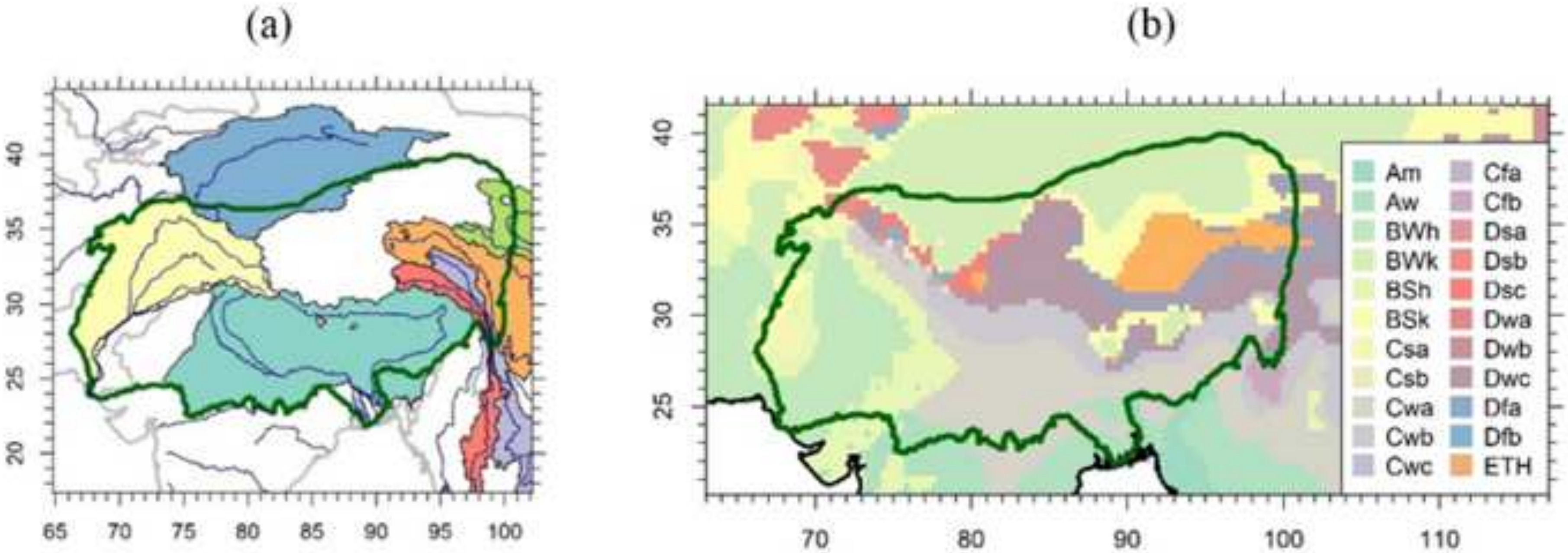

Figure
Click here to download high resolution image

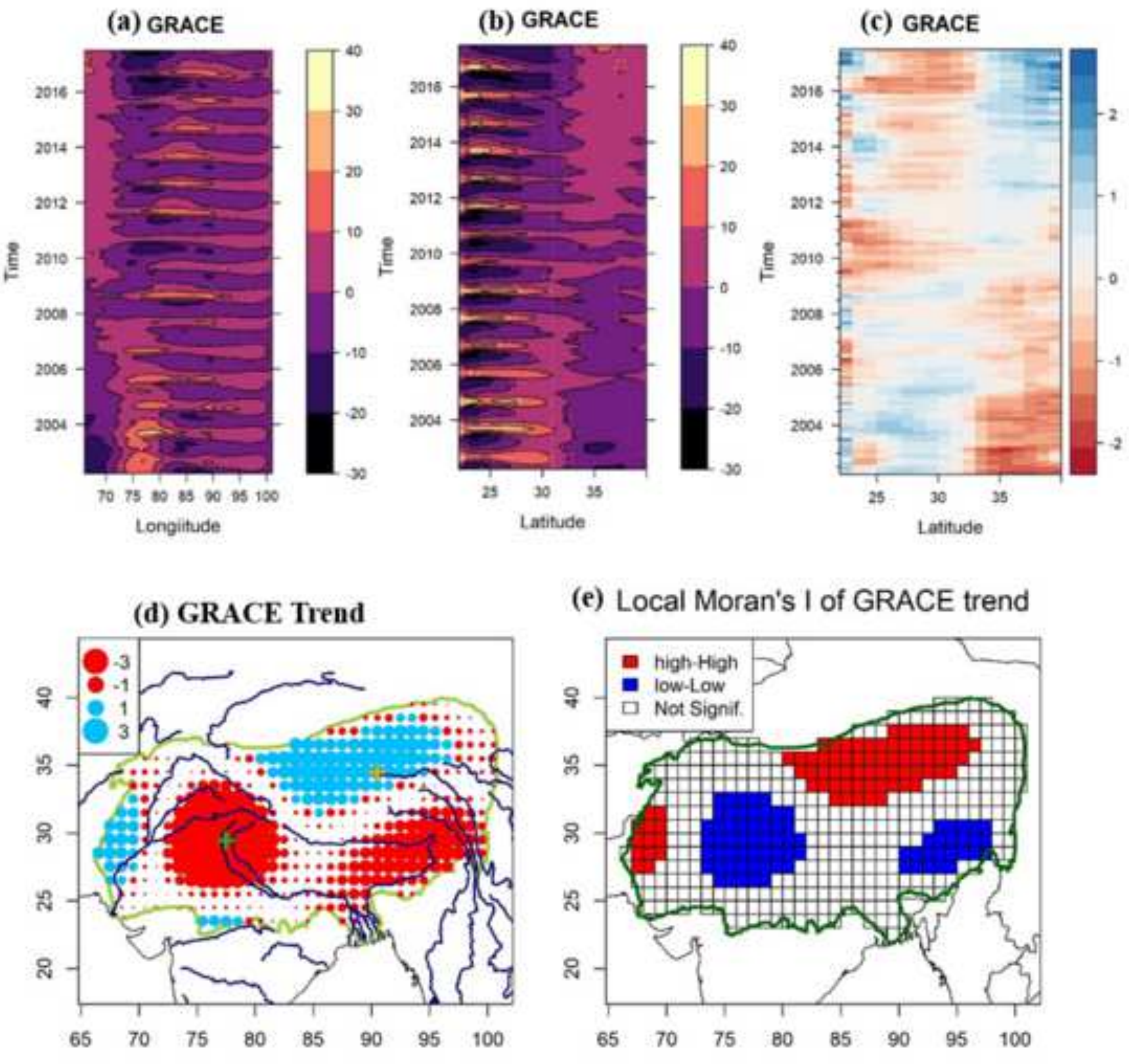

Figure
Click here to download high resolution image

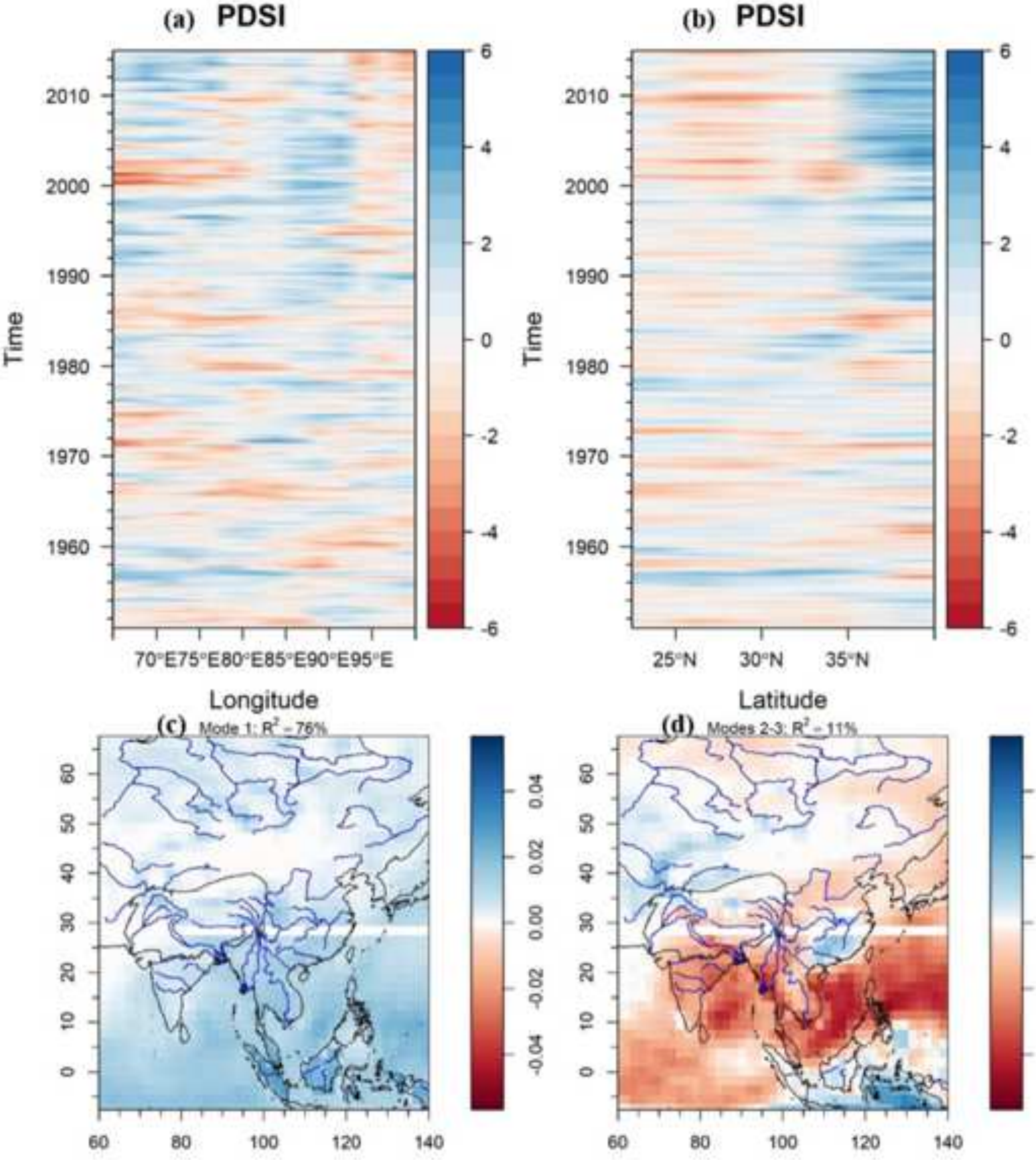

Figure
Click here to download high resolution image

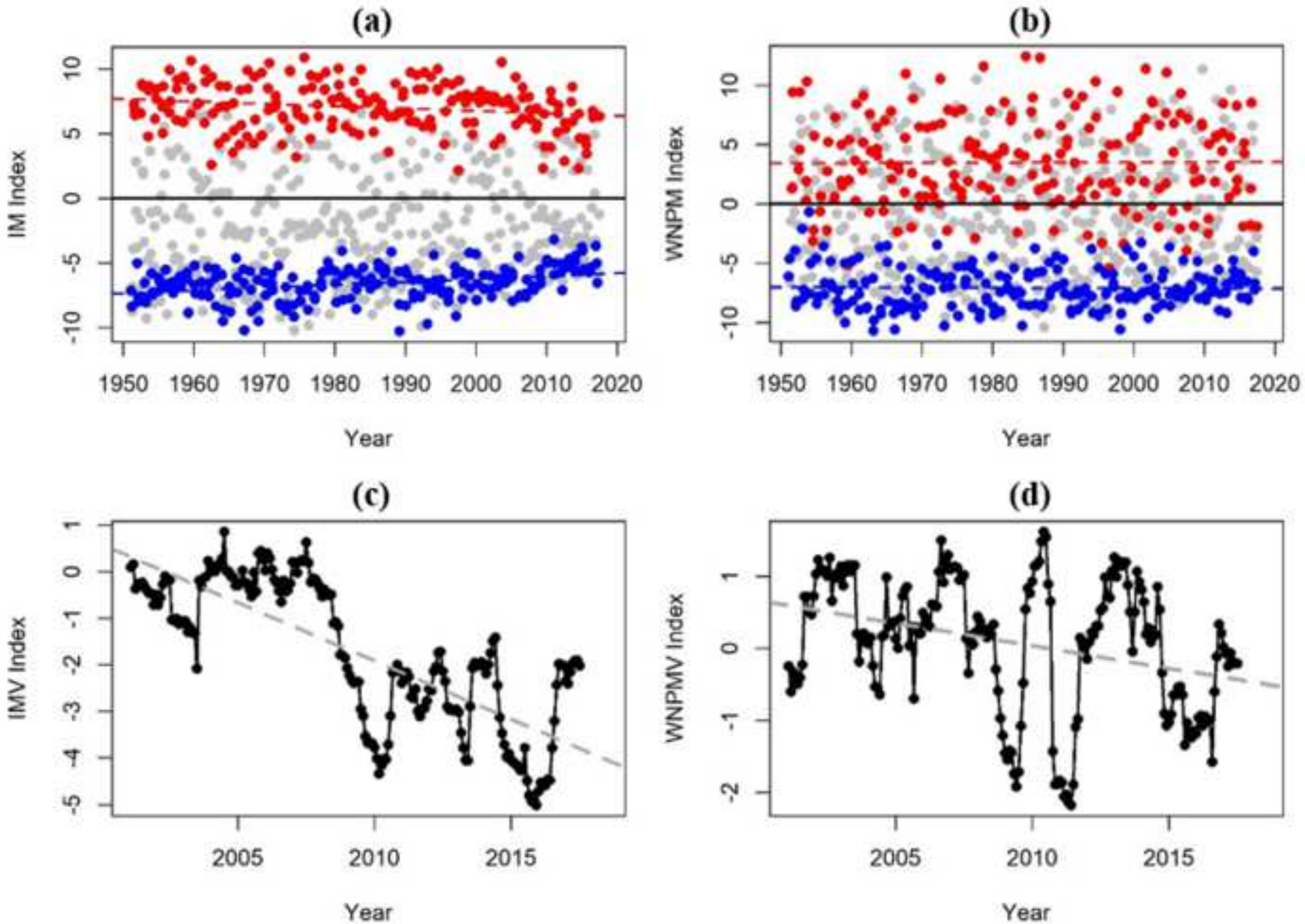

Figure

Click here to download high resolution image

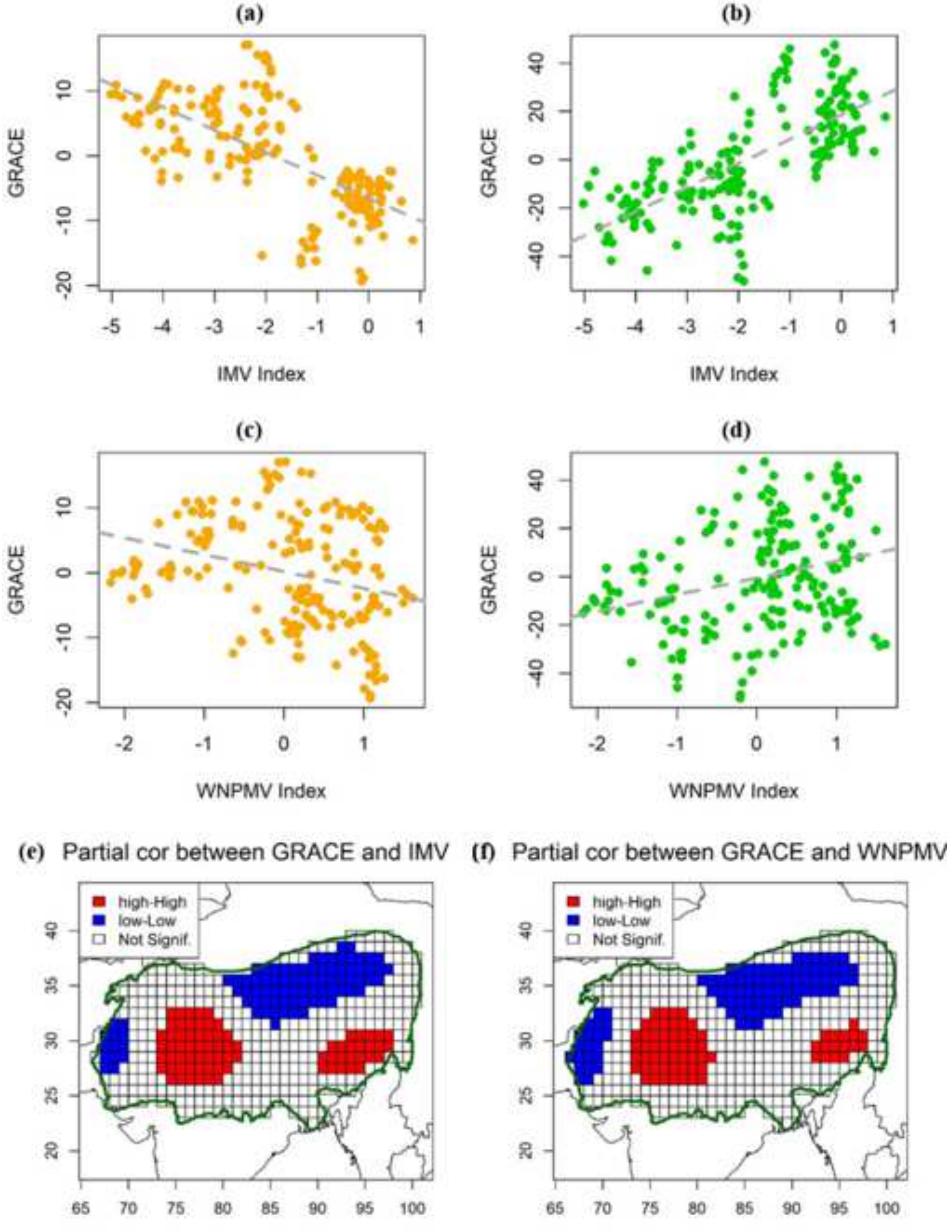

Figure
Click here to download high resolution image

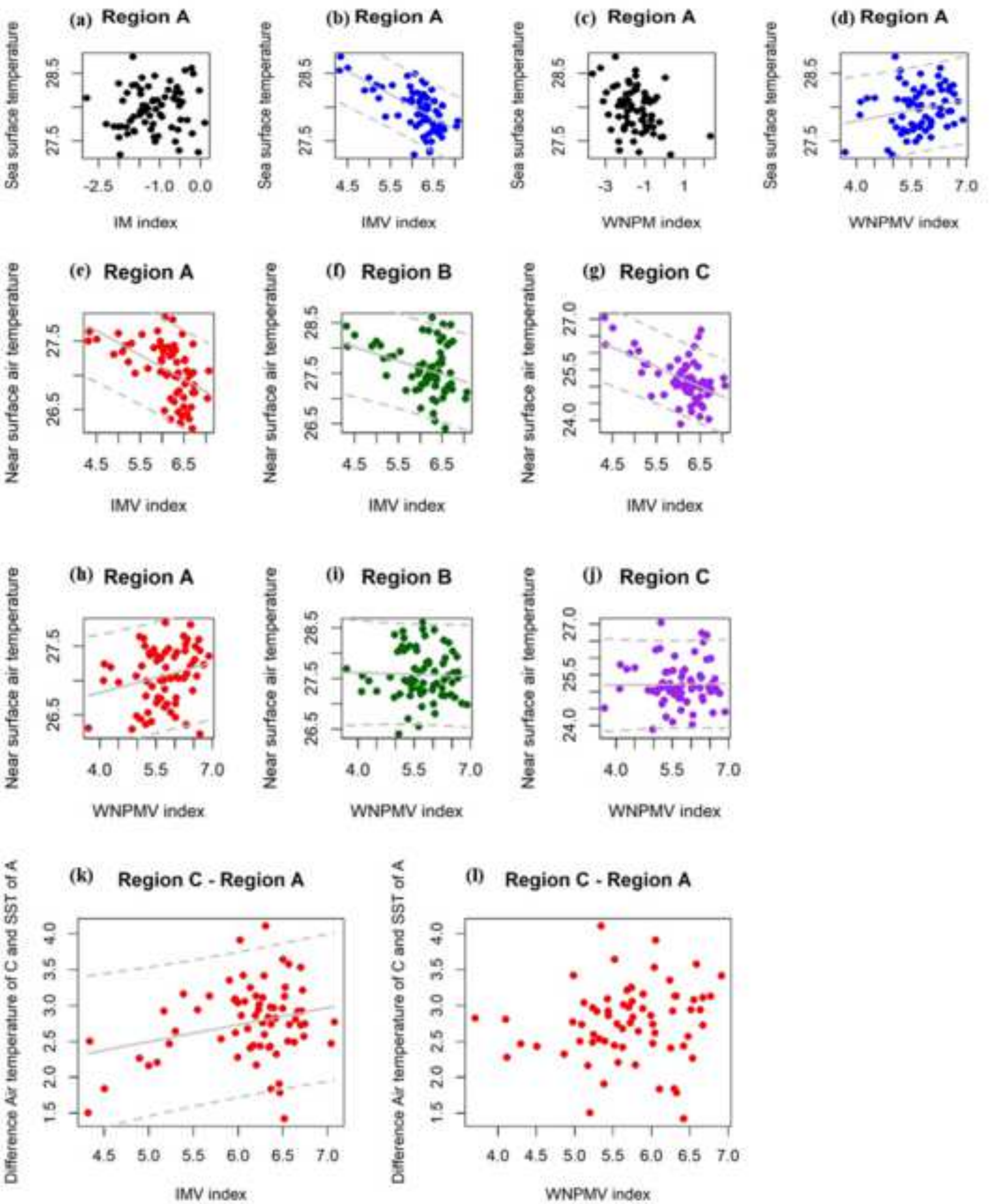

Figure
Click here to download high resolution image

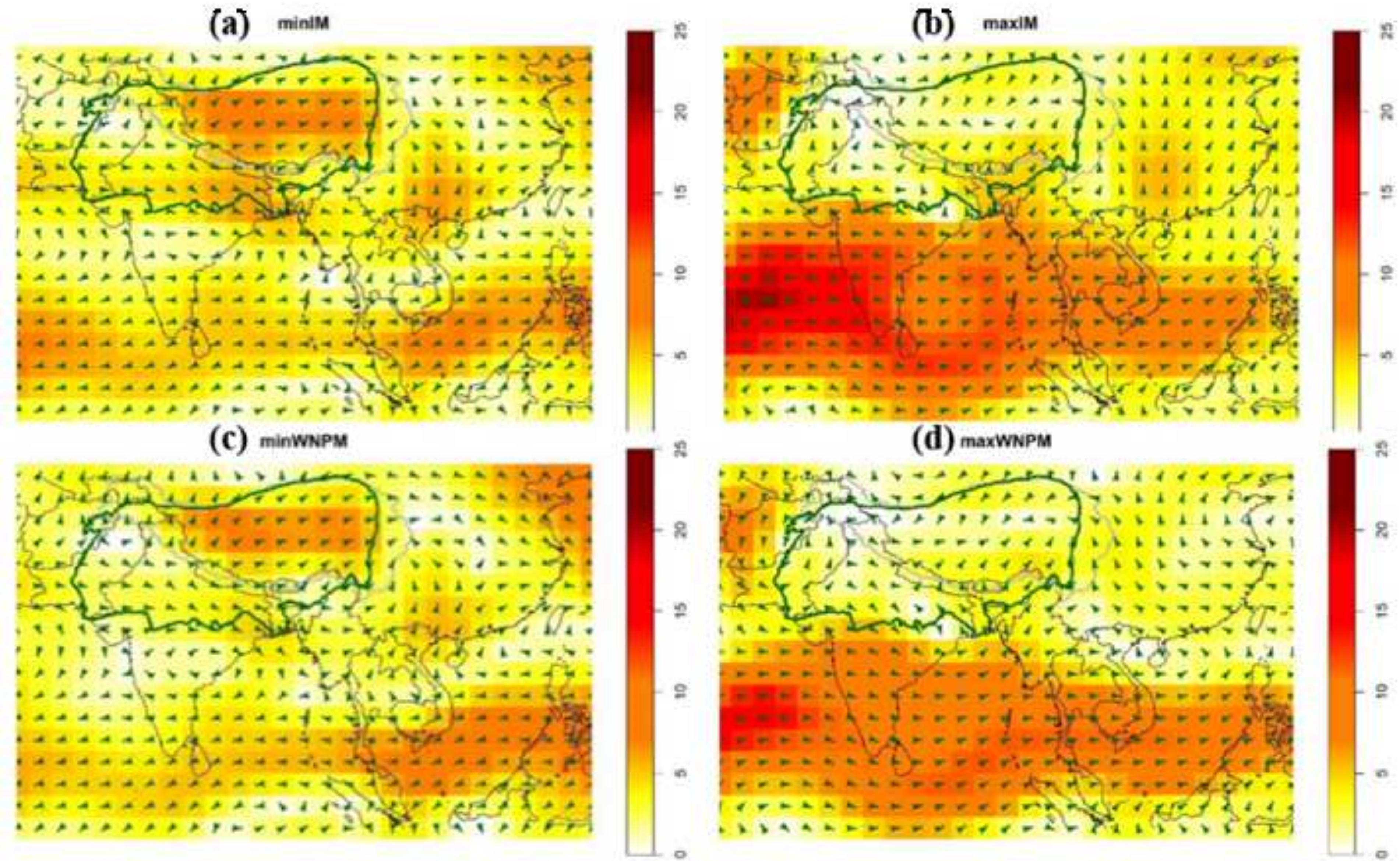

Figure

Click here to download high resolution image

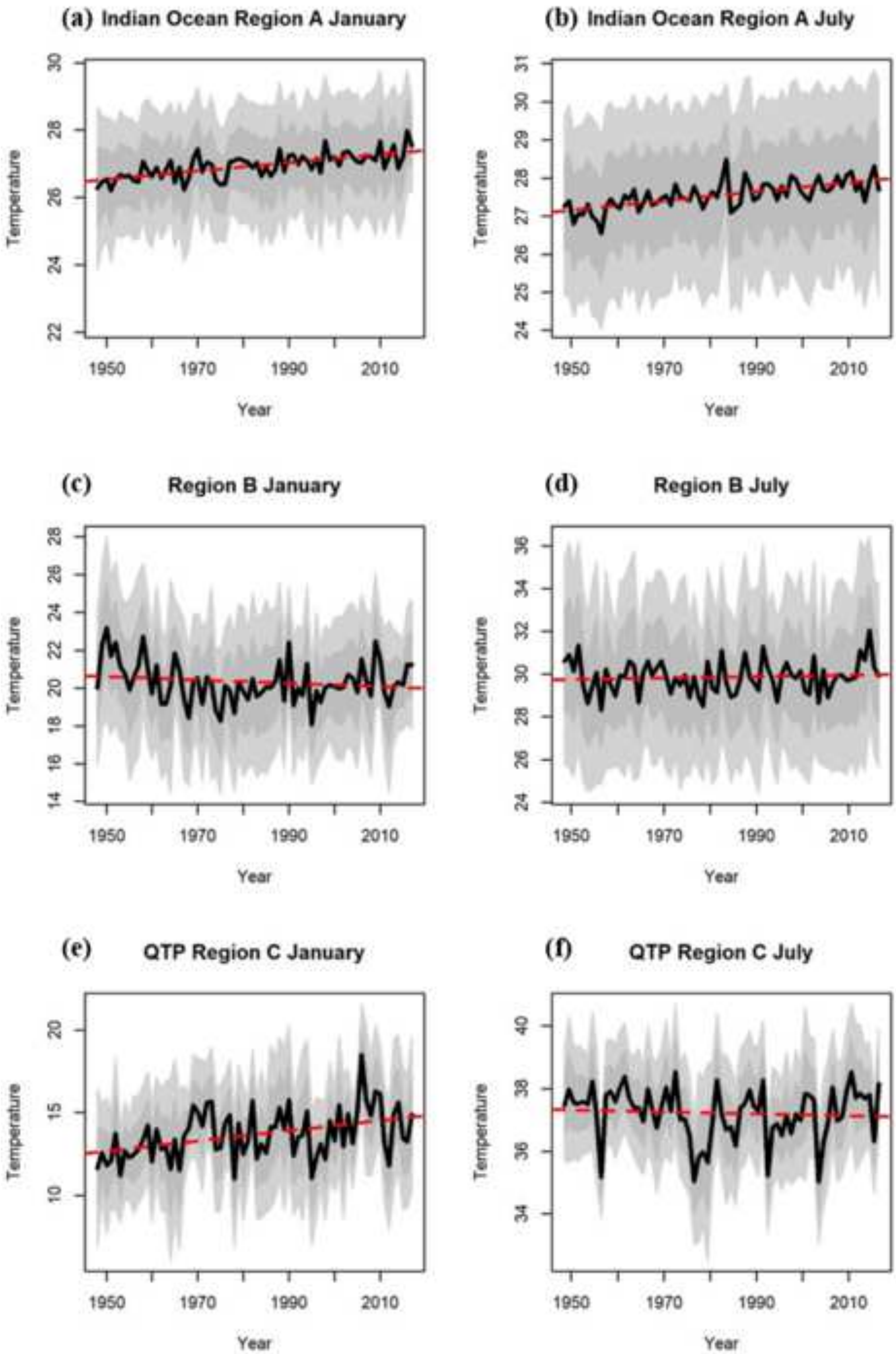

Figure
Click here to download high resolution image

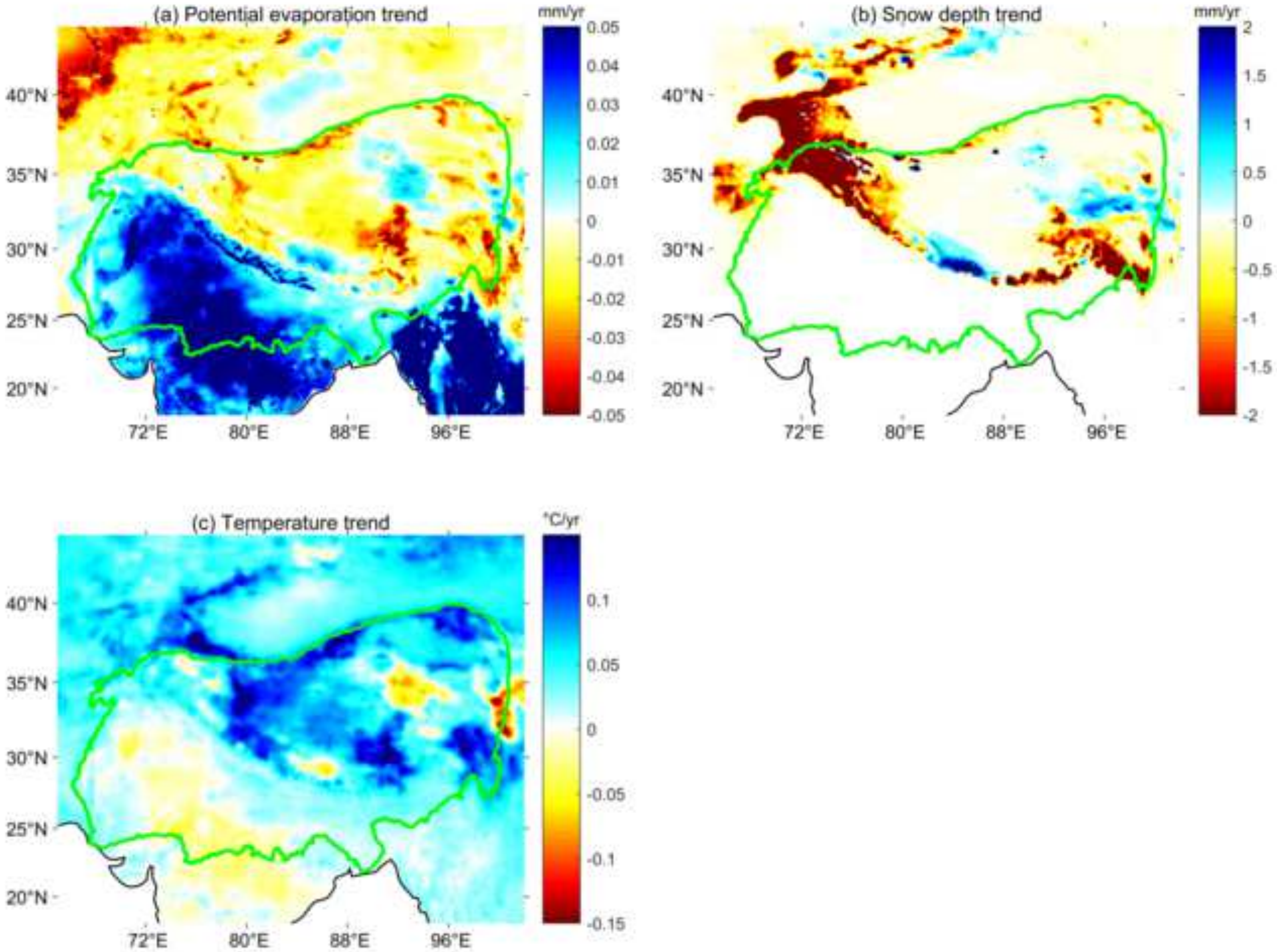

Figure
Click here to download high resolution image

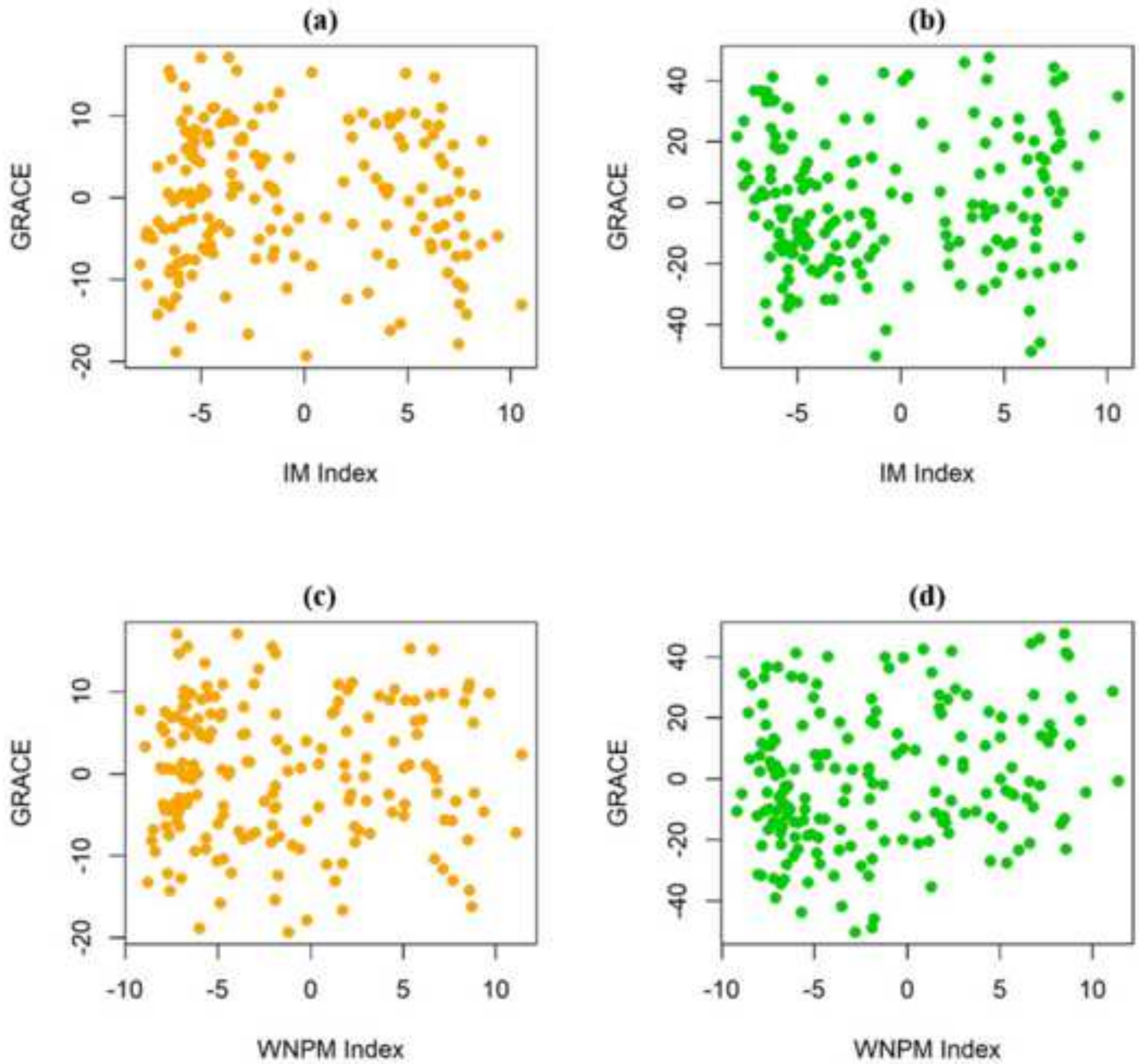

Figure
Click here to download high resolution image

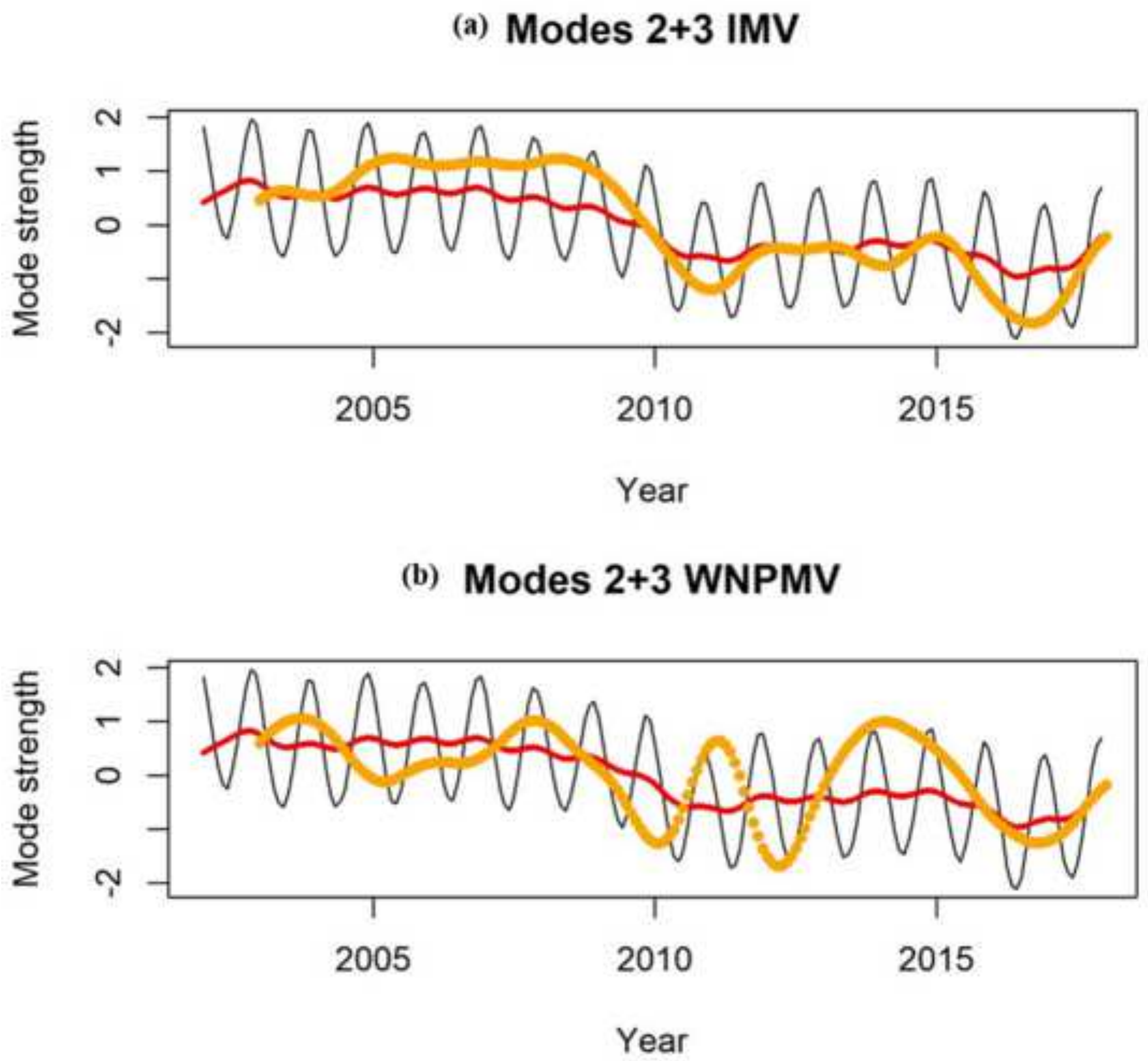

Figure
Click here to download high resolution image

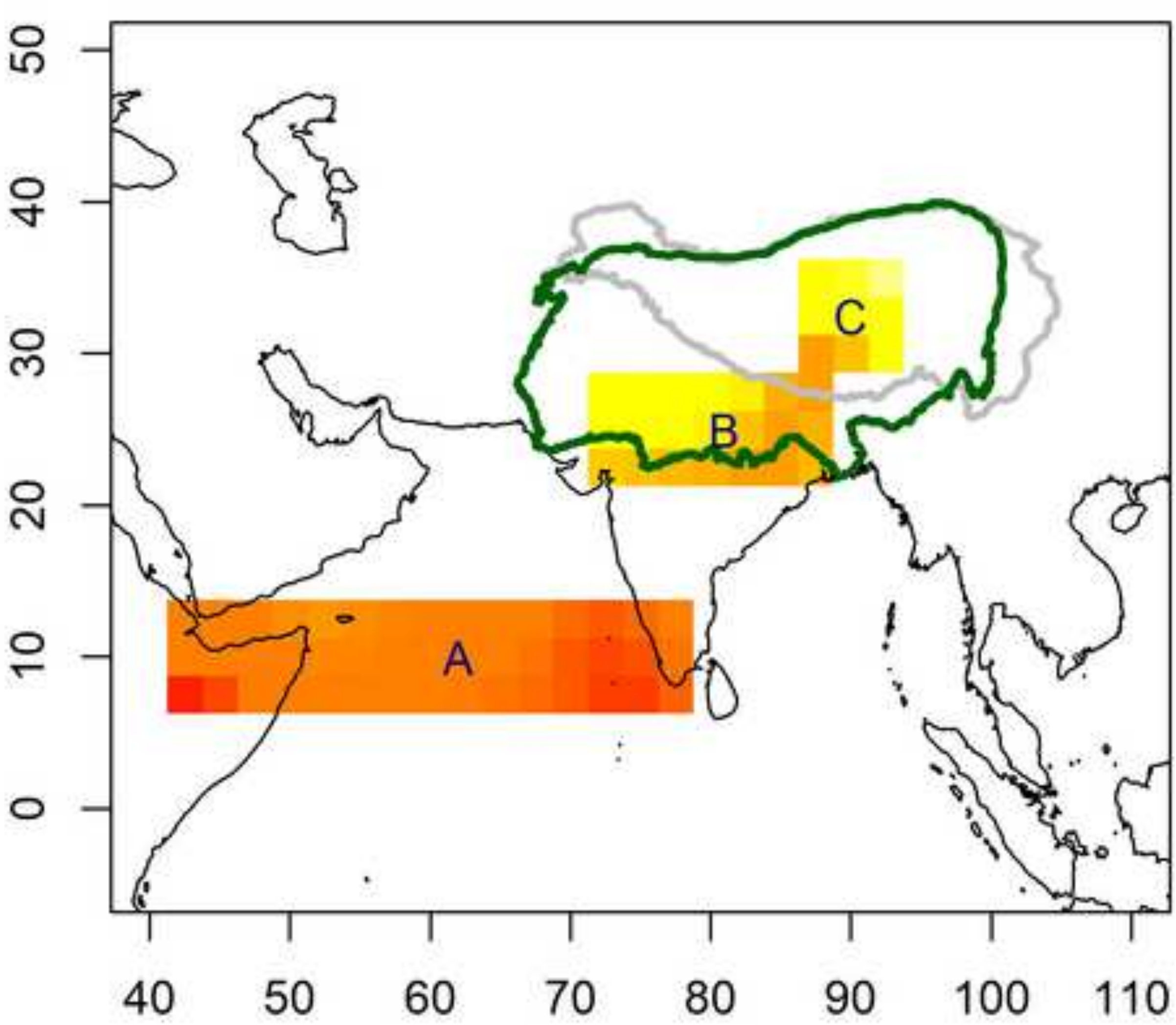

***conflict of Interest Statement**

Declaration of interests

☒ The authors declare that they have no known competing financial interests or personal relationships that could have appeared to influence the work reported in this paper.

☐The authors declare the following financial interests/personal relationships which may be considered as potential competing interests: